POLITECNICO DI MILANO

Scuola di Ingegneria Industriale e dell’Informazione

Corso di Laurea Magistrale in Ingegneria Elettrica

PHASOR MEASUREMENT UNITS AND DISTRIBUTION SMART GRIDS: APPLICATIONS AND BENEFITS

Relatore: Prof. Alberto Berizzi

Correlatore: Dott. Ing. Simone Cuni

Tesi di Laurea Magistrale di:

Giuseppe Torregrossa

Matr. 10517751

Anno accademico 2016/2017

Acknowledgements

This thesis would not have been possible without the support of many people. Many thanks to my supervisor, Professor Alberto Berizzi, who gave me the opportunity to work on an experimental project in e-distribuzione and helped make some sense of the confusion that sometimes happened to arise.

Also thanks to the Smart Grid Lab team, and in particular Gianluca Sapienza, Giovanni Valvo, and Carla Marino, who offered guidance and support. A special mention goes to Simone Cuni, for not only being my main source of advice, positive criticism and suggestions, but also providing me with all the means to complete this project with ease and keeping up the mood with his optimistic and charismatic personality. A note of appreciation to my colleagues Flavia and Mattia too, for the hand they lent me in the reviewing phase.

I am grateful to my parents Arturo e Rosaria and my sister Giorgia, whose love and care reaches me every day even from the distance that keeps us apart; to my cousins Giulio and Silvia, without whom I would have missed this great opportunity and to whom I truly owe a lot; to my grandmother Mela, a strong role-model that even now misses no opportunity to teach me rules of the world and how to survive it.

Last but not least, I want to thank the friends I met during this two-year academic adventure: Quanti (Isacco), Disagea (Davide), Foppa (Massimo), Fero (Federico) and all the people I met and learned to trust and respect living in the “Casa dello Studente” students’ residence.

Thank you all for your precious help and, most importantly, for gifting me with an existence that would not be as worth without even just one of you.

Abstract

This thesis' objective is to research the many potential applications for the PMU technologies when installed on the Italian distribution grid, with attention to the benefits DSOs could gain as a consequence.

After a brief introduction explaining the reasons why the MV and LV networks would nowadays require the use of real time monitoring and control more than ever before, the phasor theory is reviewed and the PMU technology is presented in detail. A list of potential distribution applications is then offered and its elements are presented one by one.

Only one of them, however, is chosen as the subject of an intensive experimental research: the validation of MV network parameters by a PMU-enabled real time system. This is studied in depth thanks to the help of the Real Time Digital Simulator (RDTS). Models and algorithms are created and implemented in a long series of tests, whose results are then collected and commented thoroughly.

Finally, the work ends with some considerations regarding the economic feasibility of a future potential network upgrade to implement these devices and benefit from their applications.

Astratto

L’obiettivo di questa tesi è studiare le potenziali applicazioni delle tecnologie PMU sulla rete di distribuzione Italiana, con particolare attenzione ai benefici che i DSO potrebbero trarre dal loro utilizzo.

Dopo una breve introduzione, utile a capire le ragioni per le quali le reti MT e BT al giorno d’oggi necessitino più che mai di monitoraggio e controllo in tempo reale, viene riportato un sunto della teoria dei fasori e presentata in dettaglio la tecnologia PMU. Una lista di potenziali applicazioni di tale tecnologia per le reti di distribuzione è quindi proposta, ed i punti che la compongono analizzati singolarmente.

Tuttavia uno solo fra essi viene scelto come soggetto dell’analisi sperimentale condotta: la validazione in tempo reale dei parametri di una rete MT effettuata per mezzo di un sistema automatico basato sulle PMU. Tale studio è condotto per mezzo del Real Time Digital Simulator (RTDS). Modelli ed algoritmi vengono creati ed implementati in una lunga serie di test, i cui risultati sono infine raccolti ordinatamente e commentati.

Infine, il lavoro si conclude con la presentazione di alcune considerazioni sulla praticabilità economica di un futuro miglioramento degli assetti di rete, finalizzato all’implementazione di questi dispositivi in funzione dei benefici e vantaggi che essi potrebbero portare.

Index of contents

Index of figures

INTRODUCTION

The Italian electricity market liberalization process, started in 1999 and still ongoing, brought many changes in the grid management approach. One of the most influential factors is without a doubt the massive penetration of Distributed Energy Sources (DER). In fact, the liberalized market allowed a great number of new participant, individuals that were eager to invest their however small capitals into the newly opened market. This caused a fast and radical change in the national generation assets: big and centralized conventional power plants (such as coal-fired and gas powered ones) were joined, and sometimes even substituted, by a multitude of small generators distributed all over the grid. If the former systems often required energy to be transmitted over long distances, the latter could by contrast be installed close to the load they served, thanks to their low capacities (10 megawatts or less), modularity and flexibility.

This revolution brought many benefits with it, but also a number of issues: Distribution System Operators (DSOs) had to deal with new challenges, due to the penetration of such an amount of DG plants in a portion of the network that was not originally designed to accommodate as much. The existing literature is more than exhaustive about such problems, and some of them will be described in more detail in the following chapters. The focus of this work, however, will not be on the already well-known complications, but on the possible solutions.

Among the many proposed technical alternatives, the one that this thesis focused on is the implementation of Phasor Measurement Units (PMUs, from now on) on a portion of the distribution grid under the responsibility of e-distribuzione. PMUs are measurement devices whose readings could, as will be shown, prove to be fundamental for the implementation of innovative monitoring and control techniques developed in order to solve DG-related issues and, more in general, improve system efficiency.

This work is composed by three distinct chapters. The first one goes in-depth with the description of the grid criticalities that the DSOs, and e-distribuzione in particular, must face in the new liberalized environment, as well as the theoretical and mathematical tools used for their analysis. Particular focus will be put on the definition of Phasor Measurement Units (PMU) and on the explanation of their purpose and role in said analysis.

The second chapter is dedicated to the study of the potential benefits of PMUs' installation on the national distribution grid, with emphasis on their impact on the DG-related issues previously mentioned. Several hypothetical applications will be presented and described in detail.

The third and last portion of this endeavor will illustrate the implementation of one specific PMU application to a portion of the grid managed by e-distribuzione. The experiment is conducted by means of a simulation of the actual network, run by the Real Time Digital Simulator (RTDS) and set up through the use of the RSCAD software.

CHAPTER 1
DG PENETRATION AND PMUS

As already mentioned, the focus of this work is the analysis of the impact of Phasor Measurement Units' (PMUs) implementation on a number of issues affecting the distribution network, whose prime cause is Distributed Generation (DG) penetration, and Renewable Energy Sources (RES) in particular. In order to understand the benefits the PMUs could bring to the system, first a preliminary study of the new problems plaguing it is necessary.

The following sub-chapters contain an historical overview of the Italian regulatory framework, and an explanation about how it has been the main driver for the rise of said new problems; these criticalities will then be listed and explained in detail. Additionally, this section contains specific descriptions of the theoretical assumptions and mathematical tools used to conduct the study discussed in the successive chapters.

1.1 Historical background

1.1.1 Italian electricity market liberalization process

By "regulatory framework" we refer to a system which allows governments to formalize and institutionalize its commitments to protect consumers and investors in a certain market. For what concerns the electric power industry, two main regulatory models can be identified:

- A *traditional one,* in which the electric power industry is managed by a vertically integrated monopolistic company, which is the only one in charge of providing electrical supply as a public service. According to this regulation philosophy, the chosen firm benefits from an exclusive franchise agreement with the public administration, which can last indeterminately. The lack of any form of competition in this environment calls for strict monitoring and control actions operated by an appointed regulatory body: the Regulator; this entity has many role, for example price definition based on the firm’s expenses. This regulatory approach was in force in Italy between 1962 and 1999. During this period, every aspect of the Italian electric power industry, ranging from generation to distribution to retailing, was in the hands of the Enel company.

- An *innovative one*, based on competition, that only appeared on the scenes in recent years. The first attempt was made in Chile in 1982 and it involved the separation – the so-called “unbundling” – of every activity related to the electric power provision, as a result of which most of these activities were privatized and had to be re-organized. Furthermore, a competitive pool market was created: here different generation companies (GENCOs) competed for the right of supplying a specific service by means of auction bids. This pool market mechanism serves as a non-discriminatory tool, in which each player is paid the very same quantity of money.

  In Italy, the transition to this new regulatory model occurred after the enactment of the legislative decree n.79 of March the 16th 1999, also known as “Bersani decree” by the name of its inspirer.

This normative act of the Italian Republic, transposition of the European directive 96/92/CE, determined the shift from the traditional vertically integrated structure managed by Enel as a public monopolistic company to an open market structure where a plurality of players were allowed to participate. Additionally, Enel was privatized and forced to sell a great amount of its generation capacity and, later on, also lost the ownership of the transmission network (high/very high voltage lines).

This process limited the influence of the Enel company on the pool and dispatching market, but changed almost nothing relatively to its role as a power distributor. In fact, even if the distribution business was partially opened to competition, Enel managed to prevail and assure for itself a great share of it all (as of today, it manages 85% of the national distribution network). However the transition brought new challenges, linked to an intrinsic lack of coordination in the system (one of the downsides of activities unbundling) and to the drastic increase of distributed generation.

1.1.2 Network evolution

Distribution System Operators' role

Distribution activities consist of transporting and delivering – wanting to use an analogy with material goods – electric energy to medium and low voltage customers. The decree made the former fully monopolistic distribution business into a local monopoly, meaning that inside a certain geographic enclosure defined by the territory of a municipality there must be only one distributor chosen to carry out such a service.

Enel and all the other firms operating in more than one sector of the power supply chain were forced to carry out an unbundling of their activities for the sake of transparency. This is why, as of today, business branches formerly named after their main company had to be re-named and re-organized as separate societies: for instance, the former "Enel Distribuzione" is now known as "e-distribuzione".

Distribution network structure

The Italian distribution network is a fraction of a much bigger system, one that can be synthetized as shown in Figure 1.

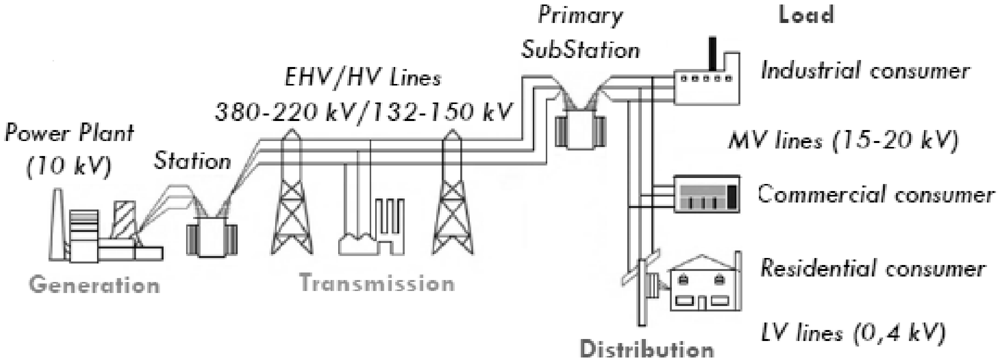

Figure 1 Italian electric power system representation.

Such a depiction, even if strongly simplified, gives an accurate description of the traditional network structure: an ensemble of interconnected devices, working together in order to produce, transmit, and distribute electric energy. Production takes place in power plants, where primary energy sources – such as coal, hydro or natural gas, just to mention some of the most relevant – are converted into electricity that is then delivered to the customers via the network. Historically, power plants have been dislocated all over the national territory, but always been connected to the transmission network only. This was true because of their high generation capacity, which would produce unbearable amounts of losses were they to be connected to lower voltage levels. (due to the higher currents)

This is however not the case anymore: thanks to the combination of a strong incentive policy focused on RES development, that had its peak in 2011, and the opening of energy markets to a plurality of private subjects, more and more small and very small plants were installed on the national grid. Due to said small capacities, these plants were connected to the Medium Voltage (MV) and Low Voltage (LV) sections of the network, with MV installation predominance. The link between incentives and RES evolution is made evident by the data collected and shown in Figure 2 (inclusive of a comparison with similar dynamics that happened to have place in Germany in that same period):

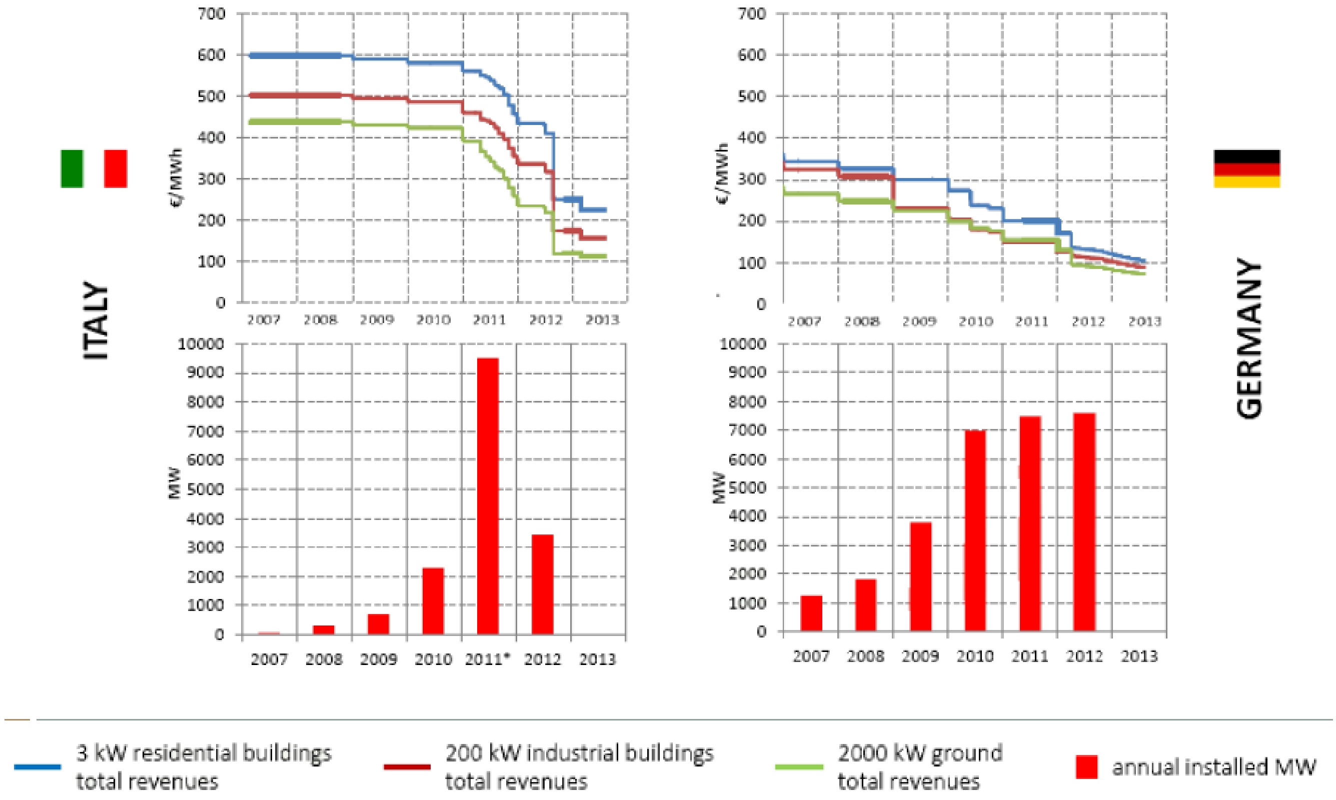

Figure 2 Photovoltaic annual installed capacity and incentives digression.

Distribution network criticalities and solutions

DG penetration is widely regarded as a positive wind of change in the generation scenario, as it bring benefits that are both economic and environmental. Efficiency gains derived by the reduction of transmission losses, higher degree of security of supply, lower energy prices due to the intrinsic CAPEX-only nature of RES investments, an abundance of balancing resources from a new category of ancillary services providers (the prosumers) can be considered economic benefits, while CO2 emissions reduction – whether it is from the generation process (less burnt coal or natural gas), the transportation industry (electrical vehicles spread) or the domestic environment (self-consumption for house heating/cooling) – are the environmental benefits.

Unfortunately, benefits do not come alone in this case. Distributed generation brought new problems with it, or worsened old ones. The following is a list of such known matters, to underline their link to the DG penetration issue:

- Reverse Power Flow (RPF);
- Unwanted islanding;
- Instability due to RES volatility;
- Network saturation (lines+transformers);
- Selectivity issues (line protection devices);
- Voltage regulation issues (slow/fast);
- Frequency regulation issues;
- Higher degree of complexity and management/reinforcement costs (telecoms/hosting capacity);
- Regulatory framework adaptation.

In simple terms, the public electrical grid was originally designed to deliver power in a uni-directional fashion: from a few big plants, into the grid and then to the final customer to consume. Nowadays, however, more and more customers are operating power generating devices – such as solar panels, windmills, etc. – for self-consumption and/or to generate income by feeding power into the grid from their end. As the electric utility cannot deny by law the this energy injection, that is on the contrary incentivized, system operators need to make sure that it does not damage the network or prejudice its good functioning.

On-field technicians and experts alike provided numerous possible solutions to every problem on the previously mentioned list, each one with its pros and cons. Just to clarify the amount of proposed viable actions to solve a single issue, voltage regulation ones are taken in consideration as an example and their solving measures are shown in the following: (a distinction is made between slow and fast variations)

- Network reconfiguration: (slow and fast)
  - Pros: cheap, easy, fast, dynamic;
  - Cons: only in MV, only for low penetration of DGs.
- Network reinforcement: (slow and fast)

    - Pros: always an option, both for LV and MV, simple;
    - Cons: expensive, slow permission/construction iter, static.
- On-load tap changer: (slow)
    - Pros: simple, dynamic, relatively cheap;
    - Cons: problems with increasing penetration.
- Booster transformers: (slow)
    - Pros: simple, both for MV and LV, relatively cheap;
    - Cons: static, slow installation.
- Reactive compensation: (slow)
    - Pros: simple, both for MV and LV;
    - Cons: must be coordinated with OLTC and load/generation;
- Storage systems: (slow and fast)
    - Pros: both for MV and LV, dynamic, allows advanced management;
    - Cons: expensive and space consuming.
- Advanced voltage control: (slow and fast)
    - Pros: highly dynamic and adaptive, it’s a set of different tools;
    - Cons: costs, TLC, complex, Smart architecture/regulation needed.
- Advanced closed-loop operation: (slow and fast)
    - Pros: those of loop configurations; (e.g. power/voltage stability)
    - Cons: Smart architecture/regulation needed, rarely seen in MV.

As it can be seen, there are both simple but scarcely efficient measures and effective but complex ones. Proposals from the two categories can be combined in order to obtain a good final result, however both their advantages and disadvantages will overlap. Any mixed solution would then be quite complex to manage, both in terms of needed starting data collection and delivery. This is the reason why modern management and control systems rely more and more on telecommunications and distributed intelligence, hence the development of Smart Grids and companion devices capable of providing the data that said Smart Grid would help to collect, transmit and elaborate on.

Among those many devices, there is one believed to be able to exponentially increase the efficiency of monitoring and control system if properly used. This instrument and its possible applications are the subject of the present study: it is the “Phasor Measurement Unit”.

1.2 Theoretical premise

In order to understand the full extension of PMUs’ potential in system management and control applications, the first thing needed is an in-depth understanding of the theoretical basis upon which these devices are built.

1.2.1 Phasor theory outlines

Electrical data analysis often requires comparisons between time-variant quantities in order to extract meaningful results from raw data. An example of such need is the case in which the voltage of an impedance must be compared to the current flowing through it in order to compute energy consumption or define the nature of the load. A common way to differentiate between capacitive and inductive load is, in fact, checking the angular difference between its measured voltage and current waveforms, given that they are at the same frequency. Once a zero-angle reference is set, then the two quantities can be compared graphically or by analyzing their expressions in the time domain (Eq. 1 shows the generic form for a sine wave), and in particular the phase parameter φ:

$$A(t) = A_m \sin(\omega t \pm \varphi) \qquad \text{Eq. 1}$$

This comparison is however not very intuitive, and mathematical operations turn out to be quite difficult to conduct in the time domain. One way to overcome these problems is to represent the sinusoids graphically within the phasor-domain form by using phasor diagrams, and this is achieved by the rotating vector method.

Basically, a “phasor” is a rotating vector whose length represents an AC quantity’s magnitude and whose direction represents, with respect to a reference angle, its phase. While the AC quantity is time-variant, the phasor representation is instead static, as if frozen at some point in time. Normally, phasors are assumed to pivot at one end around a fixed point known as “the point of origin”, freely rotating in anti-clockwise direction at an angular velocity $\omega=2\pi f$, where f is the frequency of the waveform.

The tip of the rotating vector will draw a circle every period T=2f. This means that the vector that starts rotating from point A will be back to that same exact point every T seconds. The height of its moving tip can be transferred at different angular intervals in time to a graph as shown in Figure 3.

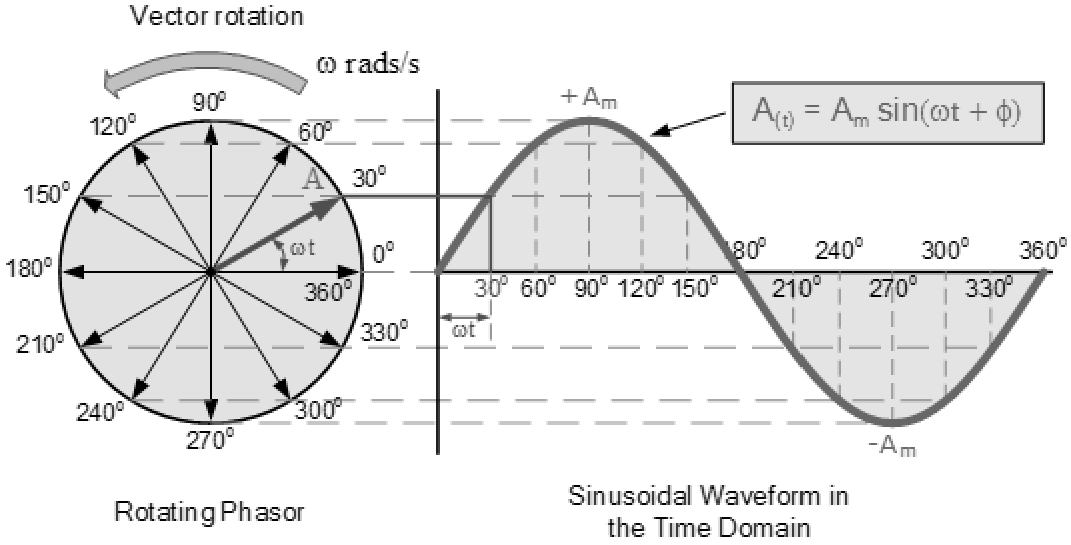

Figure 3 Phasor-wave relationship explained by graphical means.

Sometimes when analyzing sinusoidal waveforms a comparison is in order. Voltage and current, as already mentioned, should be taken into consideration simultaneously when power is computed. We assume that one of the two waveforms, for example the voltage V, starts passes through zero increasing at time t=0, while the other (the current I) does so at a later time. In order to represent the relationship between these two quantities in phasor notation, the angular difference Φ must be highlighted as shown in Figure 4.

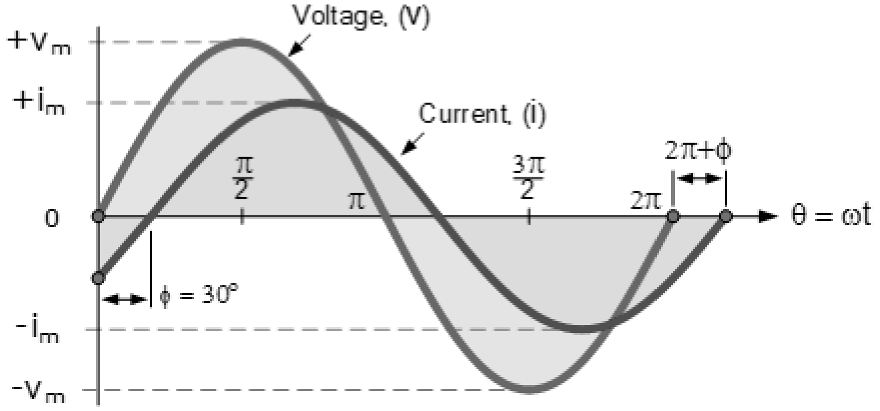

Figure 4 Example of two waveforms shifted by an angle equal to Φ.

The mathematical expressions used to define these two sinusoidal quantities are:

$$v(t) = V_m \sin(\omega t) \qquad \text{Eq. 2}$$

$$i(t) = I_m \sin(\omega t - \Phi) \qquad \text{Eq. 3}$$

The current is lagging with respect to the voltage by an angle Φ=30. This same angle will be the phase difference between the two corresponding phasors, that can be represented together as in Figure 5.

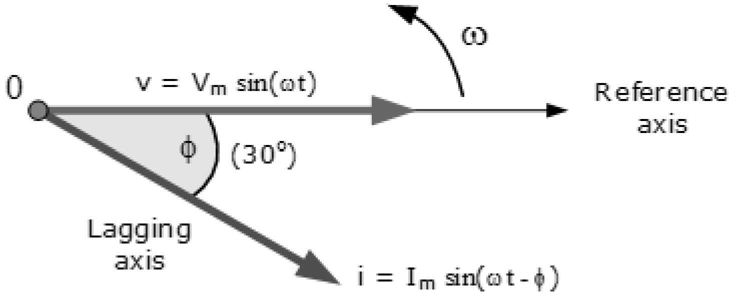

Figure 5 Phasorial representation of the two waveforms seen in Figure 4.

The phasor diagram – this is the name of such a depiction – is drawn as if the two rotating vectors were frozen at time t=0. Since the rotation's direction is anti-clockwise, the phase difference Φ is measured in that same direction.

To understand why phasors are considered to be essential tools in the study of electric phenomena, a simple applicative example is in order.

Circuital analysis often leads to the need to sum two sine waveforms. If they are in phase, that is if their phase difference Φ=0, then they can be combined as it happens with DC quantities through an algebraic sum of the respective waveforms or vectors at any given moment in time. For example, if two voltages of 50 V and 25 V of magnitude respectively are in phase, the resultant vector that will be formed by their combinations is going to be one with a 75 V of magnitude.

If however the two waveforms are not in phase, this simple computational procedure cannot and be followed. Phase difference must be taken into account, and this is much easier analyzing the problem with phasorial representation. The method applied in this case is the vector sum, carried out graphically using the parallelogram law as shown in Figure 6.

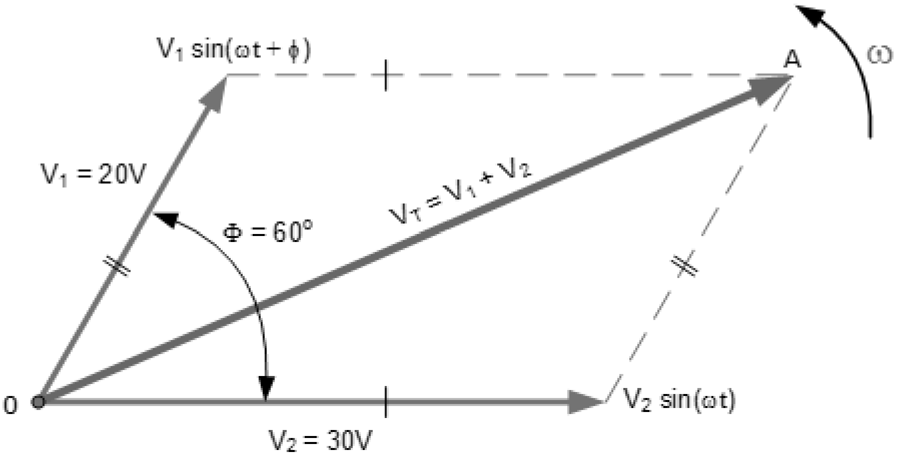

Figure 6 Example of two voltage phasors and their sum.

In this example there are two AC voltages to be summed, with the following characteristics: V1=20 V, V2=30 V and Φ=60°. (voltage V2 is lagging behind voltage V1) The total voltage V_T can be found constructing a parallelogram in which two of the sides are the voltage vectors and the remaining two are their parallels.

If the two vectors are properly drawn to scale onto graph paper, their vector sum can be easily found by measuring the length of the diagonal line of the parallelogram. Graphical resolutions like this one, however, have downsides: not only the representation takes time to be carried out, but in case of scale errors it could also produce unacceptable inaccuracies. If a high degree of precision is needed, then the solution shall be obtained by means of an analytical method.

Mathematically the resultant vector can be found by firstly finding the vertical and horizontal components of the addends, then combining them to obtain these components for the resultant vector and at last computing its magnitude making use of Pythagora's theorem. This analytical method uses sines and cosines applied to the phase difference to find the final value, and it does so by noting quantities in the so-called "rectangular form". In this form, the phasor is divided into a real part x and an imaginary part y, making the following generalized complex expression:

$$\boldsymbol{z} = x + jy \qquad \text{Eq. 4}$$

In the specific case of a voltage phasor, real and imaginary part are computed as shown in the following expression:

$$\boldsymbol{V} = V_m \cos\Phi + jV_m \sin\Phi \qquad \text{Eq. 5}$$

The sum of two phasors expressed in their rectangular form as shown in Eq. 4, whose components are computed as shown in Eq. 5, can then be easily summed by summing their components:

$$\boldsymbol{A} = x + jy \qquad \text{Eq. 6}$$

$$\boldsymbol{B} = w + jz \qquad \text{Eq. 7}$$

$$\boldsymbol{A} + \boldsymbol{B} = (x + w) + j(y + z) \qquad \text{Eq. 8}$$

The example of Figure 6 and its data are taken into consideration and a computational example is made. Voltage V2 lays on the zero-angle reference, so its vertical component is null. Hence, using Eq. 5 we obtain the following rectangular expression:

$$\boldsymbol{V_2} = 30\cos(0°) + j30\sin(0) = (30 + j0)\ V \qquad \text{Eq. 9}$$

The same computation can be made for voltage V1, which leads V2 by 60°:

$$\boldsymbol{V_1} = 20\cos(60°) + j20\sin(60°) = (10 + j17.32)\ V \qquad \text{Eq. 10}$$

Now, as explained, in order to obtain the resultant voltage V_T a vector sum is made, that is adding component by component the two vectors:

$$\boldsymbol{V_T} = \boldsymbol{V_1} + \boldsymbol{V_2} = (30 + j0) + (10 + j17.32) = (40 + j17.32)\ V \qquad \text{Eq. 11}$$

Now that both the real and imaginary values have been found, the magnitude of voltage $\mathbf{V_T}$ is determined by simply using Pythagora's Theorem as follows:

$$V_T = \sqrt{40^2 + 17.32^2} = 43.6\ V \qquad \text{Eq. 12}$$

Similar is the procedure for vector subtractions, while other operations – such as multiplication or exponentiation – is a little more complex.

1.2.2 Phasor Measurement Units

Phasor Measurement Units (PMU), sometimes wrongly addressed as "Synchrophasors", are power system measuring devices capable of collecting data from the electricity grid in a far more precise and fast fashion when compared to traditional equipment. This is possible thanks to the use of a common time source for data synchronization, meaning that every measurement made by PMUs spread all over the network will be provided of an accurate time-stamp which allows to exploit the potential of big data time correlation.

Phasors had been known and used for almost an entire century before the invention of Phasor Measurement Units, since Charles Proteus Steinmetz developed the already discussed phasor theory in 1893, while Dr. Arun G. Phadke and Dr. James S. Thorp designed the first PMU in 1988 and built the first prototype in 1992. This device had already most of the basic features modern models have, including of course the calculation of real-time phasors synchronized to an absolute time reference provided by the Global Positioning System. (GPS)

Historically, however, the absence of a proper telecommunication infrastructure, capable of managing the massive amount of data produced and exchanged by PMUs times short enough to be acceptable, prevented the growth of this technology. Another reason for its slow development was the general lack of need for it: up until twenty years ago, in fact, power was being delivered in a uni-lateral fashion through passive components to customers, so there was no interest in collecting great amounts of real-time data for monitoring and control purposes since passive grids' management is relatively simple. However, in more recent years, the exponential growth of distributed generation resources on the peripheral parts of electric networks all over the world changed the scenario. This newly emerged condition made it imperative to continuously observe both transmission and distribution networks through advanced sensor technology, namely the PMUs.

From a technical point of view, the following are the most noteworthy characteristics of a modern PMU system:

- High speed GPS-synchronized waveforms sampling – up to 50 samples per cycle – for 50/60 Hz three-phase voltages and currents, with subsequent signal digitalization;
- Top notch clock accuracy, down to one microsecond, that can be provided by alternative/additional sources other than GPS if reliable enough;
- High rate time-stamped phasors transmission from widely dispersed locations to local receivers, up to 30 observations per second; (compared to one every four seconds using conventional technology)
- Collection of a wide range of data, including three-phase voltage magnitudes and phases, three-phase current magnitudes and phases, frequency and Rate Of Change Of Frequency (ROCOF) with respect to time.

Phasor measurements that occur at the same time are called “synchrophasors”. While it is commonplace for the terms “PMU” and “synchrophasor” to be used interchangeably, they actually represent two separate technical meanings: the latter is the metered value, whereas the former is the metering device.

Thanks to the high degree of synchronization, collected data can be put in a meaningful comparison in order to assess system conditions via parameters that would be otherwise impossible (if not harmful) to use together, such as voltage magnitude differences and phase shifts. The system operators can monitor the grid with any number of PMUs, but their number and positioning are important parameters: few well-placed devices can provide good results if used in small networks or assisted by very efficient state estimators to fill the data-gaps in non-monitored nodes. Experience has however proved that, even in case of good positioning, the use of PMUs from multiple vendors could yield inaccurate results due to the immaturity of the relative standardization framework.

Telecommunication infrastructure

Traditional power system network monitoring tools use data coming from Remote Terminal Units (RTUs), protective relays and transducers to provide useful information to system operators. This information often proves to be vital for the operation of the power system, both under normal and contingency conditions. However, the mechanism most commonly used to obtain said data from the measuring devices – the Supervisory Control And Data Acquisition (SCADA) system – is asynchronous and relatively slow, implying that the obtained system representation is accurate enough during normal steady-conditions but lacks in reliability when fast dynamics are to be taken into account.

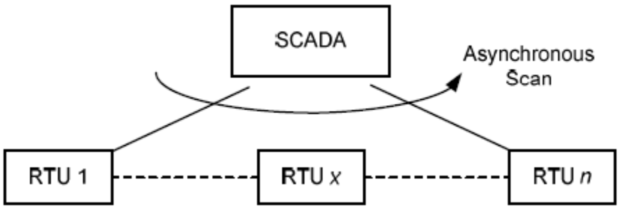

Figure 7 Example of an asynchronous scan routinely run by traditional SCADA systems.

As Figure 7 shows, the SCADA data-gathering mechanism consists in an asynchronous polling procedure, meaning that RTUs are requested to send the information they collected one by one, in an ordered fashion. One complete scan could last from 2 to 10 seconds, depending on the number *n* of polled devices. During normal steady-state conditions the long scan time is not a major concern; however, when the system state changes abruptly during the scan, the data retrieved no longer represent the system state accurately. In other words, the low data rate may be too slow to capture many short-duration disturbances on the grid, not only giving the operators an inexact view of its condition but also potentially triggering unwanted automatic control responses.

However nowadays, due to the increasing complexity of network dynamics and higher availability of Global Positioning System (GPS) receivers, an alternative to the traditional SCADA system is on the rise: PMU-enabled Wide Area Monitoring Systems (WAMS). This new mechanism makes use of synchrophasor technology in order to reproduce the functionalities of legacy systems and implement the missing ones, thanks to the quasi-real time data availability. Even if information is sent in a much faster way, however, this technology still has limits: it is, in fact, well suited for steady state and quasi-steady state phenomena analysis, but not for transient conditions like faults.

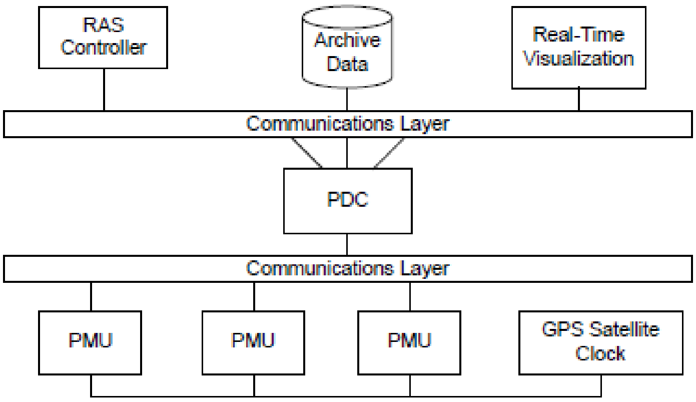

Figure 8 Communication network for PMU-based applications.

Figure 8 illustrates the building blocks scheme of a synchrophasor-based monitoring system. PMUs dispersed all over a vast geographical area receive GPS their clock signal from a common GPS satellite source, then produce synchrophasors that will be sent to a Phasor Data Concentrator at a rate of 10 to 50 messages per second, depending on the installed technology. Upon receiving synchrophasors from all the PMUs, a PDC has the role to time-align them taking into account PMU-PDC transmission delays: the device arranges a message-waiting time window to receive data from every PMU, then bundles it in a compact packet with a common time-stamp, as shown in Figure 9. In case of missing data, the PDC flags the relative PMU as “out-of-synchronism” and a self-healing procedure is bound to commence.

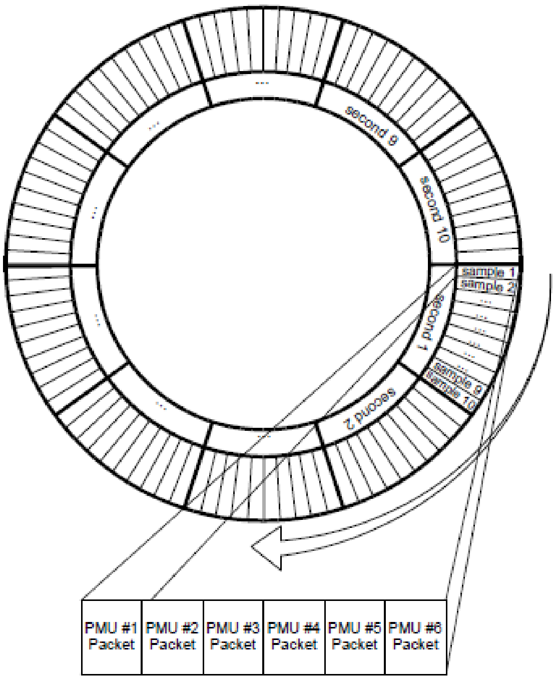

Figure 9 PDC data bundling example, with six PMUs forwarding synchrophasor packets every 100 ms to form a single time-stamped sample.

Packets are then sent to control centers, where they could be used for different purposes: fed to Remedial Action Schemes controllers to implement system protection schemes that need very accurate data to process advanced control mechanisms on the monitored network stocked into historical archives to be used as pseudo-measurements in future state estimation runs or for post-mortem analysis purposes, and finally used to implement reliable real-time visualization tools for operators to use.

Lastly, PMU-PDC and PDC-data center transmission is implemented through different physical means and communication protocols.

Criticalities

PMUs hold the potential to greatly improve the effectiveness of distribution monitoring and control systems. However, alongside benefits, innovation also brings a number of criticalities that need to be addressed in order to efficiently exploit said potential. The following is a list of known issues that operators have to face while dealing with PMU-based measurement systems:

- Data rate and storage requirements: a major characteristic of PMUs is their high sampling rate, responsible for a superior degree of measurements resolution but also for the resulting great stream of information, without which it would not be possible. As a c0nsequence, the telecommunication network on which the data will travel should be designed in a suitable way, with appropriate bandwidth and transmission characteristics. This, however, translates to high costs, that become even higher when considering derived expenses, such as those related to the acquisition of more capacious data storage devices or the upgrade of on-field equipment (e.g. switchgears) to their “intelligent” counterparts. (IEDs)
- Complex modeling and computational power: data coming from PMUs have to be processed by different algorithms in order to be useful to network control and automation procedures. However, the required computations are more complex for distribution systems than for transmission systems, because of some approximations that are considered admissible at higher voltage levels but not at lower ones. The main ones are the following:
  - Line resistances are no more negligible;
  - The three phases of a line can no longer be assumed to behave the same way, since load unbalance cannot be disregarded anymore.

  The superior complexity of the above-mentioned processes calls for enhanced computational tools, hence additional costs.

- Cyber-security risk: the more information travels along a communication line, the more it is susceptible to intentional external influences or theft. The data-flow must be protected from such dangers, in order to preserve own or customers' sensible data from industrial espionage or sabotage attempts. This is not, however, a costless effort since it requires technical expertise that was not needed with legacy system.
- Optimized device placement: a PMU network is no different from a traditional measurement system under the device-positioning point of view. State estimators, in fact, are known to produce more accurate results when measurement are provided by specific nodes. In order to pinpoint such optimal installation points for PMUs, however, it is impossible to use the same algorithms used the SCADA system so new ones need to be developed.
- Physical differences with respect to the transmission network: most of the available knowledge about PMUs and their use nowadays comes from experience matured through applications on the high voltage networks, where they were first introduced. This experience, however, cannot be fully exploited for MV installations, due to the differences between the two grid typologies. Higher degree of measurement accuracy is required for lower voltage installations, for example, since shorter distances between distribution networks' nodes imply smaller amplitude and phase differences between the respective synchrophasors: in order to properly compare them, μPMUs need to be accurate to the tenth of a degree.

  Another aspect to take into consideration is the faster dynamics that are to be expected when dealing with Smart Grids (e.g. the intermittent behavior of generators, loads and storage devices), which may require time responsiveness beyond the limits defined by the current standards, since those refer to PMUs used in HV.

CHAPTER 2
POTENTIAL PMU APPLICATIONS ON DISTRIBUTION NETWORKS

So far, synchrophasors have been considered "a solution waiting for a problem". Their undeniable theoretical potential has been in fact mostly ignored due to economic reasons and limitations derived from the luck of a suitable telecommunication infrastructure, but also by a lack of need for such advanced measurement tools. Historically, in fact, passive networks did not require real-time monitoring and control. However, as already mentioned, in time the evolution of distributed energy resources gave birth to new problems that could be addressed by the implementation of PMU systems. The truth is, however, that synchrophasors are a tool that may or may not be appropriate to solve said problems. This is where research and experimentation come in, and this chapter's aim in particular is to verify the feasibility of a number of possible PMUs' applications on the Italian distribution grid, evaluate their advantages and disadvantages and compare them to alternative solutions already in place (both from a technical and an financial standpoint).

2.1 Anti-islanding

Islanding is a condition where a part of the power system, consisting of both loads and generation, becomes isolated from the rest of the power grid, and generators continue to energize the isolated network. [1] Two types of islanding can occur in a power system: intentional islanding or unintentional islanding. The former is performed for either maintenance or load-shedding purposes to protect the rest of the power grid and avoid a blackout, with the isolated generators operating in voltage and frequency control mode to provide constant voltage to local loads while maintaining the isolated grid frequency; the latter, instead, occurs due to equipment failure or severe faults resulting in the opening of circuit breakers that interconnect the island with the rest of the power system. Unintentional islanding may result in hazards in power system operation and may lead to safety risks for maintenance staff. In addition, during unintentional islanding, the isolated network suffers from significant voltage and frequency variations that can damage both loads and generators within the island. Furthermore, the autoreclosure of the tie line, which is a standard and automated procedure followed in case of temporary faults, results in out-of-phase and unsynchronized reclosing when the system is subject to unintentional islanding.

2.1.1 Unintentional islands detection

Almost real-time event detection is nowadays made possible thanks to Smart Grids and modern measurement technologies such as PMUs. For example, the Frequency monitoring NETwork (FNET) is a low cost and quickly deployable wide-area phasor measurement system at the distribution level, developed by researchers of the University of Tennessee. [2] It is a tool characterized by high dynamic accuracy and minimal installation costs that deploys a number of single-phase Phasor Measurement Units spread across the monitored area in order to collect voltage, angle and frequency measurements at distribution level. These measurements are then transmitted across the Internet to a central location, where they are used as starting data for one of two available detection methods: the Frequency Difference Method or the Change of Angle Difference Method.

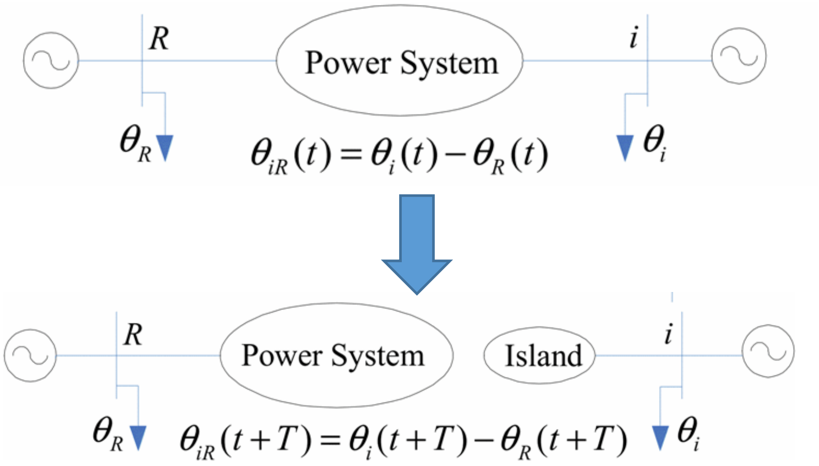
R
Power System
i
θ_R
$\theta_{iR}(t)=\theta_i(t)-\theta_R(t)$
θ_i
R
Power System
Island
i
θ_R
$\theta_{iR}(t+T)=\theta_i(t+T)-\theta_R(t+T)$
θ_i

Figure 10 A simple example of islanding event for a two-bus system.

Figure 10 shows an electric system before and after an islanding event. Voltage angles θ_R and θ_i are collected at both nodes at time *t* and *t*+*T*, as well as frequency measurements f_i and f_R, then the data is sent to operational centers for elaboration.

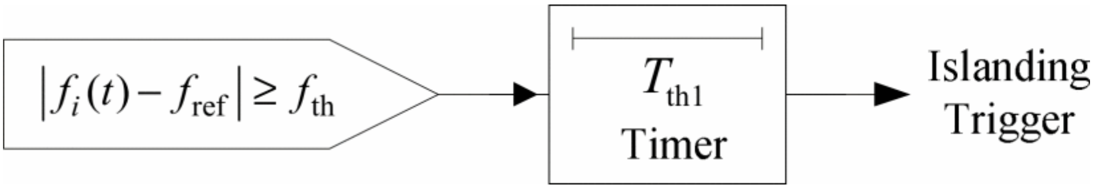

Figure 11 Frequency difference method block scheme.

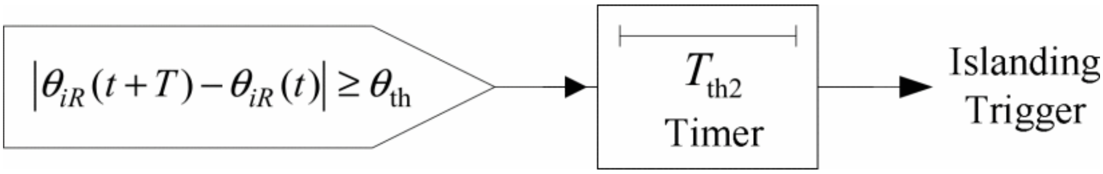
$|\theta_{iR}(t+T) - \theta_{iR}(t)| \geq \theta_{\text{th}}$
T_{th2}
Timer
Islanding
Trigger

Figure 12 Change of angle difference method block scheme.

Figure 11 and Figure 12 are graphical representations of the algorithms used in the data center to process information incoming from the PMUs in order to detect a case of islanding.

Figure 11 is relative to the “Frequency difference method”, that operates the difference between the measured frequency $f_i(t)$ and a reference value f_{ref} . f_{ref} is usually obtained as the median of all the frequency measurements collected at the same time instant t. The obtained value is then compared to a threshold f_{th}: if the threshold is violated for more than T_{th1} seconds, then an islanding alarm is triggered and appropriate control commands are sent.

Figure 12 is relative to the “Angle difference method”, that computes $\theta i_R(t+T)$, the difference between θ_R and θ_i for each instant of time. This value is then compared with the value obtained in the previous measurement interval $\theta i_R(t)$: if the difference between the two is higher or equal to the threshold θth for more than T_{th1} seconds, then an islanding alarm is triggered and appropriate control commands are sent.

During tests on six case studies, both methods proved to be effective in detecting islanding events while simultaneously successfully ignoring load shedding or generators’ tripping events. However, experience on the field proved the change of angle difference method to be more performing.

2.1.2 Island management

Synchrophasor technology can be employed to detect both unwanted islanding events, as previously explained, and to prevent them. But a third possibility is explored by Riga Technical University’s researchers, and that is active unwanted islands management. [3] Small portions of the distribution grid that are suddenly shifted to an islanded condition can in fact be managed as autonomous microgrids, given the presence of three fundamental elements: a PMU-enabled wide-area measurement system, an efficient communication framework already in place and DG-side actuators able to receive and implement orders from a centralized control room. Distributed generators whose communications are not cut off by the islanding phenomenon can in fact balance their output in response to the sudden event that caused it, thanks to the very fast readings of PMUs placed in the island itself. If suitably placed, the measurements of these devices can be elaborated by a remote control system that automatically computes the new production profiles that generators have to follow in order to maintain balance, or by a local intelligent device able to at least implement pre-determined algorithms selected as a function of the specific scenario.

Furthermore, these very same devices could be useful during the restoration phase. When the criticality that caused the creation of the island in the first place is solved, the open breaker must be closed with great caution since the island is still energized. This means that the voltage phasors may not be synchronized with those of the main grid and a sudden reclosure could lead to a plethora of negative consequences, ranging from temporary voltage instability to dangerous high currents. All this is made possible only thanks to the quick response of PMUs, that provide data at a rate high enough to react to fast dynamic events such as the creation of an unwanted island.

2.2 Phase identification

As service quality becomes a more important issue to engineers and regulators, the simple matter of phase identification becomes more important than it was decades ago. Having improper phase identification can lead to issues with load balance, fault location, metering and other reliability issues. However, even in case of relatively simple distribution junction – such as the one shown in Figure 13 –, it is clear that phase identification is not a trivial matter.

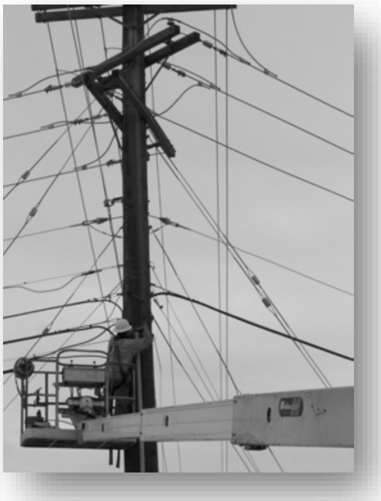

Figure 13 Dual feed and underground transition on distribution feeder.

While it is true that phase identification tools are already available to operators to use on the field, it is also true that employing a team of technicians every time phase information is needed often proves to be a waste of both time and money. PMUs could solve the problem, thanks to their unique angle measurement feature, but devices should be installed on a huge number of nodes and the cost/benefit ratio is definitely too high to justify such an investment. [4] However, if PMUs were to be deployed for different purposes, then the phase identification capability would be a very well welcomed side effect. Its advent would not only bring improvements to load balancing and fault detection, as already mentioned, but also be useful in the future when advanced tripping techniques – such as the adaptive multi-phase tripping or the single-phase tripping – will be implemented in the network control systems. Backfeeding automation schemes would also greatly benefit from this data, since to backfeed any portion of the distribution grid a well-timed closure of the end-switch is needed in order to avoid damages to the system.

2.3 Model validation

Network topology, that is the ensemble of data regarding lines and devices belonging to a portion of the distribution grid and their connection, is a fundamental piece of information for system operators. Not only grid management systems are easier to program and utilize when technicians have a clear and user-friendly virtual representation of the physical grid thanks to the information stored in dedicated databases, but also the automation itself would be impossible to be effectively implemented without a precise knowledge of every part of the system under control. Operators rely on system models to know how power flows will change as a result of manual or relay-initiated changes to topology – such as line tripping, capacitor bank insertion or generator starting. Accurate knowledge of the response of the grid in terms of energy flows as a result of topology variations is vital to both economic optimization and security of system assets.

Network characteristics, however, change with time. And if it is true that databases are periodically updated in order to provide the most accurate picture of the current status, it is also true that traditional inspection methods are not always reliable: assets aging, unrecorded switching and undetected capacitive insertions are only some of the elements that may turn an otherwise trustworthy network depiction into an unreliable, and therefore unusable, representation. Hence, a model validation tool would be needed in order to guarantee optimal and secure network management.

One way to guarantee the validity of a database-stored model is to frequently update its data with new information coming from the grid, but this is not always possible. Measurement of lines' impedances, for example, are not operated frequently; on the contrary, sometimes their virtual values are set when they are constructed and never changed thereafter. And even when changes are recorded with appropriate regularity, the scan output could still suffer from inaccuracies due to the slowness of legacy methods. To cope with these issues, a PMU-based wide area measurement system would be extremely useful, as will be proved by the following example of a fast line impedance value's update method. [5]

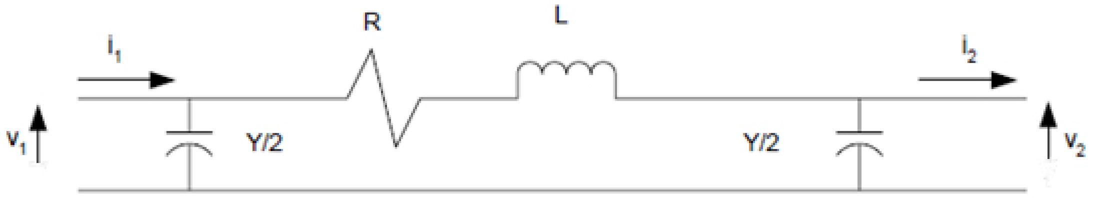

Figure 14 Simplified distribution line model.

Consider the two-bus system shown in Figure 14: the aim of said update method is the computation of the interconnecting line's electrical parameters, under the assumption of using a simple π-model to mathematically represent the link. Applying Kirchhoff's laws to the circuit in Figure 14:

$$\boldsymbol{I_1} = \boldsymbol{V_1} * \frac{\boldsymbol{Y}}{2} + \frac{(\boldsymbol{V_1} - \boldsymbol{V_2})}{\boldsymbol{Z}} \quad \text{Eq. 13}$$

$$\boldsymbol{I_2} = \frac{(\boldsymbol{V_1} - \boldsymbol{V_2})}{\boldsymbol{Z}} - \boldsymbol{V_2} * \frac{\boldsymbol{Y}}{2} \quad \text{Eq. 14}$$

Where both currents I1 and I2 and voltages V1 and V2 are measured bus phasor quantities, and both Z and Y are complex line parameters that can be written as:

$$\boldsymbol{Z} = R + j\omega L \quad \text{Eq. 15}$$

$$\boldsymbol{Y} = G + j\omega C \quad \text{Eq. 16}$$

Where Z is the line's impedance, Y is its admittance, R and G are its resistance and conductance respectively, L and C its inductance and capacitance, and ω is the angular frequency that can also be expressed as 2πf.

The system of equations made by Eq. 13 and Eq. 14 can be solved for the line constants as follows: (G is considered small enough to be negligible)

$$\boldsymbol{Z} = \frac{\boldsymbol{V_1^2} - \boldsymbol{V_2^2}}{\boldsymbol{I_1}\boldsymbol{V_2} + \boldsymbol{I_2}\boldsymbol{V_1}} \quad \text{Eq. 17}$$

$$R = Re(\boldsymbol{Z}) \quad \text{Eq. 18}$$

$$L = Im(\boldsymbol{Z})/2\pi f \qquad \text{Eq. 19}$$

$$\boldsymbol{Y} = 2 \cdot \frac{\boldsymbol{I_1} - \boldsymbol{I_2}}{\boldsymbol{V_1} + \boldsymbol{V_2}} \qquad \text{Eq. 20}$$

$$C = Im(\boldsymbol{Y})/2\pi f \qquad \text{Eq. 21}$$

All these equations existed before synchrophasors, so why would they be needed in order to effectively execute the model validation algorithm? It is a matter of data availability: in order to give out meaningful results, the processors need to elaborate voltage and current inputs that have been measured at the exact same point in time; the busses could be however very distant from a topological perspective, so it proved difficult for their measurement devices to have the same time reference. Phasor Measurement Units now provide, thanks to the GPS-delivered high precision clock signal, the correct time labeling to every data packet set to data center, so that calculations such as the previous one can finally be run properly.

2.4 Low frequency oscillations detection

This phenomenon traditionally affected transmission networks only, since low frequency oscillations of some grid parameters (e.g. rotor speed→ rotor angle δ → generators' power output) around their equilibrium point are caused by the presence of control systems – more and more intensively employed in modern networks – and variable loads. Additionally, in some occasions researchers witnessed seemingly spontaneous displays of this phenomenon: the reason behind this is still debated today, with someone indicating tripping in electrically remote locations as a possible indirect cause, and others instead pointing out similar but different small disturbances.

While it is true that up until now this has been of concern to transmission operators only, it is also undeniable that the evolution of distribution systems from passive to active networks is leading to an always more striking resemblance between the two typologies of grid. DG-induced dynamicity and the spread of control systems to lower voltage levels are the main causes for the propagation of such issues to a portion of the network that was traditionally exempt from them.

Damping systems with the specific purpose of solving this problem have already been developed, even if some of them are still prototypes, but their employment has been prevented by a lack of data coming from the field: this is where PMUs come in, with their higher-than-standard data rate. Since legacy measurement systems proved to be too slow to observe dynamic phenomena such as these – confusing them for normal power fluctuations or not detecting them at all –, high-resolution data provided by advanced WAMS may be the key to improvement in this field. The use of control solutions to avoid instability issues, since underdamped oscillations could lead to system collapse, will finally be possible.

2.5 Parallel bus voltage monitoring

Figure 15 shows an example of two distribution busses (bold vertical lines) connected in parallel at the same time. In normal operating conditions this network setup is quite rare and most of the times only temporary in the Italian distribution system, since MV networks are meshed but managed radially. However, today this configuration is typical of post-backfeeding restoration phases and could, in a not distant future, become more frequent in case of an evolution of the grid management philosophy towards a meshed-oriented approach. [6]

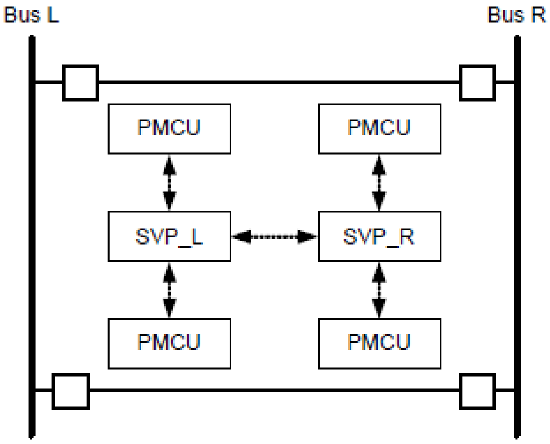

Figure 15 Two-bus distribution system example.

Phasor Measurement and Control Units (PMCUs) are advanced PMUs, capable of implementing basic control algorithms if instructed to do so. These instructions could either come from data centers or from a local Synchrophasor Vector Processor (SVP), a device capable of collecting synchronous phasor measurements and logical inputs and then perform scalar/vector calculations. Its outputs that could either be data packets to send to the data center or commands to dispatch local automation. A simple SVP application could be collecting synchrophasors from two ends of a distribution line, comparing their voltage angles and issuing a warning to an operator if a threshold has been exceeded. The one presented here, however, is a little more advanced application, even if somewhat similar.

Voltage phasors at both ends of a distribution line should be identical when the two busses are connected in parallel, or at least close enough to avoid a useless, detrimental and undesired power flow between the two of them. Thanks to their communication capabilities, SVPs can share synchrophasors with each other and detect said voltage discrepancies.

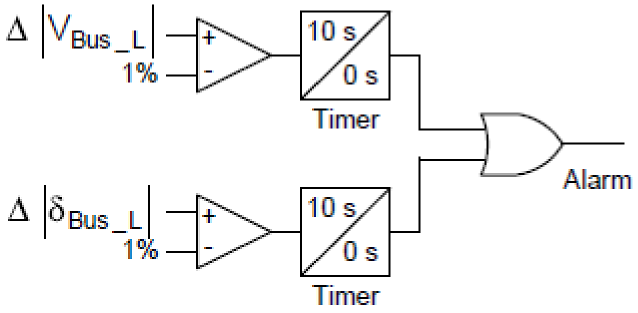

Figure 16 Bus voltage monitoring system.

Each SVP can implement the logic shown in Figure 16. That, in particular, demonstrates how the device placed on Bus L can evaluate the voltage phasors' difference in terms of both magnitude and phase: if one of the two differences exceeds a 1% threshold, then an alarm signal is sent to the data center, where a suitable remedial will be elaborated. Using a similar configuration at the remote bus, SVP_R can perform the same monitoring function: this guarantees a high degree of reliability for this function, due to the redundancy.

Data exchange between SVP also allows for an additional measurement quality check, such as the one described by Eq. 22:

$$\boldsymbol{V_{Bus\_L}} = \boldsymbol{V_{Bus\_R}} + \boldsymbol{Z} * \boldsymbol{V_{Bus\_L}} \qquad \text{Eq. 22}$$

Using synchrophasor information communicated by Bus R, the SVP can calculate the expected value of Bus L's voltage and compare it to the value sent to him by Bus L itself, effectively validating the measurements coming from both devices. This overlapping check procedure is a tool that cannot be available to operators without having synchrophasors at their disposal.

2.6 State Estimation (SE)

The condition of a power system can be determined if the model of the network and the phasor voltages at all busses are known. All this data put together, in fact, leads to a precise knowledge of current flows and thus active power, reactive power and losses. Unfortunately, however, the SCADA system does not provide voltage phasors, but voltage magnitudes alone: therefore, voltage angles have to be computed from measured magnitudes and active/reactive injections at every bus. Figure 17 clearly explains this situation.

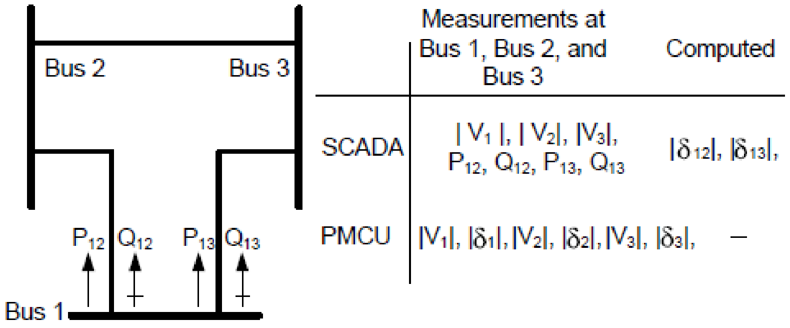

	Measurements at Bus 1, Bus 2, and Bus 3	Computed
SCADA	$\lvert V_1 \rvert, \lvert V_2 \rvert, \lvert V_3 \rvert,$ $P_{12}, Q_{12}, P_{13}, Q_{13}$	$\lvert \delta_{12} \rvert, \lvert \delta_{13} \rvert,$
PMCU	$\lvert V_1 \rvert, \lvert \delta_1 \rvert, \lvert V_2 \rvert, \lvert \delta_2 \rvert, \lvert V_3 \rvert, \lvert \delta_3 \rvert,$	–

Figure 17 SCADA and SVP direct state measurements.

When voltage/power data from one or more busses is missing, it has to be replaced by pseudo-measurement (historically coherent data) or “guessed” through a DSSE run. This procedure contributes to error propagation, for many different reasons: possible inaccuracies in the parameters that constitute the admittance matrix used by the algorithm to model the grid, communication errors or misrepresentation of the network due to the fact that the measurements are not taken simultaneously. [7]

Using PMUs as data gathering tools solves most of the above-mentioned issues, and this is particularly true for the last one. Data collected over a period of few seconds – as it is usual with SCADA measurements – could be used to represent a merged version of two different physical systems if a fast event, such as the operation of a breaker, were to happen in the middle of the scan. [6] When the power system state is changing quickly, measurements taken in a single SCADA scan are inconsistent. The key to avoid such a problem is the superior scan rate of PMU-based wide-area measurement systems: traditional state estimators can fail to converge if the system state is changing faster than the chosen tool’s scan rate, but this time-skew source of error is eliminated by the PMU technologies. Additionally, synchrophasors get rid of the need for active and reactive power measurements: the data concentrator collects and directly elaborates phasor information from all the devices scattered on the observed grid, deriving any other wanted electrical data from it.

However, despite being advantageous under so many aspects, PMU-based distribution system state estimators are still rarely adopted by DSOs. The reason behind such a choice is not related to the technical maturity of the measurement devices *per se* – those are already highly efficient and fast –, but rather to the scarce level of development of a suitable telecommunication infrastructure. Economical causes do exist, as for example the financial burden that a complete replacement of the SCADA system would place on the taxpayers’ shoulders, but plans for a gradual evolution tend to mitigate them. The idea is to incorporate phasor data into the already existing state estimation algorithms, re-writing portion of the code in order for the estimators to accept the new data format and adapt it to the pre-existing scalar computational environment.

This is called “single-stage SE approach”, as opposed to the “two-stage SE approach” that instead has two separated calculation steps to keep the different data sets apart. The first one is more difficult to design (i.e. more expensive) but more performing, while the second one is less effective – since phasor data is only used to validate the results obtained through the use of SCADA measurements in the first step – but definitely cheaper. Both solutions, however, have common advantages with respect to the plain old SCADA state estimator in terms of resolution, redundancy, precision and the possibility of real-time monitoring. These benefits come with downsides: the cost of a significantly increased computational burden, the need to deal with the so-called “data tsunami” issue (i.e. both hardware and software portions of the state estimator need to be able to manage the increased data rate of PMU systems) and the necessity to somehow synchronize time-stamped and not-time-stamped data for it to be meaningful.

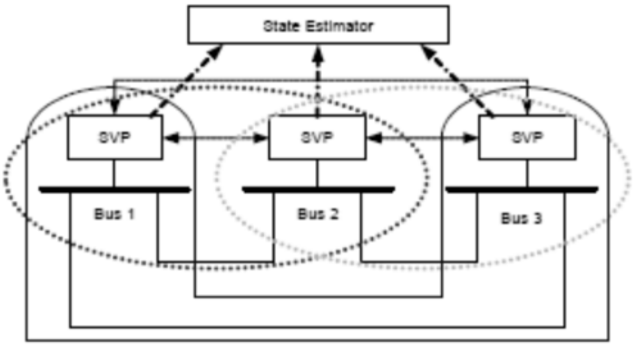

Figure 18 SVP peer-to-peer communication.

Further advantages of PMU-based DSSEs come from the capability of SVPs to implement peer-to-peer communication among themselves, allowing for additional features such as data redundancy and initial validation. As Figure 18 shows, SVPs gather information from PMUs under their responsibility (in the example, all those connected to a certain bus) and send them both to the data center where the estimator is located and to a number of adjacent devices in order to store voltage, current, associated phase angles and bus topologies in order to provide backup communication paths to the state estimator in the event that the primary communication link becomes disabled. Should the communication channel between an SVP and the state estimator fail, in fact, an adjacent SVP could forward the data, keeping the state estimator running.

Another viable approach is that of local data collection and on-site validation. The communication infrastructure needed for this application is a little more complex than the one shown before, and it is depicted in Figure 19. Bus SVPs belonging to the same local area all exchange synchrophasors with each other, but also forward them to a special concentrator appointed as the main one in that area. This special SVP has advanced computational capabilities, enough to allow a local-area state estimation and send the results to the wide-state estimator, all in order to reduce the computational burden on the centralized servers. Moreover, running local SEs can lead to topology discrepancies detection (e.g. wrong breaker status exposed thanks to current measurement) in the early stages of the estimation procedure, and this contributes to the reduction of the non-convergence risk in the main SE run.

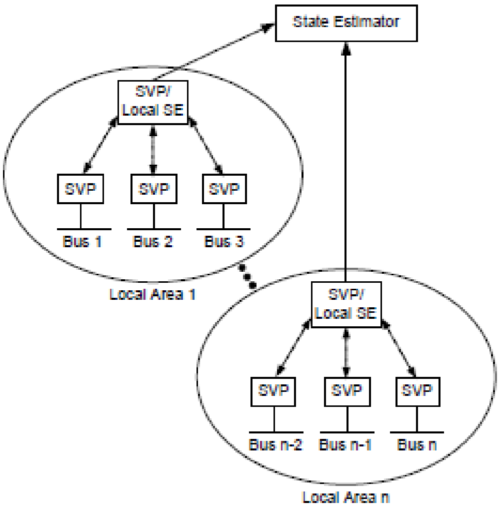

Figure 19 SVP local-area state estimation.

2.7 Real time monitoring and Remedial Action Schemes (RAS)

System monitoring, as already mentioned before, is the aspect of grid management that would benefit the most from the introduction of a PMU-based WAMS. As clearly shown by the example of Figure 18, PMU data reveal dynamic behavior as the system response to disturbances, dynamics that would be otherwise hidden and ignored by the operators. In the example, the blue line shows a certain bus voltage magnitude sampled by the SCADA system every two minutes: it shows some fluctuations, but small enough not to trigger any alarm. The red curve, however, reveals how dangerous the situation about to unfold really is. Sampling the voltage at a much higher rate allowed exposing how its magnitude is not just varying: it is oscillating. This is symptomatic of a grid where two or more power plants are working out of frequency. In essence, when two power plants operate out of phase, the least powerful one acts as a load to the other, leading to an unwanted energy exchange that could potentially lead to lines and power devices overheating. Left undetected, this kind of situation could lead to very dangerous and harmful consequences. This is just one of many examples of how a better monitoring system can help grid engineers to be aware of the health state of their network and make better-informed decisions.

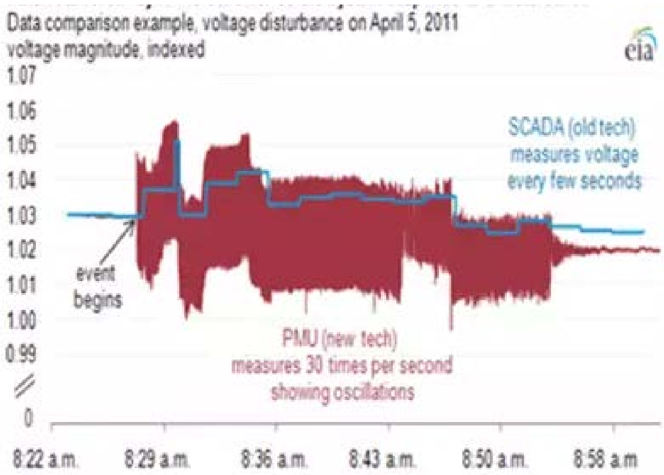

Figure 20 Voltage oscillations detected by a PMU and ignored by older equipment.

It has been proved [9] that PMUs can contribute the most to distribution network analysis when installed on the MV side of the primary substations. This is true because HV-side installed devices are able to detect only global disturbances, such as frequency drops caused by the loss of a big generator connected to the transmission network, whereas MV-side ones can also observe local issues, for example voltage fluctuations. An advanced monitoring system, one that makes use of modern Distribution System State Estimation (DSSE) techniques, is the foundation for a number of related power system automation solutions: selective and cost-efficient load shedding and demand response, mainly concerning the user, or Remedial Action Schemes (RAS) implementation, regarding the DSO.

"A RAS is a scheme designed to detect predetermined system conditions and automatically take corrective actions that include generation tripping, load curtailing, system reconfiguration, ..." [8]. Once it receives quasi-real time data from PDCs, the centralized automation intelligence can implement pre-made solutions as a response to specific scenarios, if those happen to arise. For example, consider an overflow event on a line caused by a local production/demand excess: there could be a RAS dedicated to this contingency, capable of enacting remedial actions such as local voltage control implemented by sending command signals to local generators or capacitor banks. The purpose of these schemes is to guarantee the system stability, maintaining voltage and power flow levels inside the defined boundaries and avoiding the propagation of disturbances, which could possibly lead to a disastrous cascading escalation.

2.8 Post-event analysis

Network condition's analysis post relevant events (e.g. a fault) is a procedure traditionally run via SCADA system to assess the causes and the consequences of such an accident, in order to elaborate appropriate strategies for system restoration and prevent it from happening again in the future. Legacy method are already quite effective, however the introduction of PMUs could boost post-event analysis efficiency thanks to synchrophasors' superior data resolution: a more accurate post-mortem analysis is very likely to lead to a more specific and fast resolution of the original issue. However, while it is true that having a great amount of information available is often a positive news for operator, it also brings two negative consequences: the need for both a suitable data storage system and a fast and efficient data-mining algorithm. Both this conditions mean additional costs for the grid operator.

A fast and detailed analysis can help, for example, ensuring a safe system restoration to its pre-event status, thanks to the possibility to assess the network parameters immediately after the destructive occurrence. Continuous monitoring allows for the detection of abnormal system conditions that would prevent a correct restoration by regular means: the presence of power oscillations after a fault, for example, would go undetected by the SCADA system; this could lead to instability and, in extreme cases, to grid collapse after incautious breaker reclosure. Knowledge about the real state of the network post-event will then be vital to elaborate alternative restoration procedures to solve the issue.

2.9 Fault management

Phasor measurement units can enhance the effectiveness of many fault-related automated operations, dedicated to both network and users' protection. In particular, there are four categories in which the topic can be subdivided: fault prevention, fault detection, fault localization and fault resolution. For each of them an application example will be described, among many possible ones that are currently under research.

2.9.1 Fault prevention

On August 14th 2003, 50 million people across Ontario and eight northeastern U.S. states lost electric power. [9] The combination of a hot afternoon and an unexpected breakdown of a coal-fired generating station near Cleveland set off a chain reaction that within 94 minutes left most of northeastern America in the dark. It took more than 24 hours to get power restored to most parts of the power grid, and fully restoring production capacity to meet demand in the region took almost two weeks. It will be remembered as The Great Blackout of 2003.

It came as a surprise to most grid operators that a seemingly innocent event far away could cause the entire power grid to collapse. A situation in Cleveland was allowed to go undetected for just over 90 minutes when transmission lines were operating close to maximum capacity. The hot summer air was generating high demand for electric energy to power air conditioners across the region. When a coal-fired generating station went offline, a local transmission line overloaded, causing the wires of the line to extend and sink towards the ground. When the line touched a tree that had been allowed to grow below the transmission line, the line short-circuited to ground, causing the automatic circuit protection to break. This put more stress on the remaining lines. One hour later, three other lines failed, and a catastrophic surge of electric power rushed in through the remaining lines in Ohio, triggering several other circuit breakers. As the remaining transmission lines had insufficient capacity to carry the required energy across the region, the entire grid collapsed within 90 seconds. This left consumers without electrical energy. Unable to deliver the energy they were generating, several nuclear power plants were forced to follow emergency procedures and shut down their nuclear reactors, causing harm to the nuclear reactors. It took almost four days to restore power on the grid, and nearly two weeks to bring all reactors back up to full capacity.

An investigation of The Great Blackout revealed that the power grid control systems were outdated and largely unable to monitor and protect the health of the grid. Time was never an issue. It took 31 minutes from the moment the Cleveland power station failed until the first transmission line collapsed. The situation looked manageable for another 61 minutes, until more transmission lines started burning out. The men and women controlling the grid were caught completely off guard because they had no means to detect warning signals from the power grid. Without access to real time information, the power grid control rooms were unable to predict where the next error would occur and plan corrective actions. The investigation concluded that the disaster could have been avoided if the power grid had been equipped with better monitoring systems. The U.S. Department of Energy considers the US-Canada blackout in 2003 to be the single most important motivator behind the Smart Grid initiative.

2.9.2 Fault detection

It is fairly easy to detect fault events most of the times, since the majority of them is characterized by high values of current magnitudes. The detection method, in these cases, is both effective and straightforward: overcurrent relays are triggered by these exceptionally abundant flows and are disposed of when protections trip, after a suitably short set time. There are occasions, however, in which this simple system cannot guarantee timely response to a fault event, thus potentially leading to harmful consequences for both people and equipment's safety. One of such cases is, for example, a high impedance fault. (HIF)

Table 1 Typical current levels for MV HIFs.

Surface	Current (A)
Dry asphalt	0
Dry sand	0
Concrete (non-reinforced)	0
Wet sand	15
Dry sod	20
Dry grass	25
Wet sod	40
Wet grass	50
Concrete (reinforced)	75

High impedance faults usually happen when an energized conductor comes in contact with a quasi-insulating object such as a tree, structure or equipment, or falls to the ground (typical current values relative to a number of these cases are shown above in Table 1). The significance of these previously undetectable faults is that they represent a serious public hazard as well as a risk of arcing ignition of fires. This occurrence is rare but very dangerous, so the operators have to resort to alternative detection methods in order to assure well-timed resolutive actions. Mechanical HIF detection methods have been tested for decades now and proved to be relatively effective, but their susceptibility to adverse weather conditions (ice, wind, tree growth) and installation costs prevented their employment. A simple example is that of a pole-mounted device placed below the line to protect and connected to ground through a low impedance: in case of conductor downing, a spring inside the device is released and it ejects a bus bar that makes contact with the conductor and allows the flow of a current high enough for the relays to detect the fault and act on the breakers. Electrical HIF detection methods have been object of study, but none succeeded in becoming widely spread among grid operators.

Recent advances in PMU technologies have enabled alternative solutions that are not only capable of detecting these faults, but that can also trip the affected circuit section in the narrow time window between the moment of the break and the time the conductor hits the ground. The affected circuit section is de-energized while the conductor is still falling, eliminating the risk of an arcing ground fault or energized circuits on the ground. Three different methods have been developed to achieve this goal: the dV/dt detection method, the Inverse and Zero Sequence Voltage Magnitude detection method and the Inverse and Zero Sequence Voltage Phase detection method. [10]

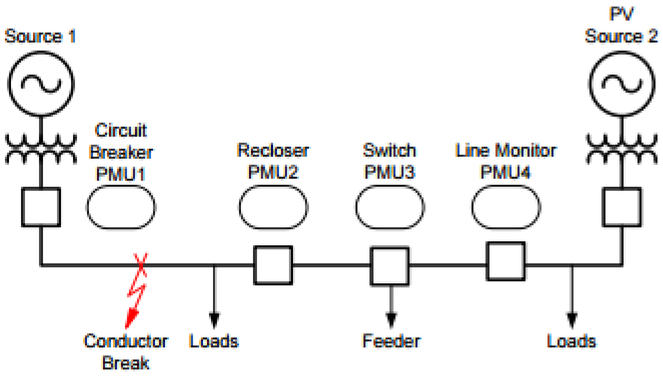

Figure 21 MV conductor break event example.

Figure 21 will be useful to briefly explain the working principle of the dV/dt detection method. In the example, two power sources supply the load on a MV feeder: source 1 is the HV network while source 2 is a PV plant connected at the end of the feeder itself. Both of them contribute to satisfy the power requirements of loads and sub-feeders, so current flows into them from both sides. In the case of a conductor break, as shown in the picture, the current supply from the left-hand side would be cut off. This not only implies a higher, possibly difficult to bear, generation burden requested to the PV plant, but also a change in the voltage profile along the line: on the left of the break it will rise, since there is no more current flowing there, and on the right it will drop due to the increase of power request from that side only. This will imply a very rapid change in voltage that PMUs installed along the line are able to detect: dV/dt measurements can be compared to set limits and the conductor break can be detected before the conductor itself reaches ground, avoiding any harmful circumstances. Some false positives, however, could results in case the application is experimented on highly dynamic distribution feeders.

2.9.3 Fault localization

Distribution lines faults are caused by different reasons (e.g. tree branches touching naked conductors, storms, birds) and they often result in mechanical damage to power lines that must be repaired before they return into service. Faulted lines must be located accurately to allow maintenance crews to arrive at the scene and repair the broke section as soon as possible. Since terrain conditions and overall geographical layout could cause some sections of power lines to be difficult to reach, the accuracy of fault location algorithms is an important requirement that must be guaranteed even when the system is operating under abnormal conditions. Generally, fast and accurate fault location will expedite supply restoration and enhance the supply quality and reliability. In addition, this will minimize the customer inconvenience. Therefore, fault location can be considered as one of the first functions to be integrated into modern control systems.

Varieties of fault-location algorithms have been developed and presented in the literature. Depending on the availability of the fault-locator input signals, fault location algorithms can be categorized as one-end, two-end and multiend. [11]

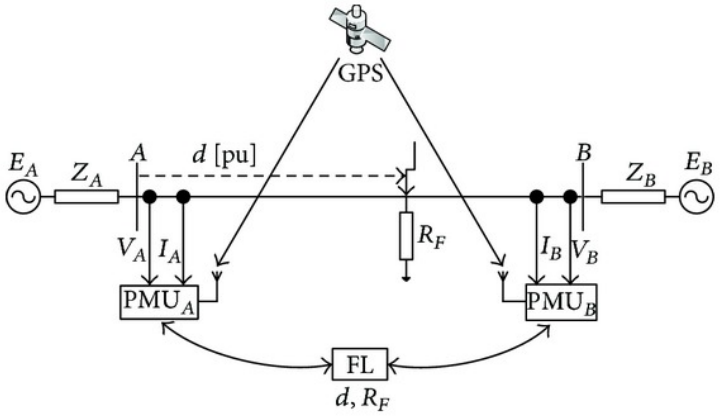

Figure 22 Two-ends synchronized fault-location arrangement.

The potential uses of subsecond GPS-synchronized phasor data collected from various locations within an electric power system promise endless benefits for the applications targeting reliable operation of electric power systems. [12] Various PMU-based fault location applications have been implemented in transmission and distribution grids, often merging information from PMUs, SCADA and nonoperational data to improve the effectiveness of alarm processing, accuracy of fault location and ability to detect cascades. Among them, two-end fault location algorithms have been proposed with the aim of overcoming the limitations of the one-end techniques and improving overall accuracy. A schematic diagram for this solution is shown in Figure 22.

There is a very high number of case-specific location algorithms based on two-end synchronized measurements, using either complete or incomplete two-end measurements. With the use of complete two-end measurements the three-phase voltages and currents are utilized. In case of incomplete two-end measurements, the following options are of interest:

i. three-phase voltages from both ends with three-phase current from only one end,
ii. three-phase currents from both ends with three-phase voltage from only one end,
iii. three-phase voltages from both ends.

Various fault location algorithms utilizing complete two-end synchronized measurements have been studied. Both iterative and noniterative methods have been proposed to locate faults on a single line. In the noniterative method, an analytical synchronization of the unsynchronized voltage and current measurements from two ends of a line is performed with use of the determined synchronization operator. Then, the synchronized measurements are used to calculate the distance to fault. Simultaneous usage of two kinds of symmetrical components for determining the synchronization operator makes the calculations simple and highly accurate.

2.9.4 Fault resolution

Once a fault has occurred and its location has been pinpointed, it needs to be extinguished in due time. Network protection systems effectively do so most of the times, but they can lack responsiveness during particular and rare events. Relay settings are, in fact, calibrated to trip the breakers under normal grid conditions and may prove to be inefficient in case of anomalies.

Adaptive relaying is a philosophy of protection design that provides for adjustments in protection settings and/or functions automatically, as grid conditions change. (e.g. Interface Protection Systems after Annex 70) The adoption of this kind of relaying is needed to ensure timely breaker operations not only under normal circumstances but also in case of those abnormalities (e.g. cascade tripping) to face which they lack proper regulation, all leading to malfunction. Adaptive relays are already a reality, but in order to operate they need a high data rate stream coming from the network, a quasi-real-time information input that can only be supplied by special sensors placed on the observed grid, and PMUs for sure are suitable candidates.

The following list contains examples of grid operations enabled by the adaptive approach, which is not only exclusive to breakers tripping but also to more complex functionalities: [13]

- Intelligent load shedding: adoption of a smart management of load dropping schemes in emergencies, that allows to locate with precision which users to cut out in order to solve an unbalance instead of blindingly shedding pre-set blocks (or “aggregates”) of them without exactly knowing how power consumption is reduced by doing so. This approach avoids long load shed/generation trip iterative procedures to achieve balance, thus improving service power quality;
- Adaptive loss-of-field relaying: automatic setting correction for generators excitation current relays, that in unstable working conditions could happen to trip even when not supposed to;
- Oscillation damping controller: dynamic adjustments for oscillation damping systems’ (those already mentioned in section 2.4) parameters. These systems cannot, in fact, be rigid but need to adapt to different kinds of oscillation singularities that could occur.

2.10 Unmasking load behind net-metered DG

Measurements made at the customers' point of connection onto the grid can only be this useful, since they monitor a prosumer's net injection/withdrawal only. Separate data regarding load and production profiles would be of much more interest for system operators, since having it at their disposal would imply being able to prepare remedial actions for possible DG loss or rapid ramps, but also facilitate forecasting of net load by understanding its composition even when "masked" by generation.

In this predicament, PMU measurements might allow remote inference of load /DG ratio [14] without the need for customer-side access (which could be impossible or undesired for legal, technical or economic reasons), combining time series net load data with power quality measurements, that is an harmonic content analysis capable of obtaining a "fingerprint" typical of generation or load. (i.e. the load gives its specific harmonic contribution to the spectrum profile, in a way that – if properly analyzed – can unveil its hidden presence)

2.11 Reverse Power Flow (RPF) detection

Electrical networks are complex dynamic systems that need to be studied with specific tools. When an operator is interested in knowing magnitude and direction of power flows, the mathematical instruments to be used are called *load flow equations*. They can be written as follows:

$$P_i = V_i^2 Y_{ii} \cos\theta_{ii} + \sum_{j\neq i}^{n} V_i V_j Y_{ij} \cos(\delta_j - \delta_i + \theta_{ij}) \qquad \text{Eq. 23}$$

$$Q_i = V_i^2 Y_{ii} \sin\theta_{ii} + \sum_{j\neq i}^{n} V_i V_j Y_{ij} \sin(\delta_j - \delta_i + \theta_{ij}) \qquad \text{Eq. 24}$$

where:

- P_i is the net active power injection at the *i*-eth node of the network;
- Q_i is the net reactive power injection at the *i*-eth node of the network;
- V_i is the voltage magnitude of the *i*-eth node of the network;
- Y_{ii} is the magnitude of the element found at the intersection of the *i*-eth row and *i*-eth column in the network's bus admittance matrix;
- θ_{ii} is the angle of the the element found at the intersection of the *i*-eth row and *i*-eth column in the network's bus admittance matrix;
- V_j is the voltage magnitude of the *j*-eth node of the network;

- *Y_{ij}* is the magnitude of the element found at the intersection of the *i*-eth row and *j*-eth column in the network's bus admittance matrix;
- δ_j is the voltage angle of the *j*-eth node of the network;
- δ_i is the voltage angle of the *i*-eth node of the network.

When complex voltages for each node are not known variables, multiple iterative computational methods must be used in order to estimate them (since the power equations are not linear): the Gauss method and the Newton-Rhapson method are suitable examples. However, if node voltages are already known – as in the case shown in Figure 23, where real-time complex measurements are constantly taken by μPMUs –, then the apparent power flowing between two adjacent nodes can be directly computed:

$$\underline{\boldsymbol{S_{12}}} = \underline{\boldsymbol{V_1}}(\overline{\boldsymbol{Y_{11}V_1}} + \overline{\boldsymbol{Y_{12}V_2}}) \qquad \text{Eq. 25}$$

where:

- *S_{12}* is the complex power flowing from node 1 to node 2;
- *V_1* is the complex voltage of node 1;
- *V_2* is the complex voltage of node 2;
- *Y_{11}* is the element found at the intersection of the first row and first column in the network's bus admittance matrix;
- *Y_{12}* is the element found at the intersection of the first row and second column in the network's bus admittance matrix.

However, under some simplifying assumptions (all bus voltages equal to 1 p.u., negligible shunt parameters for lines and transformers and no losses), the active power flowing between two adjacent busses can be expressed as:

$$P_{12} = \frac{V_1V_2}{X_{12}}\sin(\delta_1 - \delta_2) \qquad \text{Eq. 26}$$

where:

- *P_{12}* is the complex power flowing from node 1 to node 2;
- *V_1* is the voltage magnitude of node 1;
- *V_2* is the voltage magnitude of node 2;
- *X_{12}* is the reactance of the line connecting the two nodes;
- δ_1 is the voltage angle of node 1;
- δ_2 is the voltage angle of node 2.

Under the generally realistic conditions that $V_1 \approx V_2$ and $\sin(\delta_1 - \delta_2) \approx (\delta_1 - \delta_2)$, Eq. 26 can be further simplified:

$$P_{12} = \frac{V_1^2}{X_{12}}(\delta_1 - \delta_2) \qquad \text{Eq. 27}$$

This equation points out the relationship between nodes' voltage angles and power flow on the branches connecting them. In particular, it is evident that active power will flow from the node with greatest angle to the one with the smallest, since it is their difference that defines the sign of mentioned power.

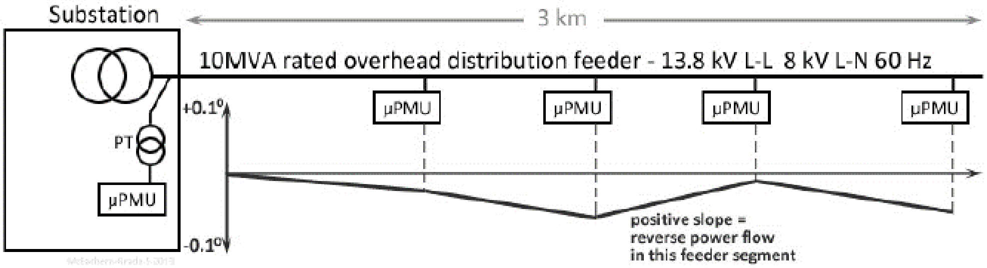

Figure 23 Reverse power flow detection on an MV feeder.

In conclusion, the installation of PMUs on distribution feeders could easily allow the detection of reverse power flow events, through the comparison of the voltage angles of subsequent nodes: if the δ angle is drawn as a function of the distance from the substation, like in the picture above, then it is sufficient to look at the slope of said function to find braches affected by reverse power flow where it becomes positive.

CHAPTER 3
PMU-BASED NETWORK MODEL VALIDATOR

After holding an exhaustive presentation on the above-mentioned PMU applications for the Italian MV grid at e-distribuzione’s Smart Grid Lab sited in Milan, in agreement with the local decisional board, one of the many proposed alternatives was selected to be studied more in depth. To be more specific, the choice fell on the development of a synchrophasor-based network model validator (as briefly described in section 2.3), its optimization in a simulated yet realistic medium voltage grid and subsequent testing with real equipment.

This study was carried out thanks to the availability of the Real Time Digital Simulator (RTDS), a powerful instrument at the Lab’s disposal capable of modeling the electric systems and its components and mimic its dynamics in real-time. The tool can in fact simulate complex networks’ responses in multiple scenarios, with both digital inputs coming from programmed elements and analog inputs from external devices. It can also elaborate said responses for analysis purposes or use them as output to be delivered to real devices, connected through suitable amplifiers, in order to test them as if they were actually placed on the field.

3.1 Real Time Digital Simulator

3.1.1 General premises

The following section is dedicated to the detailed description of the simulation tool used to perform the experiments described in the next paragraphs: the Real Time Digital Simulator. (RTDS)

"To simulate" means to develop a mathematical model that represents a physical existing system with the aid of modern informatics, and then analyze its behavior over time. During a simulation, time is intended as a variable that grows following a linear ramp. This ramp represents the time base to which any model implemented in the simulator will refer.

In general, the duration of a simulation depends on the computational power of the used calculator's processor. For instance, a very complex model in terms of number and intricacy of its defining equations will need a longer elaboration time with respect to a simpler model. In order to perform a real time simulation, therefore, the computer needs to be able to elaborate all the inputs and obtain the outputs as fast as the analyzed event evolves. This calls for very powerful processors, if the desired performance is meant to be optimal even when dealing with very fast transients occurring in complex models.

The main characteristic of the RTDS is that the simulator is able to work in real time, thanks to the extreme computational capability provided by its advanced hardware. It can in fact rapidly elaborate the mathematical models describing power systems up to a certain extension, giving outputs that realistically represent the real grid's conditions. Additionally, since the solution is in real time, the simulator can be directly connect to power and control system devices in order to study their interaction with the network where they are going to be installed even before the real installation. (very useful practice when, for example, protection equipment prototypes need to be tested in close-to-real scenarios, without neither risking damages to the grid nor lowering quality of service levels)

3.1.2 Hardware description

The Real Time Digital Simulator is a modular system produced by the homonymous Canadian company "RTDS Technologies®". It is composed of many units installed on a cabinet called "racks". The one present in the Smart Grid Lab is equipped with four of those racks, as can be seen in Figure 24.

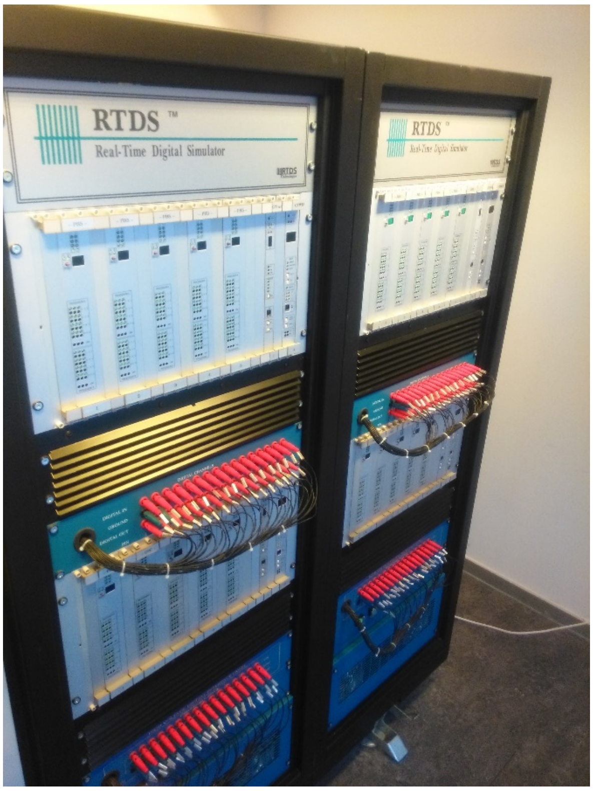

Figure 24 Real Time Digital Simulator (RTDS).

Each rack is composed by a number of elements: processor cards, analog and digital input/output cards, a power supply unit and a fire detection sensor for emergency shut-down. Processor electronic cards can be of two types: 3PC (Triple Processor Card) or GPC (Giga Processor Card). Every rack is equipped with three 3PCs and four GPCs. The two topologies differ in terms of computational capabilities and data transfer speed.

Every 3PC contains three DSPs (Digital Signal Processors) to simulate power and control devices thanks to the following technical characteristics:

- Clock speed: 40 MHz, equal to 40 MPS (Million instructions Per Second);
- Numeric format: 40 bits;
- Data transfer speed: 40 MB/s;
- RAM: 2 Mbit.

Every GPC, instead, contains two type RISC IBM Power PC processors with the following technical characteristics:

- Clock speed: 1 GHz, equal to 1 GFLOPS (FLoating point OPerations per Second);
- Numeric format: 64 bits;

- Level 1 Memory Cache: 32 kB for instructions and 32 kB for data;
- Level 2 Memory Cache: 1 MB.

Additionally, each rack has a WIF (Workstation InterFace) card installed to perform the following tasks:

- Backplane communication with the motherboard;
- Racks synchronization when simulations require the use of many of them;
- Communication between simulator and personal computer; (human-machine interface)
- Initial simulation state diagnostics.

Personal computers can be connected to the WIF card through a 10/100BASE T Ethernet interface directly using twisted cables (to eliminate electromagnetic interferences caused by external sources) or a HUB installed on a rack to guarantee simultaneous access to multiple computers.

3.1.3 Software description

The software used for programming the Real Time Digital Simulators and providing users with an intuitive interface is called “RSCAD”. Implemented in a Java environment, it is subdivided into different workspaces: two of them are HMI support tools used by the user to create and monitor (respectively) the network to experiment upon, and those are called “Draft” and “Runtime”; then a “C-Builder” section exists, allowing the user to build and test custom components to be added in the above-mentioned simulated network.

The Draft is a graphical interface through which the simulated grid’s layout and parameters can be set in order to prepare a wide variety of experiments. It has a library filled with both standard and custom components ready to be interconnected and configured. All the virtual devices can be divided into “power devices” or “control devices”: the former category includes elements such as resistors, inductors, transformers and electrical machines; the latter covers devices working with signals such as mathematical operators, logical blocks, measurement tools.

The Draft can be subdivided in separated graphical areas called “Subsystems”, each of them hosting an independent portion of the grid under analysis. A single Subsystem can be assigned to each rack, thus the RTDS in the Smart Grid Lab can manage to work with up to four Subsystems simultaneously.

The main limitation in terms of network simulation capabilities is that each rack has a maximum number of nodes that can be implemented in the Draft while building the grid's layout. For the RTDS a "node" is found in each point where a different potential can be measured. For instance, Figure 25 shows a basic electrical scheme – from left to right: three-phase 20 kV sinusoidal generator, 20/0.23 kV/kV D-Yn transformer, three-phase RLC load – made out of 7 nodes: the ground connections represent one, N1-N2-N3 is a triplet and so is N4-N5-N6.

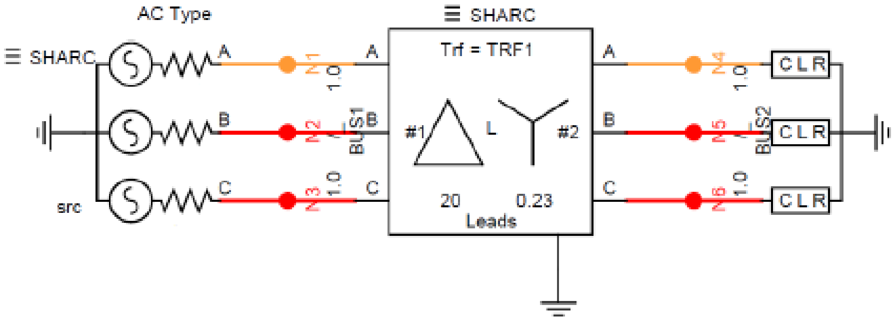

Figure 25 Small network represented through the use of the Draft functionality.

Every Subsystem can implement a network with 54 nodes at max. If the grid under test contains more than 54 nodes, then it is necessary to simulate it by using more racks in parallel.

There are two techniques in order to connect different subsystems: using a distributed parameters transmission line or decoupling transformers.

In the first case a line is chosen as the sole link between two adjacent separate portions of the network, as shown in Figure 26, under the condition of it being long enough for the waves propagating through it to reach the other side in a time interval longer than the computational time-step of the calculator. If that was not the case, in fact, the wave would reach the end of the line before the end of the source Subsystem's analysis, compromising the results.

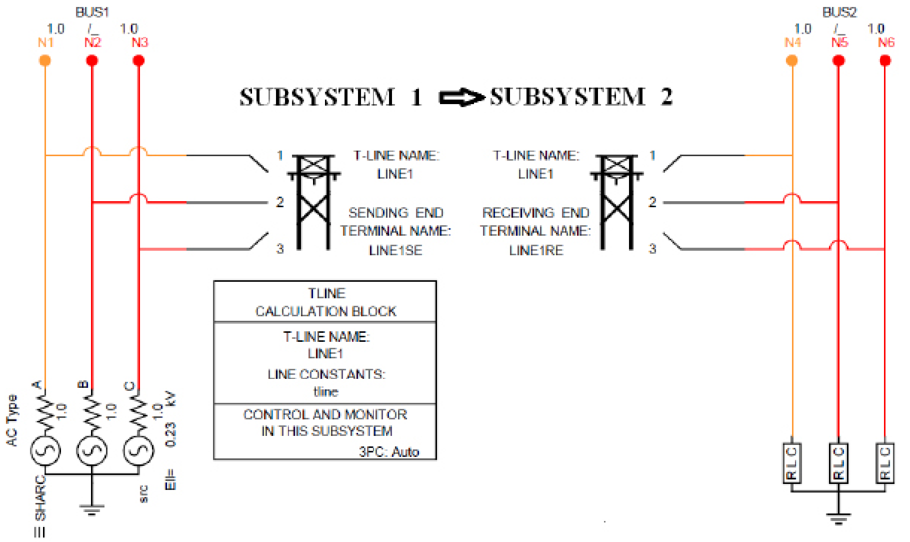

Figure 26 Separate Subsystem connected via transmission lines.

In the second case, the method that allows interaction between Subsystems is based on the use of decoupling transformers such as the ones shown in Figure 27. These blocks are no actual transformers, but rather an alternative to transmission lines (very similar in terms of internal logics too) with a small but important difference: while the transmission lines are selected among the existing ones in the real network and represented in the simulation with their own length and parameters (both series and shunt), decoupling transformers are virtual devices used in substitution to a chosen connection when the network lacks a line long enough to ensure proper communication between racks. Decoupling transformers' settings are in fact only partially subject to user modifications, since series parameters only can be changed: shunt capacitance is automatically set by the simulator in order to guarantee that the wave propagates from a rack to another in a time shorter than the computational time-step.

The per unit of length capacitance influence on the wave's propagation speed $\boldsymbol{v}$ is shown by Eq. 28:

$$\boldsymbol{v} = \frac{\mathbf{1}}{\sqrt{\boldsymbol{lc}}} \qquad \text{Eq. 28}$$

where:

- *l* is the per unit of length inductance of the line; [H/km]
- *c* is the per unit of length capacitance of the line. [F/km]

Since *l* is set by the user and thus fixed, the only parameter that can be adjusted automatically by the algorithm of the decoupling transformer is *c*.

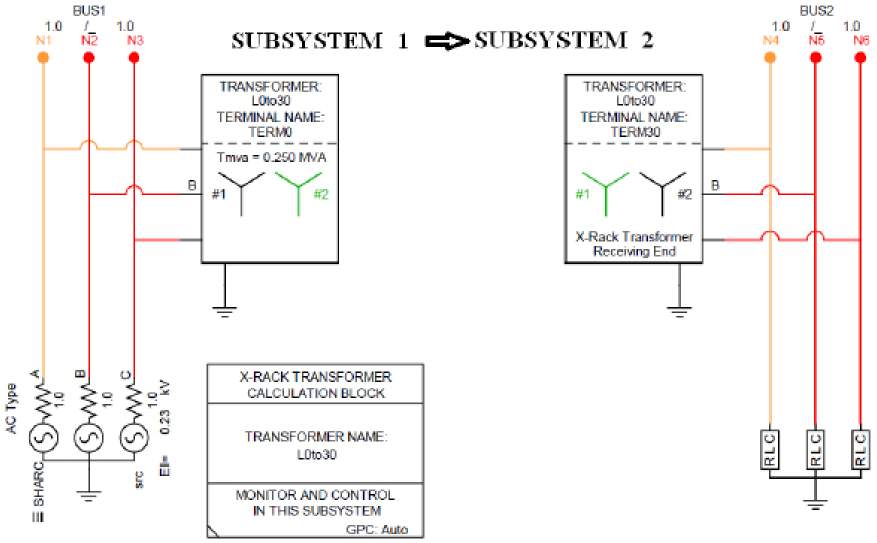

Figure 27 Separate Subsystem connected via decoupling transformers.

This is, of course, a solution that can negatively influence the accuracy of the final results. In order to avoid errors due to a wrong “propagation duration/time-step” ratio, in fact, a different kind of error is intentionally introduced: a difference between real and virtual shunt capacitance for the chosen connection line. Most of the times, however, the difference is so small that it fails to influence the final results, thus why this second solution is deemed acceptable.

The other two sections the RSCAD software is composed by are the Runtime and the C-Builder.

The Runtime is an interface that allows interactions during a simulation run between the user and the network drawn on the Draft, both in terms of inputs (e.g. breakers and sliders can be freely manipulated here) and outputs (e.g. any consequence of said manipulation can be monitored in real-time through a wide variety of meters and displays).

The C-Builder is a tool that gives the user the ability to modify any of the components’ models in the pre-loaded library and even create new ones. Many functions can thus be freely implemented in a project, and that is particularly needed in the case of this thesis since the RTDS’ library is mainly intended for HV networks. This lead to the creation of new components, fit for the MV environment: some of them for general purposes, some for this specific work.

Any element, created or modified, needs to be defined in terms of: expected inputs/outputs, block graphical form and code written in C language defining the role and function of that specific component.

3.1.4 Interface with external devices

The Real Time Digital Simulator can interact with external devices thanks to its input/output cards, both of analog and digital kind. They are listed and described as follows:

- GTAO (Gigabit Transceiver Analog Output) card;
- GTAI (Gigabit Transceiver Analog Input) card;
- GTDO (Gigabit Transceiver Digital Output) card;
- GTDI (Gigabit Transceiver Digital input) card;
- GTFPI (Gigabit Transceiver Front Panel Interface) card.

The GTAO card is capable of producing wide dynamic range analog outputs. Each GTAO card includes twelve 16 bits digital-to-analog converters (DAC) with ±10 V digital full scale, meaning that it can reproduce up to twelve independent analog signals. Each GTAO output channel can be assigned to a specific node voltage/branch current, that will be extrapolated from the simulation after being properly scaled (the scaling factor, “SF”, can be set through RSCAD).

If the desired output voltage/current needs to be higher than the ±10 V boundary, amplifiers will be needed.

The GTAI card is capable of external analog signals’ acquisition. It includes two 16 bits analog-to-digital converters (ADC) with 6 input channels each, meaning that twelve signals can be acquired at the same time. Every channel can work with differential signals, as well as single ended ones, in a range of ±10 V.

The GTDO card is capable of producing digital signals as outputs to feed to external digital devices. It is composed by 64 static switches, whose logic zero corresponds to an open contact while its one corresponds to a closed contact. The maximum voltage applicable to the switches is 24 V.

The GTDI card is capable of external digital signals’ acquisition. It is composed by 24 optically isolated digital input channels, whose state is verified once every 300 ns. Signal acquisition is performed thanks to LED-phototransistor coupling. The LED’s cathode is at reference voltage and, when a +5 V voltage is applied to its anode, a 10 mA current lights it up; the light travels to the phototransistor and causes its conduction, which corresponds to a logic 1.

The GTFPI is an input-output card connected to the front panels of the rack. On the rack there are two kind of front panels:

- Digital channels: 16 input channels and 16 output channels with a common reference. In order to have as input the logic state 1, it is necessary to short circuit a channel's terminals;
- High Voltage Digital Interface Panel: 16 digital output channels capable of providing signals whose voltage level can vary between 0 and 250 V. Typically the logical 1 within protections belongs to the 110 ÷ 220 V, so this panel can be used to connect and test protection devices.

Both panels are equipped with pin connections, represented in the Figure 28 and Figure 29. Every GPC card has two optical ports to which two independent groups of GTAO, GTAI, GTDO, GTDI and GTFPI cards can be connected in cascade. It is only possible to connect up to eight cards in any given order. The optical connection eliminates every possible electrical connection between the GPC processors and the other cards, granting the former protection from external short-circuits or overvoltages. The cascade connection previously mentioned is shown in Figure 30.

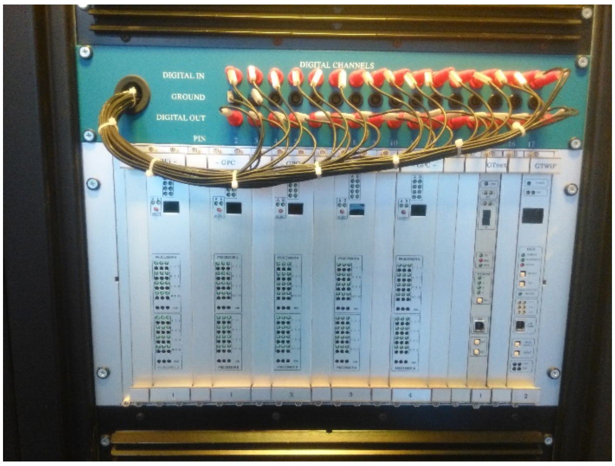

Figure 28 Digital channels input and output connections.

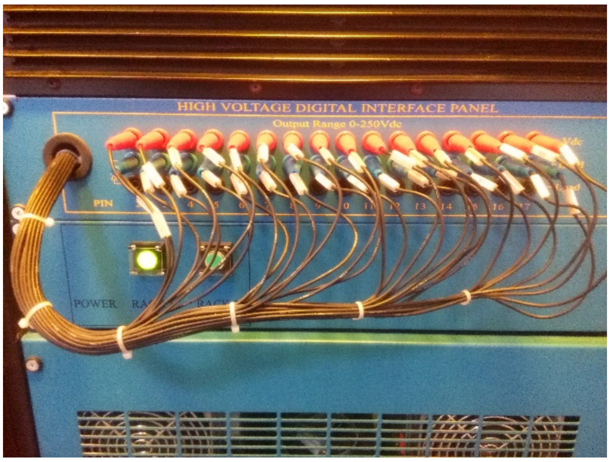

Figure 29 High Voltage Digital Interface Panel.

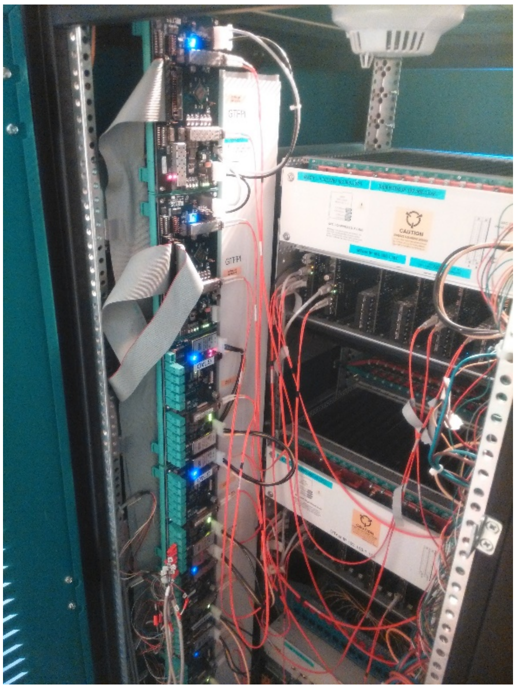

Figure 30 Input/output cards cascade connection.

3.1.5 Signal amplification

As previously mentioned, the maximum voltage that can be measured at the GTAO card's pins is ±10 V. This could pose a problem in the external devices' testing phase: if, for instance, there is an MV protection device under test, ±10 V is an inappropriate voltage range to test it. No realistic results could be extracted from such attempts, thus it is necessary to amplify the GTAO output signals in order for them to reach suited levels for the specific applications; this can be done using voltage amplifiers.

The same procedure is applicable to currents too, and it is even more true when considering protection devices, so voltage-driven current amplifiers are also needed.

Amplifiers built by the "Omicron" company were chosen in order to be able to amplify both kinds of signals: since three-phase systems are often the ones under analysis, these devices have three voltage outputs and three current outputs, independent of each other. Figure 31 shows the frontal panels of said amplifiers:

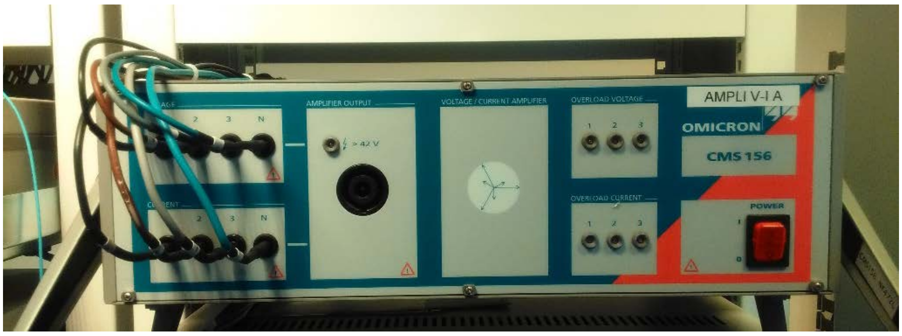

Figure 31 Omicron power amplifier.

Amplifiers are also useful when control and measurement signals need to be sent as input to external devices that would only accept them at certain voltage levels outside the ±10 V voltage range.

3.2 Network modeling and Validator development

The aim of this work, as previously mentioned, is the development and testing of a synchrophasor-based network model validator, an algorithm (from now on only referred to as “Validator”) capable of a precise estimation of the network’s parameters based on the quasi real-time measurements made by PMUs installed on strategic positions on the network.

In order to develop such a tool, some conditions are to be met. First of all, a suitable grid model needs to be available, with a full knowledge of its and all the connected devices’ electrical parameters. Then a simulation engine is needed, one able to rapidly solve the network and publish the required outputs in a fast and clear fashion. Last but not least, a software to compile and test the algorithm will complete the list.

Working with the RTDS, all the conditions are fully satisfied: the RSCAD software provides a rich library of components thanks to which any kind of network configurations can easily be arranged.

The Runtime section then allows to start the simulation, during which the network states are continuously updated following its inputs’ dynamics, and monitor the evolution of any chosen parameter in real-time. The user interface can be customized freely, based on the current test’s requirement: any network variable can be monitored through plots, meters, phasorial representations, etc. Some of them can also be controlled, for example load active and reactive power modulated using a slider or faults induced simply by pushing a button.

The C-Builder section is the programming tool that allows to create new components, compiled in C language, and make them interact with all the others already included in the simulation.

The first step in this experiment was the creation of a small MV network, far from being realistic in terms of extension but as similar as possible to real installations under any other aspect. The electrical scheme used is the one shown in Figure 32:

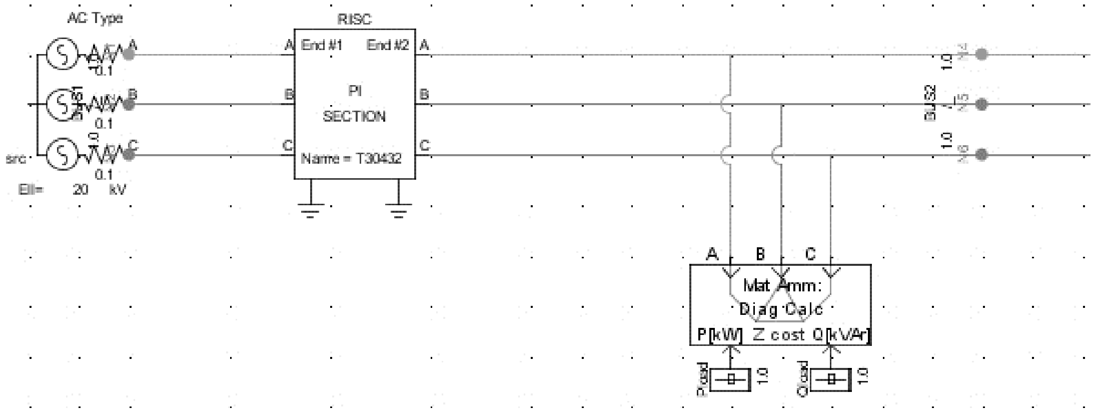

Figure 32 Simple test circuit built in the Draft section of the RSCAD software.

This simple circuit is composed by the following elements:

- An ideal 20 kV three-phase 50 Hz voltage generator, with three 0.1 ohm resistors in series to represent its internal resistance and no ground connection to follow e-distribuzione's policy on MV-side transformer grounding;
- A “PI Section” black box to a short distribution line with a condensed parameters sequence pi model, with the following known characteristics:
    - Positive sequence series resistance Rd=10.8420 Ω;
    - Positive sequence series inductive reactance X_Ld=2.5874 Ω;
    - Positive sequence shunt capacitive reactance X_Cd=75.224 kΩ;
    - Zero sequence series resistance Ro=28.2320 Ω;
    - Zero sequence series inductive reactance X_Lo=17.2920 Ω;
    - Zero sequence shunt capacitive reactance X_Co=75.224 kΩ.
- A three-phase balance delta load, with real-time controllable absorbed active and reactive power via the sliders placed below the block and in the Runtime section.

After a preliminary verification of the correct placement and parametrization of each of the installed elements, the Phasor Measurement Units were implemented. The presence of the ready-to-use component shown in Figure 33 in the pre-loaded library made easy this first approach, but in a more advanced stage it was eventually replaced for a more performing custom element.

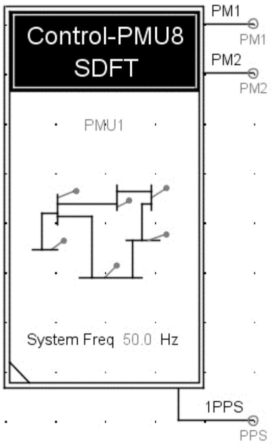

Figure 33 RTDS PMU-network simulator.

Even if the main objective of this thesis is to realize a tool capable of estimating the network parameters of a branched grid under normal working conditions, to start this work under such assumptions would have proved to be unnecessarily complex and harmful to the research itself. For this reason, it was decided that, during the first steps, only a single line would be considered as a test subject for the soon-to-come Validator tool. This is why such a small circuit was taken into consideration, and for the same reason the simulated PMUs – after a brief configuration phase – were placed right at the start and at the end of the line-block "T30432", simultaneously monitoring left-hand side and right-hand side voltage and current phasors.

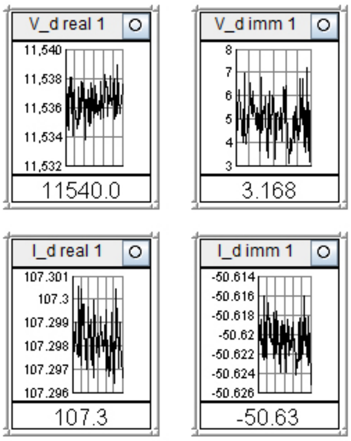

Figure 34 Runtime section monitoring system.

As Figure 34 doesn't fail to show, RSCAD's PMUs publish their outputs as real numbers only: real and imaginary part of the monitored complex quantity (in the picture the left bus direct sequence voltage $\mathbf{V_d1}$ and current $\mathbf{I_d1}$ are shown, in order not to fill the page with too many unnecessary images, but the actual amount of variables monitored by both PMUs goes up to a total of 16). This leads to the conclusion that both Eq. 17 and Eq. 20 – the formulas upon which the Validator is build, and whose proof is shown in Appendix A.1– have to be properly manipulated in order to be used in this context. Not only the PMU components do not produce complex synchrophasors as direct output, but the elements compiled in C using the C-Builder are not capable of complex calculation too. Because of this reasons, the equations have been modified accordingly:

$$\boldsymbol{Z} = \frac{\boldsymbol{V_1^2} - \boldsymbol{V_2^2}}{\boldsymbol{I_1}\boldsymbol{V_2} + \boldsymbol{I_2}\boldsymbol{V_1}} \qquad \text{Eq. 17}$$

$$\boldsymbol{Z} = \frac{(V_{1r} + jV_{1i})^2 - (V_{2r} + jV_{2i})^2}{(I_{1r} + jI_{1i})(V_{2r} + jV_{2i}) + (I_{2r} + jI_{2i})(V_{1r} + jV_{1i})} \qquad \text{Eq. 29}$$

$$\boldsymbol{Z} = \frac{V_{1r}^2 - V_{1i}^2 + j2V_{1r}V_{1i} - V_{2r}^2 + V_{2i}^2 - j2V_{2r}V_{2i}}{I_{1r}V_{2r} + j(I_{1r}V_{2i} + I_{1i}V_{2r}) - I_{1i}V_{2i} + I_{2r}V_{1i} + j(I_{2r}V_{1i} + I_{2i}V_{1r}) - I_{2i}V_{1i}} \qquad \text{Eq. 30}$$

$$\boldsymbol{Z} = \frac{(V_{1r}^2 - V_{1i}^2 - V_{2r}^2 + V_{2i}^2) + j2(V_{1r}V_{1i} - V_{2r}V_{2i})}{(I_{1r}V_{2r} - I_{1i}V_{2i} + I_{2r}V_{1i} - I_{2i}V_{1i}) + j(I_{1r}V_{2i} + I_{1i}V_{2r} + I_{2r}V_{1i} + I_{2i}V_{1r})} \qquad \text{Eq. 31}$$

The aim is to obtain an expression for **Z** that allows separate computation for real and imaginary part. In order to do so, Eq. 31 will first be simplified by means of terms substitution, then the complex numbers property shown by Eq. 33 will be applied.

The substitutions are the following:

- $a = (V_{1r}^2 - V_{1i}^2 - V_{2r}^2 + V_{2i}^2)$;
- $b = 2(V_{1r}V_{1i} - V_{2r}V_{2i})$;
- $c = (I_{1r}V_{2r} - I_{1i}V_{2i} + I_{2r}V_{1i} - I_{2i}V_{1i})$;
- $d = (I_{1r}V_{2i} + I_{1i}V_{2r} + I_{2r}V_{1i} + I_{2i}V_{1r})$.

Eq. 31 can be then rewritten as:

$$\boldsymbol{Z} = \frac{a + jb}{c + jd} \qquad \text{Eq. 32}$$

For complex numbers, it is true that:

$$\frac{a + jb}{c + jd} = \frac{(ac + bd) + j(bc - ad)}{c^2 + d^2} = \frac{(ac + bd)}{c^2 + d^2} + \frac{j(bc - ad)}{c^2 + d^2} \qquad \text{Eq. 33}$$

Once this is known, the extended formulation for **Z** can be written:

$$\boldsymbol{Z} = \frac{(V_{1r}^2 - V_{1i}^2 - V_{2r}^2 + V_{2i}^2)(I_{1r}V_{2r} - I_{1i}V_{2i} + I_{2r}V_{1i} - I_{2i}V_{1i})}{(I_{1r}V_{2r} - I_{1i}V_{2i} + I_{2r}V_{1i} - I_{2i}V_{1i})^2 + (I_{1r}V_{2i} + I_{1i}V_{2r} + I_{2r}V_{1i} + I_{2i}V_{1r})^2} +$$

$$\begin{aligned}&+\frac{2(V_{1r}V_{1i}-V_{2r}V_{2i})(I_{1r}V_{2i}+I_{1i}V_{2r}+I_{2r}V_{1i}+I_{2i}V_{1r})}{(I_{1r}V_{2r}-I_{1i}V_{2i}+I_{2r}V_{1i}-I_{2i}V_{1i})^2+(I_{1r}V_{2i}+I_{1i}V_{2r}+I_{2r}V_{1i}+I_{2i}V_{1r})^2}+\\&+\boldsymbol{j}(\frac{2(V_{1r}V_{1i}-V_{2r}V_{2i})(I_{1r}V_{2r}-I_{1i}V_{2i}+I_{2r}V_{1i}-I_{2i}V_{1i})}{(I_{1r}V_{2r}-I_{1i}V_{2i}+I_{2r}V_{1i}-I_{2i}V_{1i})^2+(I_{1r}V_{2i}+I_{1i}V_{2r}+I_{2r}V_{1i}+I_{2i}V_{1r})^2}+\\&-\frac{(V_{1r}^2-V_{1i}^2-V_{2r}^2+V_{2i}^2)(I_{1r}V_{2i}+I_{1i}V_{2r}+I_{2r}V_{1i}+I_{2i}V_{1r})}{(I_{1r}V_{2r}-I_{1i}V_{2i}+I_{2r}V_{1i}-I_{2i}V_{1i})^2+(I_{1r}V_{2i}+I_{1i}V_{2r}+I_{2r}V_{1i}+I_{2i}V_{1r})^2})\end{aligned} \qquad \text{Eq. 34}$$

The exact same reasoning can be applied to Eq. 20, leading to the following result:

$$\boldsymbol{Y}=2\cdot\frac{\boldsymbol{I_1}-\boldsymbol{I_2}}{\boldsymbol{V_1}+\boldsymbol{V_2}} \qquad \text{Eq. 20}$$

$$\boldsymbol{Y}=2\cdot\frac{(I_{1r}+jI_{1i})-(I_{2r}+jI_{2i})}{(V_{1r}+jV_{1i})+(V_{2r}+jV_{2i})} \qquad \text{Eq. 35}$$

$$\boldsymbol{Y}=2\cdot\frac{(I_{1r}-I_{2r})+j(I_{1i}-I_{2i})}{(V_{1r}+V_{2r})+j(V_{1i}+V_{2i})} \qquad \text{Eq. 36}$$

Defining the new substitution terms:

- $a'=(I_{1r}-I_{2r})$;
- $b'=(I_{1i}-I_{2i})$;
- $c'=(V_{1r}+V_{2r})$;
- $d'=(V_{1i}+V_{2i})$.

Using these new parameters in Eq. 33, we finally obtain:

$$\begin{aligned}\boldsymbol{Y}=2&\frac{(I_{1r}-I_{2r})(V_{1r}+V_{2r})+(I_{1i}-I_{2i})(V_{1i}+V_{2i})}{(V_{1r}+V_{2r})^2+(V_{1i}+V_{2i})^2}+\\+2j&\frac{(I_{1i}-I_{2i})(V_{1r}+V_{2r})-(I_{1r}-I_{2r})(V_{1i}+V_{2i})}{(V_{1r}+V_{2r})^2+(V_{1i}+V_{2i})^2}\end{aligned} \qquad \text{Eq. 37}$$

Both Eq. 34 and Eq. 37, written in a generic fashion, can be used to calculate the impedance/admittance of any of the sequences (positive, negative, zero), given the proper voltage and current measurements. Once applied, series resistance and inductive reactance and shunt capacitive reactance can be derived simply by isolation of the real/imaginary portion of the calculated impedance **Z** and admittance **Y**. Both equations were tested in MATLAB, comparing their results with the ones produced by Eq. 17 and Eq. 20 using the same inputs (see Appendix A.2 for the source code).

The results produced by both sets of equations, however, were interesting yet problematic:

- Positive sequence series resistance Rd= 10.7938 Ω; (-0.4% error)

- Positive sequence series inductive reactance X_Ld= 2.5664 Ω; (-0.8% error)
- Positive sequence shunt capacitive reactance X_Cd= 72.6130 kΩ; (-3.5% error)
- Zero sequence series resistance Ro= 6.481 kΩ; (+22856.2% error)
- Zero sequence series inductive reactance X_Lo= -1.5850 kΩ; (-9266.1% error)
- Zero sequence shunt capacitive reactance X_Co= -7.1810 kΩ. (-109.5% error)

While the positive sequence parameters were calculated with a high degree of precision, the same could not be said for the zero sequence ones. They were in fact clearly affected by some kind of issues that prevented the algorithm to obtain the correct values. After some in-depth analysis and tests involving simulated single-phase faults, it was concluded that the gross errors obtained were caused by a lack of zero sequence current, unable to circulate in such a small network. PMU measurements were, in particular, strongly affected by errors due to the currents' proximity to zero, and their oscillation around that same value. Simulating a single-line-to-ground fault, that is allowing zero sequence current to flow on the line, solved the issue:

- Positive sequence series resistance Rd= 10.8400 Ω; (-0.02% error)
- Positive sequence series inductive reactance X_Ld= 2.5880 Ω; (+0.02% error)
- Positive sequence shunt capacitive reactance X_Cd= 72.2200 kΩ; (-4.0% error)
- Zero sequence series resistance Ro= 28.2514 Ω; (+0.07% error)
- Zero sequence series inductive reactance X_Lo= 17.3125 Ω; (+0.12% error)
- Zero sequence shunt capacitive reactance X_Co= 75.2110 Ω. (-0.02% error)

Note that, in order to make the current flow during the fault simulation, a return path had to be created. This was done by connecting the generator's neutral point to ground. Even though this is no usual practice for a real MV distribution grid, it was needed for this specific test's sake. The ground connection was then removed.

The outcome of this last experiment revealed the need to carry out new ones in a different environment, a network model far more extensive and realistic. This evolution will be seen in sub-chapter 3.3, while this one will be instead closed with the description of another part of the development process, with a higher degree of priority: the creation of the first version of the Validator component (both in terms of aesthetic design and code creation in C language).

The creative process starts in the C-Builder section of RSCAD. Here, as shown in Figure 35, the user is first given the opportunity to decide the shape of the component (even though this will have no consequences on its performance whatsoever), the number and position of its input/output ports (respectively on the left/right) and the possible presence of any writings on it. In this case, the Validator assumed a rectangular shape in order to accommodate the high number of needed ports. In the simple case of two PMUs monitoring both sides of a line in order to calculate its positive and zero sequence parameters (the negative ones are of no interest for e-distribuzione), four synchrophasors will have to be collected from each of them (positive and zero sequence voltage, positive and zero sequence current); this means four complex numbers per PMU, eight in total in this situation (4*n* inputs in case of *n* PMUs considered).

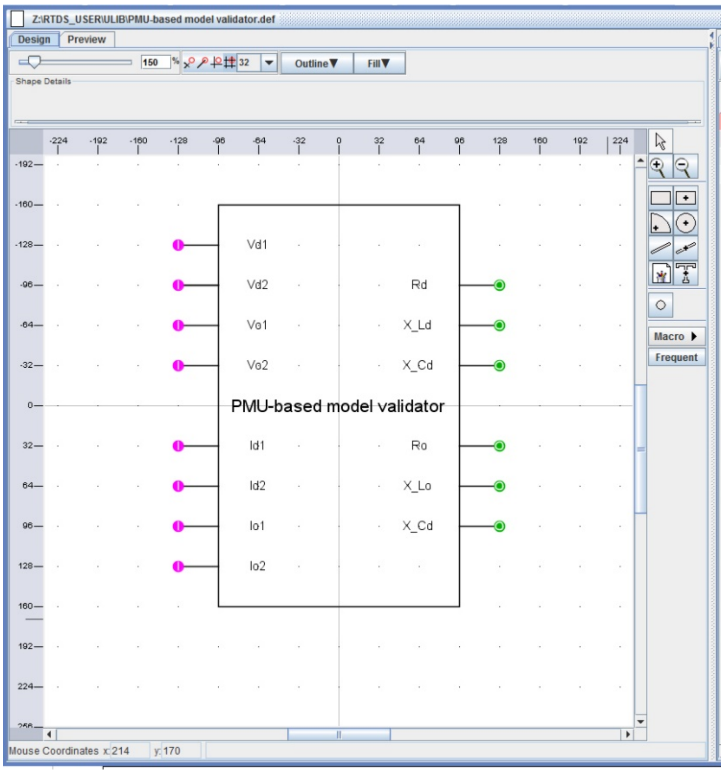

Figure 35 Design phase for the PMU-based model validator v. 1.0.

After a short configuration phase during which both inputs and outputs had to be preventively defined as integer/floating real/complex values (pink color for complex inputs/outputs, green for real ones), the code-writing phase followed. The finished product can be consulted in the Appendix A.3: more than one version of it is reported, in order to show the gradual optimization process it underwent.

The newborn component implemented in RSCAD the algorithm that was up until then run externally thanks to MATLAB, allowing not only a higher degree of precision (inputs were not imported by hand, being subject to approximation errors, but taken directly in-software) but also the possibility of real-time monitoring of the parameters under analysis. The tests run via MATLAB were in fact only instantaneous shoots, like pictures taken at a certain instant frozen in time, and that did not allow to appreciate potential variations in time (e.g. oscillations in the results). This was true in theory, however: in reality there was a major obstacle to the implementation of the Validator in the network, that is the lack of real-time inputs to feed it.

The PMU model found in the RSCAD library and used up until then, in fact, allowed only to monitor the measured quantities: their time evolution could be followed on the in-software meters, as well as their instantaneous value, but such data could not be in any way fed to another block in the Draft section. This of course proved to be more than a simple hindrance, since the whole point of these experiments is to develop a device capable of working in real-time, and the testing itself should be lead paying attention to potential dynamic disturbances' influences on the component.

Because of this problem, and many others involving the same standard component (e.g. limited amount of PMUs that can installed at the same time on a network), a decision was taken: the RSCAD component had to be abandoned, in favor of a custom one capable of producing usable synchrophasors. This custom component was previously created by the e-distribuzione R&D staff and is called "DV7203". As it can be seen in Figure 36, each DV7203 acts as a PMU, accepting 6 input quantities (i.e. three phase voltages and three line currents) and elaborating them to produce a variety of outputs: active and reactive power, line-to-line voltages, symmetric components, residual voltages and currents. Since the only quantities of interest for this work are the sequence component, the only relevant outputs are direct/zero sequence voltage and currents (the way this values are computed is shown in Appendix A.4).

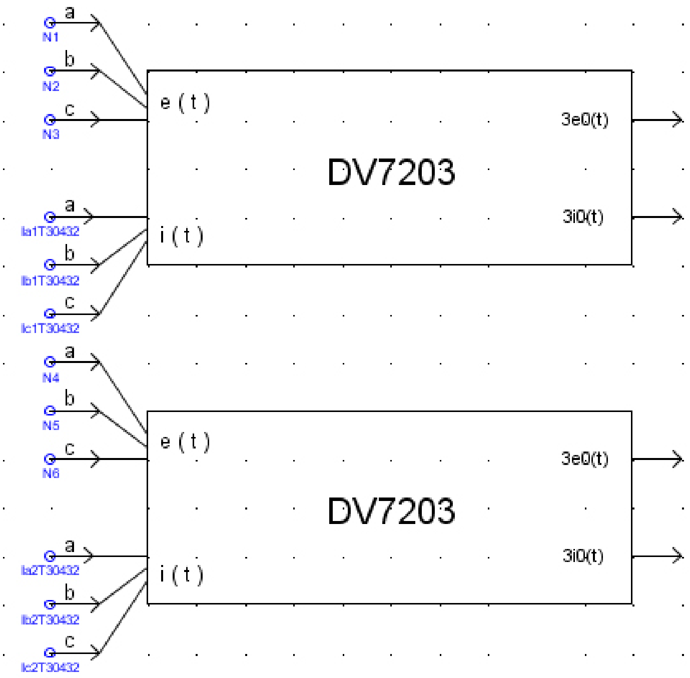

Figure 36 Two DV7203 components simulating two real PMUs placed on the grid.

The implemented DV7203 components produce, in this case, eight real numbers each: direct sequence voltage magnitude and phase, zero sequence voltage magnitude and phase, direct sequence voltage magnitude and phase, zero sequence voltage magnitude and phase. Since the output format could not be set differently, the Validator had to be modified in order to accept complex values no more, but magnitudes and phases instead. The new code for this second version of the component is shown in Appendix A.5.

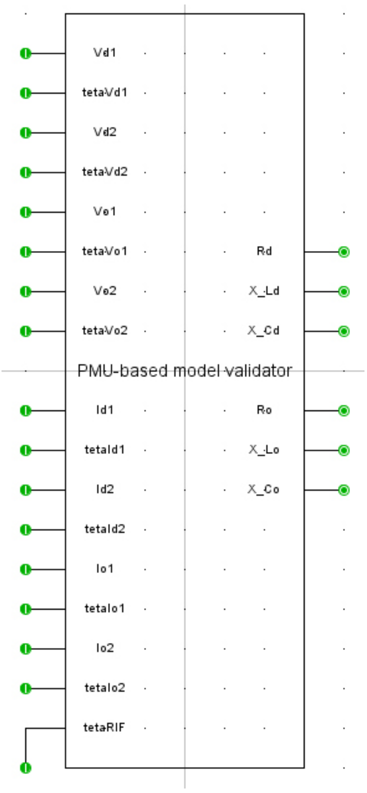

Figure 37 the PMU-based model validator v. 2.0. (final)

Figure 37 shows the new appearance of the Validator after the update. It is possible to notice that now its inputs are more than doubled, since not only it has to receive each phasor as the separate contribution of its magnitude and phase, but it also needs a phase reference pin (the last one in the column). This is needed because the DV7203 component actually offers voltage/current angles, that are time dependent quantities, and not phases since there cannot be any pre-decided common reference for the *n* devices the user decides to employ, until he decides to do so and defines a common reference application by application. This reference can be any of the involved output variables' angle: the choice, as long as it remains the same for all of the experiment's duration, is not influent on the final outcome.

Another interesting change, that is evident comparing the codes in Appendices A.3 and A.5, is the fact that a "safety switch" has been introduced in the algorithm: due to a "floating point – invalid operation" error popping up frequently, the preliminary results obtained were invalidated. It was discovered, after a short debugging session, that the error was caused by the dynamic real-time interaction of the input variables that cause some zeros to appear in some equations' denominators in the algorithm. That is the reason why the "if" portions of the code were added: they act as a protection, avoiding the zeros to influence the calculation by substituting them with a very small yet non-null constant.

After the Validator 2.0 was introduced, new tests were run. The results were positive, with small errors: this was the confirmation that the component was still working well even after the upgrade. However it proved, again, to be able to accurately compute zero sequence parameters only while simulating a single-phase-to-ground fault. This condition, completely unacceptable, needed to be studied more in depth and, if possible, overcome. In order to do so, as anticipated, another network model (that pre-existed in e-distribuzione's database) was taken into consideration, one where zero sequence currents naturally flow – even if small in magnitude – due to its size. In that new context, the Validator was expected to produce positive results even without the necessity to simulate ground faults. This hypothesis is validated in the following sub-chapter 3.3.

3.3 Validator testing in a realistic distribution network

The new network model the following tests were run in is, by e-distribuzione's will, to be kept as anonymous as possible. Due to this internal policy, no real names can be mentioned and the grid itself cannot be fully shown (also because of its sheer size, too big to be properly presented in its entirety on A4 pages). However this proves to be not a problem: only portions of said grid were interested by the research activities, and those will be described as precisely as possible.

Figure 38, in the following page, shows a small but important part of the network: on the left the HV grid's equivalent is simulated by means of a couple of three-phase 150 kV real sinusoidal voltage generators. At the top of the picture there is the 156 kV/20.8 kV HV/MV Y/Yn transformer from which a number of MV feeders depart. The vertical three-phase MV line the feeders are connected to simulates the low voltage-side busbar. The visible transformer, the only one of interest in this context, is the red one in the primary substation: five feeders are found here. The vertical three-phase HV line is connected to the green transformer, that will remain hidden since it is not needed to consider it in this study.

It is not possible to show the feeders in all their length, since they are very long and/or branch out so much that it would be too encumbering on the document's layout to show them all. However some of them, the ones that are going to be studied in depth, will be described with words and partial graphical representation, as needed case by case.

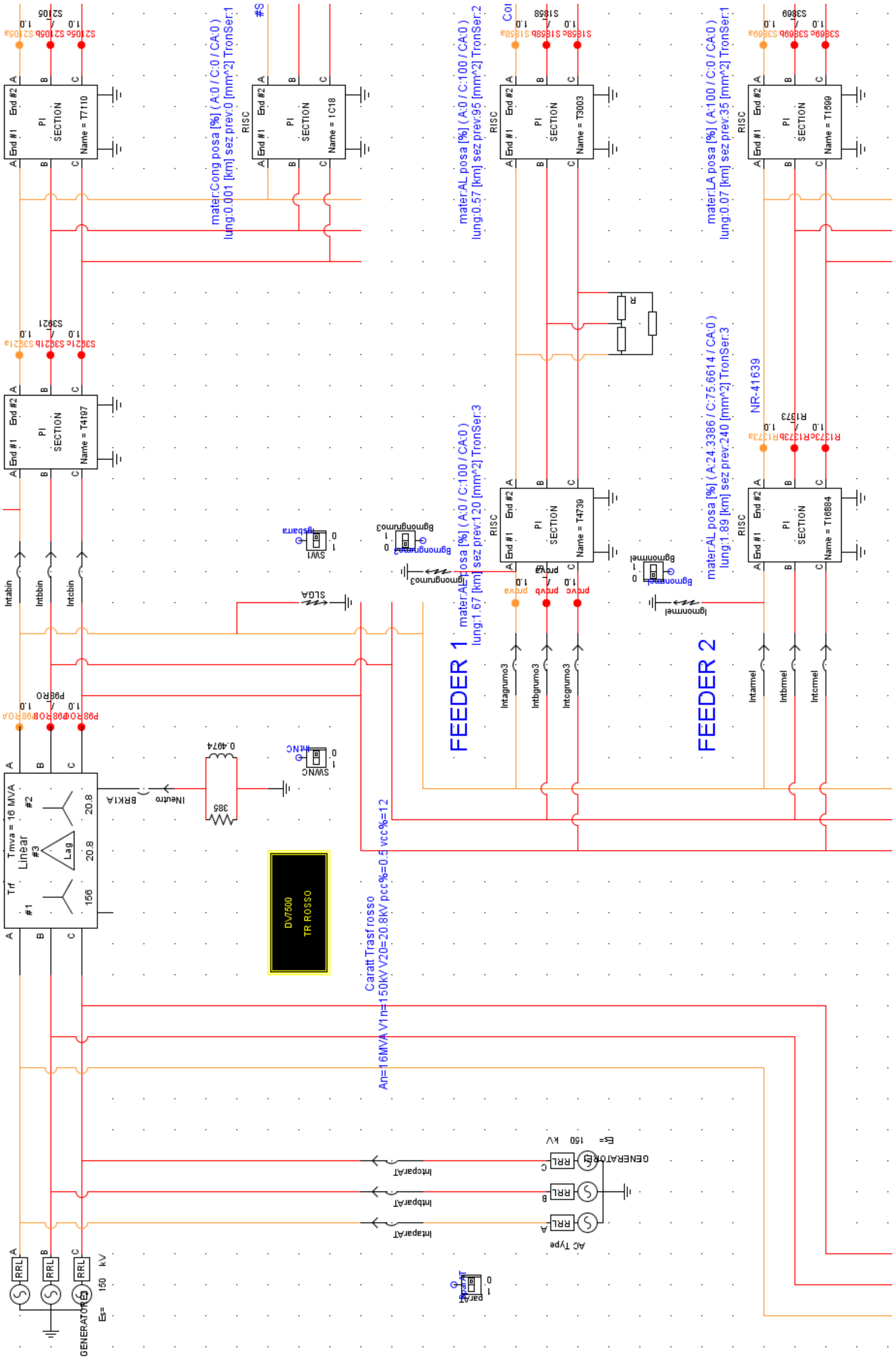
FEEDER 1
FEEDER 2
mater:Cong posa [%] (A:0 / C:0 / CA:0)
lung:0.001 [km] sez prev:0 [mm^2] TronSer:1
mater:AL posa [%] (A:0 / C:100 / CA:0)
lung:0.57 [km] sez prev:95 [mm^2] TronSer:2
mater:LA posa [%] (A:100 / C:0 / CA:0)
lung:0.07 [km] sez prev:35 [mm^2] TronSer:1
mater:AL posa [%] (A:0 / C:100 / CA:0)
lung:1.67 [km] sez prev:120 [mm^2] TronSer:3
mater:AL posa [%] (A:24.3386 / C:75.6614 / CA:0)
lung:1.89 [km] sez prev:240 [mm^2] TronSer:3
NR-41639
Caratt Trasf rosso
An=16MVA V1n=150kV V20=20.8kV pcc%=0.5 vcc%=12
DV7500
TR ROSSO
Trf
Tmva = 16 MVA
Linear
Lag
Name = T7110
Name = 1C18
Name = T3003
Name = T4197
Name = T4739
Name = T16884
PI
SECTION
RISC
GENERATOR
Es= 150 kV
AC Type
RRL
Intabin
Intbbin
Intcbin
Intagrumo3
Intbgrumo3
Intcgrumo3
Intaelmel
Intbelmel
Intcelmel
Intaparaf
Intbparaf
Intcparaf
INeutro
BRKIA
SWNC
SLGA
385
0.4974

Figure 38 Realistic distribution grid model’s portion as represented in the Draft section.

The feeders are represented, as in can be seen in Figure 38, as cascades of many black boxes that are none other than condensed parameters pi line models. Each black box can be studied by looking at two possible representation: the three-phase model shown in Figure 39 or the single-phase sequence equivalent shown in Figure 40. Since the parameters are by default to be configured in the sequence domain (as it is evident looking at Figure 41, were also the definitions for the parameters shown in Figure 40 can be found), the sequence equivalent model will be the one this study will be mostly referring to from now on.

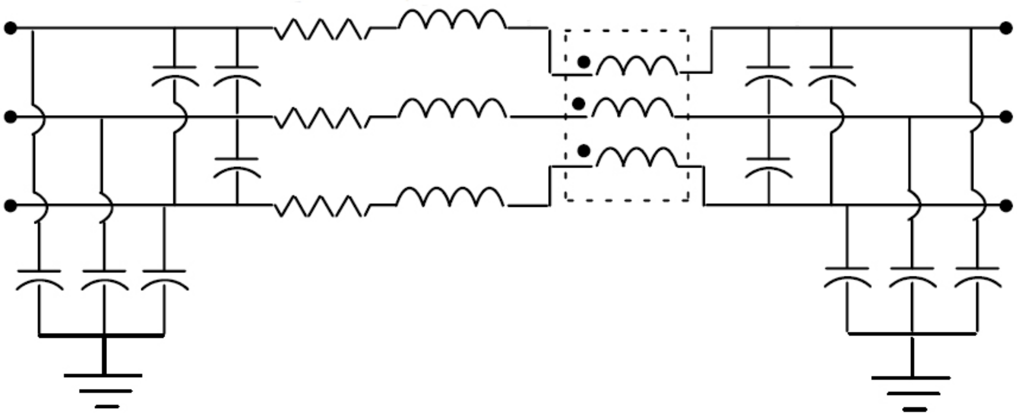

Figure 39 Three-phase pi line model.

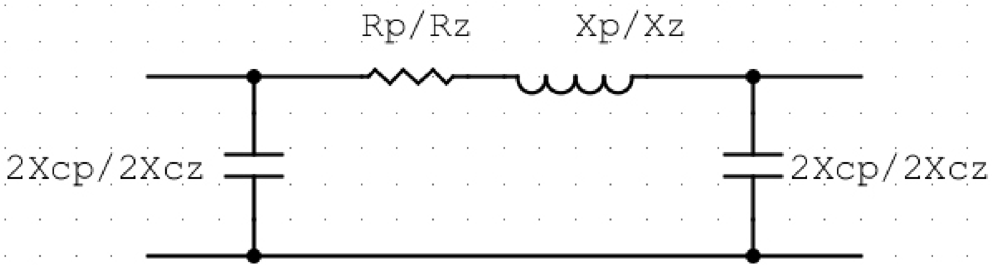

Figure 40 Single-phase symmetrical pi line model. (for positive and zero sequence only)

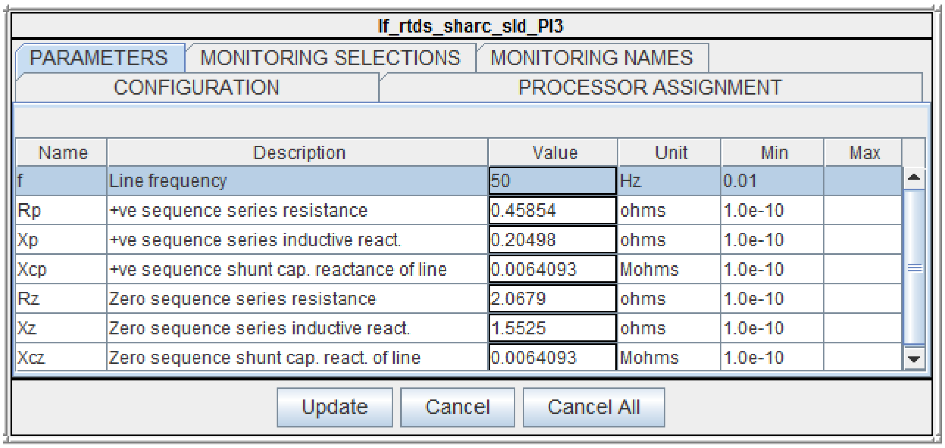

Name	Description	Value	Unit	Min	Max
f	Line frequency	50	Hz	0.01	
Rp	+ve sequence series resistance	0.45854	ohms	1.0e-10	
Xp	+ve sequence series inductive react.	0.20498	ohms	1.0e-10	
Xcp	+ve sequence shunt cap. reactance of line	0.0064093	Mohms	1.0e-10	
Rz	Zero sequence series resistance	2.0679	ohms	1.0e-10	
Xz	Zero sequence series inductive react.	1.5525	ohms	1.0e-10	
Xcz	Zero sequence shunt cap. react. of line	0.0064093	Mohms	1.0e-10	

Figure 41 Line sequence parameters’ configuration window example.

The first experiments were carried out in a no-load condition: all the lines were interested only by a current flow caused by the presence of shunt capacitances, and nothing else. It was decided to proceed like this, at least at first, in order to simplify the Validator's effectiveness preliminary testing phase: loads were added in a second phase, following a progressive increase in complexity plan for the network that the component had to work in. To be more precise, the plan was the following these steps:

1. Verifying the Validator's effectiveness/efficiency when used on a short linear unloaded feeder;
2. Verifying the Validator's effectiveness/efficiency when used on a long linear unloaded feeder;
3. Verifying the Validator's effectiveness/efficiency when used on a long branched unloaded feeder;
4. Verifying the Validator's effectiveness/efficiency when used on a long branched loaded feeder.

The chosen distribution network luckily offers lines that fit all four possible scenarios, that will now be analyzed one by one.

3.3.1 Short linear unloaded feeder

The line chosen to conduct these tests is "Feeder 3", a relatively short one (4.6 km) fragmented into eight portions. (the first three of them are shown in Figure 42)

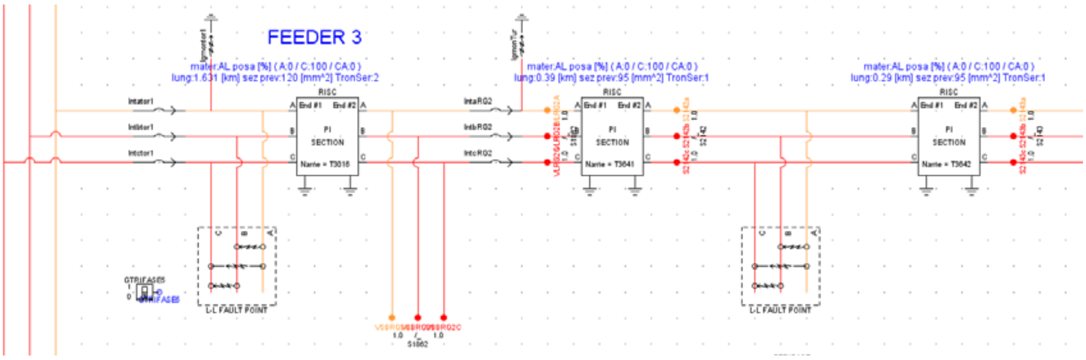
FEEDER 3
mater:AL posa [%] (A:0 / C:100 / CA:0)
lung:1.631 [km] sez prev:120 [mm^2] TronSer:2
mater:AL posa [%] (A:0 / C:100 / CA:0)
lung:0.39 [km] sez prev:95 [mm^2] TronSer:1
mater:AL posa [%] (A:0 / C:100 / CA:0)
lung:0.29 [km] sez prev:95 [mm^2] TronSer:1
RISC
End #1
End #2
PI
SECTION
Name = T3016
Name = T3641
Name = T3642
Intator1
Intbtor1
Intctor1
IntaRG2
IntbRG2
IntcRG2
L-L FAULT POINT
GTRIFASE5
S1862
1.0

Figure 42 "Feeder 3" partial view as represented in the Draft section.

This test aims to prove that the Validator is able to correctly compute the cumulative symmetrical line parameters (positive and zero sequence) not only when applied to a single pi-model, but also when their number increases and the total considered length with it. (in order to understand if there is any precision drop working with longer lines) To validate the test results however, that is to understand if the outputs of the Validator are correct or not, a MATLAB model of the line needs to be built. The objective of this model is to elaborate, starting from the data from each of the eight sections the line is split in, an equivalent pi-model (one for each sequence) whose parameters must coincide to the ones computed by the Validator.

Before showing the MATLAB code that was created with this specific intent, it is necessary to explain the theoretical basis on which it was built. The core concept is that to each pi-model corresponds a transmission matrix: once the eight transmission matrices are calculated, the black boxes' cascade can be analytically translated into the ordered multiplication of said matrices, until a single one is obtained. This single transmission matrix represents the equivalent of the entire line (in terms of symmetrical variables) and can finally be transformed back into a pi-model, ready to be compared with the Validator's results.

The rigorous step-by-step mathematical demonstration of what has been stated here can be found in Appendix 101A.6, together with the MATLAB algorithm that implements this procedure for Feeder 3.

The eight sections of the line under analysis are called, from left (busbar) to right (end switch): T3016, T3641, T3642, T3017, T3650, T3649, T3009 and T3647. The following list compares the line parameters of interest – positive sequence series resistance *Rd*, series inductive reactance *X_Ld*, shunt capacitive reactance *X_Cd* and zero sequence series resistance *Ro*, series inductive reactance *X_Lo*, shunt capacitive reactance *X_Co* – as obtained from the MATLAB algorithm (on the left) and from the Validator in the simulation (on the right), underlining in brackets the percent difference between the two measurements.

One branch section at a time, all of them will be included in the analysis by moving the second PMU toward the right:

T3016

- Rd=0.4585 Ω, while the Validator's output is 0.4809 Ω; (+0.05%)
- X_Ld=0.2050 Ω, while the Validator's output is 0.2051 Ω; (+0.05%)
- X_Cd=6409.3 Ω, while the Validator's output is 6406 Ω; (-0.05%)
- Ro=2.0679 Ω, while the Validator's output is 2.090 Ω; (+1.1)
- X_Lo=1.5525 Ω, while the Validator's output is 1.553 Ω; (0.03%)
- X_Co=6409.3 Ω, while the Validator's output is 6406 Ω; (-0.05%)

T3016 and T3641

- Rd=0.5833 Ω, while the Validator's output is 0.5893 Ω; (+1.03%)
- X_Ld=0.2549 Ω, while the Validator's output is 0.2539 Ω; (-0.39%)
- X_Cd=5220 Ω, while the Validator's output is 5218 Ω; (-0.04%)

- Ro=2.5360 Ω, while the Validator’s output is 2.5470 Ω; (-0.43%)
- X_Lo=1.9425 Ω, while the Validator’s output is 1.9350 Ω; (-0.39%)
- X_Co=5221 Ω, while the Validator’s output is 5218 Ω; (-0.06%)

T3016, T3641 and T3642

- Rd=0.6761 Ω, while the Validator’s output is 0.6869 Ω; (+1.60%)
- X_Ld=0.2920 Ω, while the Validator’s output is 0.2905 Ω; (-0.51%)
- X_Cd=4588 Ω, while the Validator’s output is 4585 Ω; (-0.07%)
- Ro=2.8842 Ω, while the Validator’s output is 2.9040 Ω; (+0.69%)
- X_Lo=2.2324 Ω, while the Validator’s output is 2.2180 Ω; (-0.65%)
- X_Co=4588 Ω, while the Validator’s output is 4585 Ω; (-0.07%)

T3016, T3641, T3642 and T3017

- Rd=0.8272 Ω, while the Validator’s output is 0.8470 Ω; (+2.39%)
- X_Ld=0.3524 Ω, while the Validator’s output is 0.3500 Ω; (-0.68%)
- X_Cd=3832 Ω, while the Validator’s output is 3830 Ω; (-0.05%)
- Ro=3.4509 Ω, while the Validator’s output is 3.4870 Ω; (+1.05%)
- X_Lo=2.7044 Ω, while the Validator’s output is 2.6780 Ω; (-0.98%)
- X_Co=3832 Ω, while the Validator’s output is 3830 Ω; (-0.05%)

T3016, T3641, T3642, T3017 and T3650

- Rd=0.9631 Ω, while the Validator’s output is 0.9530 Ω; (-1.05%)
- X_Ld=0.4073 Ω, while the Validator’s output is 0.4033 Ω; (-0.98%)
- X_Cd=3329 Ω, while the Validator’s output is 3328 Ω; (-0.03%)
- Ro=3.9683 Ω, while the Validator’s output is 3.9820 Ω; (+0.35%)
- X_Lo=3.1325 Ω, while the Validator’s output is 3.0950 Ω; (-1.20%)
- X_Co=3330 Ω, while the Validator’s output is 3327 Ω; (-0.09%)

T3016, T3641, T3642, T3017, T3650 and T3649

- Rd=1.2399 Ω, while the Validator’s output is 1.2160 Ω; (-1.93%)
- X_Ld=0.5180 Ω, while the Validator’s output is 0.5108 Ω; (-1.39%)

- X_Cd=2637 Ω, while the Validator’s output is 2636 Ω; (-0.04%)
- Ro=5.0075 Ω, while the Validator’s output is 5.0270 Ω; (0.39%)
- X_Lo=3.9972 Ω, while the Validator’s output is 3.9270 Ω; (-1.76%)
- X_Co=2638 Ω, while the Validator’s output is 2636 Ω; (-0.08%)

T3016, T3641, T3642, T3017, T3650, T3649 and T3009

- Rd=1.2639 Ω, while the Validator’s output is 1.2440 Ω; (-1.57%)
- X_Ld=0.5276 Ω, while the Validator’s output is 0.5202 Ω; (-1.4%)
- X_Cd=2591 Ω, while the Validator’s output is 2589 Ω; (-0.08%)
- Ro=5.0977 Ω, while the Validator’s output is 5.1230 Ω; (0.4%)
- X_Lo=4.0722 Ω, while the Validator’s output is 3.9999 Ω; (-1.8%)
- X_Co=2591 Ω, while the Validator’s output is 2589 Ω; (-0.08%)

T3016, T3641, T3642, T3017, T3650, T3649, T3009 and T3647

- Rd=1.4099 Ω, while the Validator’s output is 1.3380 Ω; (-4.49%)
- X_Ld=0.5859 Ω, while the Validator’s output is 0.5776 Ω; (-1.4%)
- X_Cd=2339 Ω, while the Validator’s output is 2338 Ω; (-0.04%)
- Ro=5.6458 Ω, while the Validator’s output is 5.7310 Ω; (+1.51%)
- X_Lo=4.5279 Ω, while the Validator’s output is 4.4320 Ω; (-2.12%)
- X_Co=2339 Ω, while the Validator’s output is 2337 Ω; (-0.09%)

The test results in a success, since very small errors are met in the process. Small enough to be considered negligible: the error threshold imposed by e-distribuzione’s technician was +/-5%, so the Validator’s measurements successfully passed this first exam. However, even if already considered acceptable, this errors can be further reduced taking into consideration their causes: parallax errors in the readings, influence of circuital components not taken in consideration in the MATLAB model (e.g. breakers resistance) on the measurements and error propagation during the calculations. With those considered, the difference between the two algorithms tends to zero.

3.3.2 Long linear unloaded feeder

The line chosen to conduct these tests is "Feeder 1", a relatively long one (9.048 km) fragmented into fifteen portions. (the first three of them are shown in Figure 43)

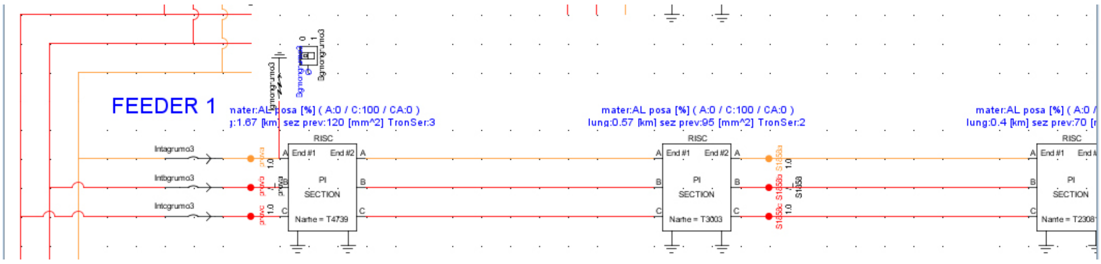
FEEDER 1
nater:AL posa [%] (A:0 / C:100 / CA:0)
:1.67 [km] sez prev:120 [mm^2] TronSer:3
mater:AL posa [%] (A:0 / C:100 / CA:0)
lung:0.57 [km] sez prev:95 [mm^2] TronSer:2
mater:AL posa [%] (A:0 /
lung:0.4 [km] sez prev:70 [
Intagrumo3
Intbgrumo3
Intcgrumo3
RISC
End #1
End #2
A
B
C
PI
SECTION
Name = T4739
Name = T3003
Name = T2308
S1858
1.0

Figure 43 "Feeder 1" partial view as represented in the Draft section.

This test aims to prove that the Validator is able to correctly compute the cumulative symmetrical line parameters (positive and zero sequence) also in case of very long lines. This experiment was conducted as the previous one was, with the gradual addition of the line sections and step-by-step parameters' reading from both the simulation and MATLAB: (starting from the first couple of branch portions on the left, since the effectiveness of the method on the single segment has been already proved)

T4739 and T3003

- Rd=0.6530 Ω, while the Validator's output is 0.6486 Ω; (-0.67%)
- X_Ld=0.2859 Ω, while the Validator's output is 0.2848 Ω; (-0.38%)
- X_Cd=4781 Ω, while the Validator's output is 4779 Ω; (-0.04%)
- Ro=2.8572 Ω, while the Validator's output is 2.8570 Ω; (-0.01%)
- X_Lo=2.1710 Ω, while the Validator's output is 2.1540 Ω; (-0.78%)
- X_Co=4853 Ω, while the Validator's output is 4850 Ω; (-0.06%)

T4739, T3003 and T23081

- Rd=0.8210 Ω, while the Validator's output is 0.8062 Ω; (-1.80%)
- X_Ld=0.3399 Ω, while the Validator's output is 0.3373 Ω; (-0.76%)
- X_Cd=4135 Ω, while the Validator's output is 4133 Ω; (-0.05%)
- Ro=3.3951 Ω, while the Validator's output is 3.3600 Ω; (-1.03%)
- X_Lo=2.5621 Ω, while the Validator's output is 2.526 Ω; (-1.41%)

- X_Co=4189 Ω, while the Validator's output is 4186; (-0.07%)

T4739, T3003, T23081 and T19459

- Rd=0.9429 Ω, while the Validator's output is 0.9203 Ω; (-2.40%)
- X_Ld=0.3790 Ω, while the Validator's output is 0.3752 Ω; (-1.00%)
- X_Cd=3776 Ω, while the Validator's output is 3764 Ω; (-0.32%)
- Ro=3.7851 Ω, while the Validator's output is 3.761 Ω; (-0.7%)
- X_Lo=2.8456 Ω, while the Validator's output is 2.827 Ω; (-0.6%)
- X_Co=3811 Ω, while the Validator's output is 3809 Ω; (-3.3%)

T4739, T3003, T23081, T19459 and T3656

- Rd=1.3415 Ω, while the Validator's output is 1.2990 Ω; (-3.17%)
- X_Ld=0.5225 Ω, while the Validator's output is 0.5151 Ω; (-1.42%)
- X_Cd=2822 Ω, while the Validator's output is 2821 Ω; (-0.04%)
- Ro=5.1833 Ω, while the Validator's output is 5.1300 Ω; (-1.03%)
- X_Lo=3.9197 Ω, while the Validator's output is 3.878 Ω; (-1.06%)
- X_Co=2847 Ω, while the Validator's output is 2845 Ω; (-0.07%)

T4739, T3003, T23081, T19459, T3656 and T12820

- Rd=1.4893 Ω, while the Validator's output is 1.4420 Ω; (-3.18%)
- X_Ld=0.5761 Ω, while the Validator's output is 0.5683 Ω; (-1.35%)
- X_Cd=2563 Ω, while the Validator's output is 2562 Ω; (-0.04%)
- Ro=5.6998 Ω, while the Validator's output is 5.6470 Ω; (-0.93%)
- X_Lo=4.3259 Ω, while the Validator's output is 4.2810 Ω; (-1.04%)
- X_Co=2584 Ω, while the Validator's output is 2582 Ω; (-0.08%)

T4739, T3003, T23081, T19459, T3656, T12820 and T3600

- Rd=1.6200 Ω, while the Validator's output is 1.5690 Ω; (-3.15%)
- X_Ld=0.6236 Ω, while the Validator's output is 0.6151 Ω; (-1.36%)
- X_Cd=2371 Ω, while the Validator's output is 2369 Ω; (-0.08%)
- Ro=6.1671 Ω, while the Validator's output is 6.1050 Ω; (-1.01%)

- X_Lo=4.6855 Ω, while the Validator's output is 4.638 Ω; (-1.99%)
- X_Co=2388 Ω, while the Validator's output is 2386 Ω; (-0.08%)

T4739, T3003, T23081, T19459, T3656, T12820, T3600 and T7013

- Rd=1.6914 Ω, while the Validator's output is 1.633 Ω; (-3.45%)
- X_Ld=0.6465 Ω, while the Validator's output is 0.6371 Ω; (-1.45%)
- X_Cd=2295 Ω, while the Validator's output is 2294 Ω; (-0.04%)
- Ro=6.3860 Ω, while the Validator's output is 6.324 Ω; (-0.97%)
- X_Lo=4.8516 Ω, while the Validator's output is 4.800 Ω; (-1.06%)
- X_Co=2312 Ω, while the Validator's output is 2310 Ω; (-0.09%)

T4739, T3003, T23081, T19459, T3656, T12820, T3600, T7013 and T12247

- Rd=1.8775 Ω, while the Validator's output is 1.805 Ω; (-3.86%)
- X_Ld=0.7101 Ω, while the Validator's output is 0.6993 Ω; (-1.52%)
- X_Cd=2099 Ω, while the Validator's output is 2098 Ω; (-0.05%)
- Ro=7.0088 Ω, while the Validator's output is 6.9340 Ω; (-1.07%)
- X_Lo=5.3243 Ω, while the Validator's output is 5.2660 Ω; (-1.09%)
- X_Co=2113 Ω, while the Validator's output is 2111 Ω; (-0.09%)

T4739, T3003, T23081, T19459, T3656, T12820, T3600, T7013, T12247 and T6824

- Rd=2.0343 Ω, while the Validator's output is 1.968 Ω; (-3.26%)
- X_Ld=0.7731 Ω, while the Validator's output is 0.7639 Ω; (-1.19%)
- X_Cd=1918 Ω, while the Validator's output is 1917 Ω; (-0.05 %)
- Ro=7.6021 Ω, while the Validator's output is 7.5540 Ω; (-0.63%)
- X_Lo=5.8169 Ω, while the Validator's output is 5.7620 Ω; (-0.94%)
- X_Co=1930 Ω, while the Validator's output is 1928 Ω; (-0.10%)

T4739, T3003, T23081, T19459, T3656, T12820, T3600, T7013, T12247, T6824 and T3661

- Rd=2.1317 Ω, while the Validator's output is 2.0690 Ω; (-2.94%)
- X_Ld=0.8120 Ω, while the Validator's output is 0.8037 Ω; (-1.02%)

- X_Cd=1821 Ω, while the Validator's output is 1820 Ω; (-0.05%)
- Ro=7.9681 Ω, while the Validator's output is 7.9370 Ω; (-0.39%)
- X_Lo=6.1206 Ω, while the Validator's output is 6.0680 Ω; (-0.86%)
- X_Co=1832 Ω, while the Validator's output is 1830 Ω; (-0.11%)

T4739, T3003, T23081, T19459, T3656, T12820, T3600, T7013, T12247, T6824, T3661 and T3665

- Rd=2.4006 Ω, while the Validator's output is 2.2980 Ω; (-4.27%)
- X_Ld=0.8983 Ω, while the Validator's output is 0.8849 Ω; (-1.49%)
- X_Cd=1663 Ω, while the Validator's output is 1662 Ω; (-0.06%)
- Ro=8.8312 Ω, while the Validator's output is 8.7390 Ω; (-1.04%)
- X_Lo=6.7456 Ω, while the Validator's output is 6.6700 Ω; (-1.12%)
- X_Co=1672 Ω, while the Validator's output is 1670 Ω; (-0.12%)

T4739, T3003, T23081, T19459, T3656, T12820, T3600, T7013, T12247, T6824, T3661, T3665 and T3004

- Rd=2.6537 Ω, while the Validator's output is 2.5390 Ω; (-4.32%)
- X_Ld=0.9897Ω, while the Validator's output is 0.9749 Ω; (-1.50%)
- X_Cd=1510 Ω, while the Validator's output is 1509 Ω; (-0.07%)
- Ro=9.7169 Ω, while the Validator's output is 9.6240 Ω; (-0.96%)
- X_Lo=7.4382 Ω, while the Validator's output is 7.3570 Ω; (-1.09%)
- X_Co=1517 Ω, while the Validator's output is 1515 Ω; (-0.13%)

T4739, T3003, T23081, T19459, T3656, T12820, T3600, T7013, T12247, T6824, T3661, T3665, T3004 and T16518

- Rd=2.9664 Ω, while the Validator's output is 2.8550 Ω; (-3.76%)
- X_Ld=1.1084 Ω, while the Validator's output is 1.0970 Ω; (-1.03%)
- X_Cd=1342 Ω, while the Validator's output is 1341 Ω; (-0.07%)
- Ro=10.8951 Ω, while the Validator's output is 10.8200 Ω; (-0.69%)
- X_Lo=8.3286 Ω, while the Validator's output is 8.2760 Ω; (-0.63%)
- X_Co=1348 Ω, while the Validator's output is 1346 Ω; (-0.15%)

T4739, T3003, T23081, T19459, T3656, T12820, T3600, T7013, T12247, T6824, T3661, T3665, T3004, T16518 and T3666

- Rd=3.0932 Ω, while the Validator's output is 2.9880 Ω; (-3.40%)
- X_Ld=1.1572 Ω, while the Validator's output is 1.1480 Ω; (-0.80%)
- X_Cd=1282 Ω, while the Validator's output is 1281 Ω; (-0.08%)
- Ro=11.4033 Ω, while the Validator's output is 11.3300 Ω; (-0.64%)
- X_Lo=8.6826 Ω, while the Validator's output is 8.6630 Ω; (-0.23%)
- X_Co=1287 Ω, while the Validator's output is 1285 Ω; (-0.16%)

The results are once again positive: not even one measurement error exceeds the +/-5% imposed threshold and the range of the recorded ones suggests that, again, the small inconsistencies are caused not by the length of the line under test but only by minor differences between the RSCAD network model and that analytically built on MATLAB.

3.3.3 Long branched unloaded feeder

The line chosen to conduct these tests is "Feeder 2", one that is branched like many others on the Italian distribution grid. Its layout can be seen in Figure 44:

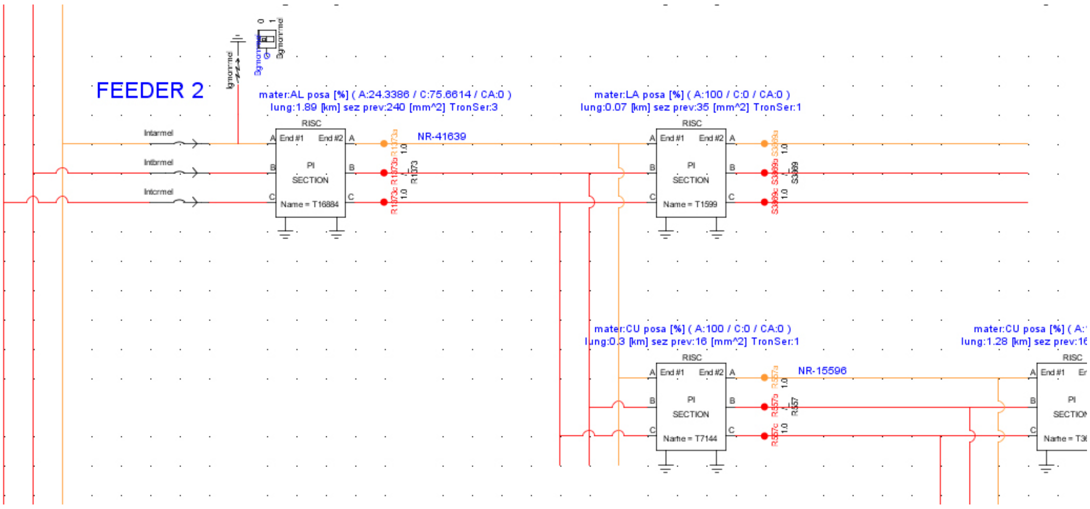
FEEDER 2
mater:AL posa [%] (A:24.3386 / C:75.6614 / CA:0)
lung:1.89 [km] sez prev:240 [mm^2] TronSer:3
RISC
End #1
End #2
PI
SECTION
Name = T16884
NR-41639
R1873
mater:LA posa [%] (A:100 / C:0 / CA:0)
lung:0.07 [km] sez prev:35 [mm^2] TronSer:1
Name = T1599
S3069
mater:CU posa [%] (A:100 / C:0 / CA:0)
lung:0.3 [km] sez prev:16 [mm^2] TronSer:1
Name = T7144
NR-15596
R557
mater:CU posa [%] (A:
lung:1.28 [km] sez prev:16

Figure 44 "Feeder 2" partial view as represented in the Draft section.

This test aims to prove that the Validator is able to correctly compute the equivalent symmetrical line parameters (positive and zero sequence) also in presence of ramifications, meaning that the Validator is able to correctly handle them. The results of this experiment are more interesting with respect to the ones obtained in the previous two, so they are commented step-by-step:

T16884

- Rd= 0.7011 Ω, while the Validator’s output is 0.7107 Ω; (-1.40%)
- X_Ld= 0.3519 Ω, while the Validator’s output is 0.3522 Ω; (+0.08%)
- X_Cd=5612 Ω, while the Validator’s output is 5609 Ω; (-0.05%)
- Ro=2.1838 Ω, while the Validator’s output is 2.1500 Ω; (-1.5%)
- X_Lo=1.8791 Ω, while the Validator’s output is 1.8800 Ω; (+0.05%)
- X_Co=5635 Ω, while the Validator’s output is 5632 Ω; (-0.05%)

The presence of a successive ramification has no effect on the measurements made on a single line section. This could be easily imagined, but it was worth verifying. The small errors are, once again, due to slight discrepancies in MATLAB’s and RSCAD’s grid models.

T16884 and T1599 (with T7144 as a branch in the middle)

- Rd= 0.7664 Ω, while the Validator’s output is 1.3790 Ω; (+77.61%)
- X_Ld= 0.3789 Ω, while the Validator’s output is 0.6420 Ω; (+69.44%)
- X_Cd=5606 Ω, while the Validator’s output is 983 Ω; (-82.47%)
- Ro=2.2595 Ω, while the Validator’s output is 2.5800 Ω; (+14.18%)
- X_Lo=1.9927 Ω, while the Validator’s output is 2.3250 Ω; (+16.68%)
- X_Co=5632 Ω, while the Validator’s output is 4449 Ω; (-21.00%)

This is where problems start to arise: as it can be easily inferred by the huge difference between the measurements, the Validator is influenced by the branching of the line. The same happens when the PMU is moved to the other branch, even if with smaller consequences:

T16884 and T7144 (with T1599 as a branch in the middle)

- Rd=1.0321 Ω, while the Validator’s output is 1.0100 Ω; (-2.14%)
- X_Ld=0.4776 Ω, while the Validator’s output is 0.4658 Ω; (-2.47%)
- X_Cd=5589 Ω, while the Validator’s output is 5580 Ω; (-0.16%)
- Ro=2.5594 Ω, while the Validator’s output is 2.5200 Ω; (-1.54%)
- X_Lo=2.3747 Ω, while the Validator’s output is 2.3230 Ω; (-2.18%)
- X_Co=5626 Ω, while the Validator’s output is 5621 Ω; (-0.09%)

The errors are low, but still higher than the average with respect to the previous experiments. This is true because most of the energy flows in the direction of branch T7144 (from which the rest of the feeder develops), thus the role of T1599 as a "disturbing element" is limited by its small current withdrawal. (since there is no network development from there on)

The question here was: does the Validator correctly measure the equivalent parameters, taking in proper consideration the ramification? Or are its outputs inconsistent with the true network parameters? In order to answer to these questions, the MATLAB model needs to be modified accordingly, including the branched section as it is shown in Appendix A.7. The following are the results obtained from the new model compared to the same Validator's outputs seen in the previous step.

T16884 and T7144 (with T1599 as a branch in the middle)

- Rd=1.0321 Ω, while the Validator's output is 1.0100 Ω; (-2.14%)
- X_Ld=0.4776 Ω, while the Validator's output is 0.4658 Ω; (-2.47%)
- X_Cd=5582 Ω, while the Validator's output is 5580 Ω; (-0.04%)
- Ro=2.5594 Ω, while the Validator's output is 2.5200 Ω; (-1.54%)
- X_Lo=2.3747 Ω, while the Validator's output is 2.3230 Ω; (-2.18%)
- X_Co=5623 Ω, while the Validator's output is 5621 Ω; (-0.05%)

The only difference here is a reduction of the shunt parameters (both positive and zero sequence), and that seems reasonable considering that the model has to take into consideration the shunt capacitances of the branch section and this contributes to the overall reduction of the equivalent shunt reactance that can be witnessed above. In order to be sure of the correct modeling, a branch derivation (T1599) is added to Feeder 1, just to experiment the consequences of such an addition in terms of algorithm coherence. What follows is a comparison between two experiments, with and without addition:

T4739 and T3003

- Rd=0.6530 Ω, while the Validator's output is 0.6486 Ω; (-0.67%)
- X_Ld=0.2859 Ω, while the Validator's output is 0.2848 Ω; (-0.38%)
- X_Cd=4781 Ω, while the Validator's output is 4779 Ω; (-0.04%)
- Ro=2.8572 Ω, while the Validator's output is 2.8570 Ω; (-0.01%)
- X_Lo=2.1710 Ω, while the Validator's output is 2.1650 Ω; (-0.28%)

- X_Co=4853 Ω, while the Validator’s output is 4850 Ω; (-0.06%)

T4739 and T3003 (with T1599 as a branch in the middle)

- Rd=0.6530 Ω, while the Validator’s output is 0.6486 Ω; (-0.67%)
- X_Ld=0.2859 Ω, while the Validator’s output is 0.2848 Ω; (-0.38%)
- X_Cd=4777 Ω, while the Validator’s output is 4774 Ω; (-0.06%)
- Ro=2.8573 Ω, while the Validator’s output is 2.8570 Ω; (-0.01%)
- X_Lo=2.1709 Ω, while the Validator’s output is 2.1650 Ω; (-0.28%)
- X_Co=4851 Ω, while the Validator’s output is 4848 Ω; (-0.06%)

As can be clearly seen from the data above, the insertion of a branch changes shunt parameters only, and the errors remain almost perfectly constant in the two cases, meaning that the Validator reacts to the new element as the MATLAB model does. This is the desired result, that is confirmed by a last experiment conducted on Feeder 1 with the exact same condition as the last one, but one thing: the branching section had its parameters modified by a great deal (series/shunt components multiplied/divided by ten) to confirm that the Validator correctly works even with different kind of branches. (longer ones, in this case)

T4739 and T3003 (with a modified T1599 as a branch in the middle)

- Rd=0.6530 Ω, while the Validator’s output is 0.6486 Ω; (-0.67%)
- X_Ld=0.2859 Ω, while the Validator’s output is 0.2848 Ω; (-0.38%)
- X_Cd=4737 Ω, while the Validator’s output is 4734 Ω; (-0.06%)
- Ro=2.8572 Ω, while the Validator’s output is 2.8570 Ω; (-0.01%)
- X_Lo=2.1710 Ω, while the Validator’s output is 2.1650 Ω; (-0.78%)
- X_Co=4832 Ω, while the Validator’s output is 4830 Ω; (-0.04%)

Despite the alteration, errors are still very low. This result lead to optimistic hopes regarding the Validator’s ability to take into account correctly the line parameters’ variation also in normal working conditions. (presence of load)

3.3.4 Long branched loaded feeder

This last experiment had place on Feeder 1, with a particular focus on its first and second line sections. As Figure 45 clearly shows, a three-phase load is placed between them as a derivation from which power is withdrawn. The connection typology's choice was not casual: delta connections are a custom for distribution installations, whether they are common MV direct loads, capacitor banks or primary windings of MV/LV transformers.

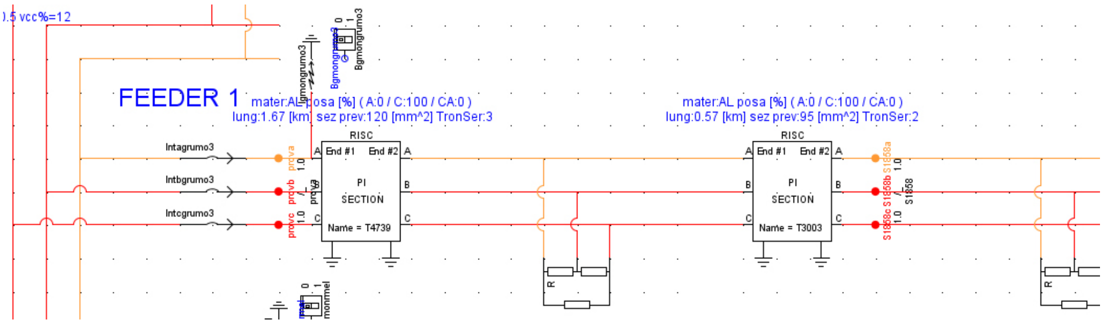

Figure 45 "Feeder 1" partial view as represented in the Draft section with load.

Similarly to a line derivation, a three-phase load withdraws current from the line that is monitored by the PMUs (placed immediately before T4739 and after T3003 pi sections), but it does so way more in comparison. This means that the current difference between the two ports widens the more the power requested increases, possibly influencing the Validator's outputs negatively.

The objective of this experiment is to understand if the device is capable of maintaining its ability to precisely estimate the line's sections cumulative sequence parameter, taking into account the load's contribution. Of course its presence implies that the results produced by the Validator will no longer be referred to the line only, but will somehow include the inference of the load itself. This is where an interesting prospective lies: if the relationship between actual line parameters (that are known) and measured ones under load conditions (variable in time and different from the previously mentioned ones) could be uncovered and expressed through an equation, then a decoupling action could be possible and the load fluctuations could be recorded and interpreted "translating" their influence on the measured parameters. The result is that a very high-resolution load profile monitoring could be possible on MV networks, a feat that is not yet realizable with the technologies installed nowadays on the grid.

As a first step in this direction, the mathematical model of the "line section – load – line section" system must be realized, in order to compare its results in terms of cumulative parameters to the one produced by the Validator. If the two were to coincide, in fact, it would prove that the Validator successfully and precisely keeps track of the load influence on them, thus further researches can be conducted on how to extrapolate data regarding load fluctuations from its readings. The MATLAB model in this case is very similar to the one developed and explained in Appendix A.7, so in order to avoid useless repetitions only the differences have been highlighted in the dedicated Appendix A.8, where the three-phase load model for a symmetrical components' circuit is created. Once this is done, the equivalent load can be introduced in the algorithm and the reference cumulative parameters calculated.

Once the reference parameters are available, the next step is creating a number of load scenarios and collect the parameters produced by the Validator in each of it in order to compare them with the firsts. The cases will be differentiated by load total impedance and power factor:

Z=500 Ω and cos φ=1:

- Rd=0.6535 Ω, while the Validator's output is 0.6941 Ω; (+6.21%)
- X_Ld=0.2864 Ω, while the Validator's output is 0.3041 Ω; (+6.18%)
- X_Cd=5 Ω, while the Validator's output is 5053 Ω; (+86074%)
- Ro=2.8572 Ω, while the Validator's output is 2.8565 Ω; (-0.02%)
- X_Lo=2.1710 Ω, while the Validator's output is 2.1479 Ω; (-1.06%)
- X_Co=4853 Ω, while the Validator's output is 4851 Ω; (-0.04%)

Z=1000 Ω and cos φ=1:

- Rd=0.6533 Ω, while the Validator's output is 0.6751 Ω; (+3.34%)
- X_Ld=0.2861 Ω, while the Validator's output is 0.2956 Ω; (+3.32%)
- X_Cd=23 Ω, while the Validator's output is 4889 Ω; (+20980%)
- Ro=2.8572 Ω, while the Validator's output is 2.8550 Ω; (-0.08%)
- X_Lo=2.1710 Ω, while the Validator's output is 2.1430 Ω; (-1.29%)
- X_Co=4853 Ω, while the Validator's output is 4851 Ω; (-0.04%)

Z=5000 Ω and cos φ=1:

- Rd=0.6531 Ω, while the Validator's output is 0.6578 Ω; (+0.72%)
- X_Ld=0.2860 Ω, while the Validator's output is 0.2879 Ω; (+0.66%)
- X_Cd=518 Ω, while the Validator's output is 4796 Ω; (+826%)
- Ro=2.8572 Ω, while the Validator's output is 2.8550 Ω; (-0.08%)
- X_Lo=2.1710 Ω, while the Validator's output is 2.1480 Ω; (-1.06%)
- X_Co=4853 Ω, while the Validator's output is 4848 Ω; (-0.10%)

Z=8000 Ω and cos φ=1:

- Rd=0.6531 Ω, while the Validator’s output is 0.6560 Ω; (+0.44%)
- X_Ld=0.2859 Ω, while the Validator’s output is 0.2872 Ω; (+0.45%)
- X_Cd=1135 Ω, while the Validator’s output is 4789 Ω; (-322%)
- Ro=2.8572 Ω, while the Validator’s output is 2.8530 Ω; (-0.15%)
- X_Lo=2.1710 Ω, while the Validator’s output is 2.1410 Ω; (-1.38%)
- X_Co=4853 Ω, while the Validator’s output is 4850 Ω; (-0.06%)

Z=590.5 Ω and $\cos\varphi$=0.85: (inductive)

- Rd=0.6535 Ω, while the Validator’s output is 0.6925 Ω; (+5.97%)
- X_Ld=0.2860 Ω, while the Validator’s output is 0.2827 Ω; (-1.15%)
- X_Cd=107 Ω, while the Validator’s output is -401.8 Ω; (-472%)
- Ro=2.8572 Ω, while the Validator’s output is 2.8500 Ω; (-0.25%)
- X_Lo=2.1710 Ω, while the Validator’s output is 2.1420 Ω; (-1.34%)
- X_Co=4853 Ω, while the Validator’s output is 4848 Ω; (-0.10%)

Z=1048 Ω and $\cos\varphi$=0.95: (inductive)

- Rd=0.6533 Ω, while the Validator’s output is 0.6760 Ω; (+3.47%)
- X_Ld=0.2861 Ω, while the Validator’s output is 0.2889 Ω; (+0.98%)
- X_Cd=124 Ω, while the Validator’s output is -1539 Ω; (-1341%)
- Ro=2.8572 Ω, while the Validator’s output is 2.8610 Ω; (+0.13%)
- X_Lo=2.1710 Ω, while the Validator’s output is 2.1470 Ω; (-1.11%)
- X_Co=4853 Ω, while the Validator’s output is 4849 Ω; (-0.08%)

Z=1181 Ω and $\cos\varphi$=0.85: (inductive)

- Rd=0.6533 Ω, while the Validator’s output is 0.6738 Ω; (+3.47%)
- X_Ld=0.2860 Ω, while the Validator’s output is 0.2835 Ω; (-0.87%)
- X_Cd=221 Ω, while the Validator’s output is -877 Ω; (-497%)
- Ro=2.8572 Ω, while the Validator’s output is 2.8440 Ω; (-0.46%)
- X_Lo=2.1710 Ω, while the Validator’s output is 2.1400 Ω; (-1.43%)
- X_Co=4853 Ω, while the Validator’s output is 4850 Ω; (-0.06%)

The outcome of these few experiments is clear: there is no full consistency between the measurements, so one of the two models (the one implemented in MATLAB or the Validator's algorithm) must be at fault. An easy way to understand which of the two methods was bearing incorrect results was to create a transmission matrix from each of the two sequence parameters' sets provided, then use it in the formula shown in Eq. 38 (see Appendix A.6 to deepen the subject) together with actual sequence voltage/current measurements taken at the secondary port of the "line section – load – line section" system in the simulation. The comparison between the results and the readings of those same quantities in the simulation pointed out the right choice: only the equivalent matrix obtained by means of cascading satisfied the equation below.

$$\begin{bmatrix} \boldsymbol{V_1} \\ \boldsymbol{I_1} \end{bmatrix} = \begin{bmatrix} \boldsymbol{A} & \boldsymbol{C} \\ \boldsymbol{B} & \boldsymbol{D} \end{bmatrix} \begin{bmatrix} \boldsymbol{V_2} \\ \boldsymbol{I_2} \end{bmatrix} \qquad \text{Eq. 38}$$

As observed, the Validator seemed to be unable to properly take into account loads connected on portions of the line under the monitoring action of two PMUs, for what concerns direct sequence parameters' estimation; it works fine under any working condition, instead, while measuring zero sequence components.

The reason why direct sequence parameters are affected by these errors when a load is considered was investigated. After some tests, it was discovered that it depended on an unforeseen condition: the equivalent pi model obtained in the presence of load always presents two different values for its shunt reactances, while in the no load case they are almost perfectly identical. Since the equations the Validator is based upon are obtained from a pi model assumed to have identical shunt parameters, as it is shown in Appendix A.1, they lose their validity with the load introduction.

When a load is considered, new equations for the Validator should be created starting from a pi model with two different shunt impedances, as the one shown in Figure 46:

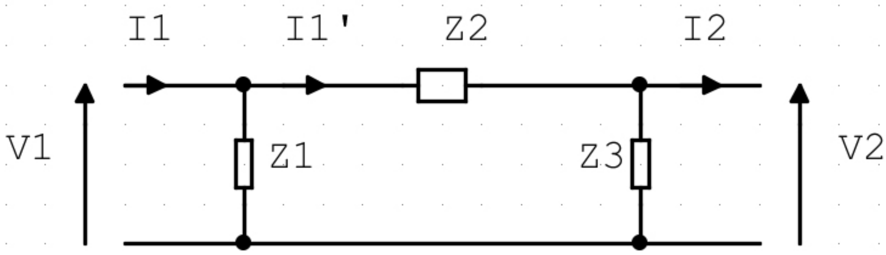

Figure 46 Distribution line pi model, with two different shunt impedances.

Kirchhoff laws are applied to obtain the following equations:

$$\begin{cases} \boldsymbol{V_2} = \boldsymbol{V_1} - \boldsymbol{I_1}'\boldsymbol{Z_2} = \boldsymbol{V_1} - \left(\boldsymbol{I_1} - \dfrac{\boldsymbol{V_1}}{\boldsymbol{Z_1}}\right)\boldsymbol{Z_2} & \text{Eq. 39} \\ \boldsymbol{I_2} = \boldsymbol{I_1} - \dfrac{\boldsymbol{V_1}}{\boldsymbol{Z_1}} - \dfrac{\boldsymbol{V_2}}{\boldsymbol{Z_3}} & \text{Eq. 40} \end{cases}$$

The problem with this method, despite being coherent with the situation, is that there are too many unknown variables: three of them, against two equations only. As it is, the system cannot be solved. However, if one of the three impedances were to be known (for example **Z2**), then the other two could be easily computed as shown by Eq. 41 and Eq. 42:

$$\begin{cases} \boldsymbol{Z_1} = \dfrac{\boldsymbol{V_1}\boldsymbol{Z_2}}{\boldsymbol{V_2} - \boldsymbol{V_1} + \boldsymbol{I_1}\boldsymbol{Z_2}} & \text{Eq. 41} \\ \boldsymbol{Z_3} = \dfrac{\boldsymbol{V_2}\boldsymbol{Z_2}}{\boldsymbol{V_1} - \boldsymbol{V_2} - \boldsymbol{I_2}\boldsymbol{Z_2}} & \text{Eq. 42} \end{cases}$$

Parametric equations like these bring solutions only if the parameter can be somehow assumed as known. **Z2** was not chosen randomly, in this regard. Since series parameters are the ones less affected by the error caused by the improper use of the "identical shunt impedances model" (as proved by the results obtained in the previous tests), those are the ones best suited to be assumed as known.

This means that a first algorithm run with the wrong model could be used to collect data (**Z2**) for a second one, based on Figure 46. Eq. 41 and Eq. 42 can be solved thanks to the approximate knowledge of **Z2**, which is not exact but close enough, producing results for **Z1** and **Z3** that are closer to reality than those previously obtained:

Z=500 Ω and cos φ=1:

- X_Cd=5 Ω, while the Validator's output is 4.7794 Ω; (-4.41%)

Z=1000 Ω and cos φ=1:

- X_Cd=23 Ω, while the Validator's output is 16.4047 Ω; (-28.68%)

Z=5000 Ω and cos φ=1:

- X_Cd=518 Ω, while the Validator's output is 326.2888 Ω; (-37.01%)

Z=8000 Ω and cos φ=1:

- X_Cd=1135 Ω, while the Validator's output is 744.6114 Ω; (-34.40%)

Z=590.5 Ω and cos φ=0.85: (inductive)

- X_Cd=107 Ω, while the Validator's output is 100.8556 Ω; (-5.74%)

Z=1048 Ω and cos φ=0.95: (inductive)

- X_Cd=124 Ω, while the Validator's output is 78.2072 Ω; (-36.93%)

Z=1181 Ω and cos φ=0.85: (inductive)

- X_Cd=221 Ω, while the Validator's output is 190.2606 Ω; (-13.91%)

The error on the shunt parameters' estimation is drastically decreased. In order to further reduce it, the application of an iterative error minimization method – for example one similar to the Weighted Least Squares formulation used for System State Estimation – could prove to be a useful solution. This however will be the subject of future studies, based on the results of this one.

3.4 Validator testing with real PMUs

Standing on the technical basis developed during the simulation-based experiments, the study of real PMUs' interactions with the simulated network was the last step of the work in the laboratories. The objective was to both develop technical expertise working with real PMUs and to verify the ability of the RTDS to interact with external devices.

In this particular case, the RDTS acted as data publisher for the PMUs. After the required software setting and cabling connection phase, analog signals were streamed through the GTAO cards in real time, reaching the input pins of the SEL machinery as shown in Figure 47. The RTDS outputs were the following: the three phase voltages and three line currents measured at the beginning of section T4739 of Feeder 1, and then the same quantities measured at the end of section T3003. Those were sent as inputs to the two PMU at disposal: the SEL 411L model and the SEL AXION model. Their analog input ports were called "Y" for voltages and "W" for currents.

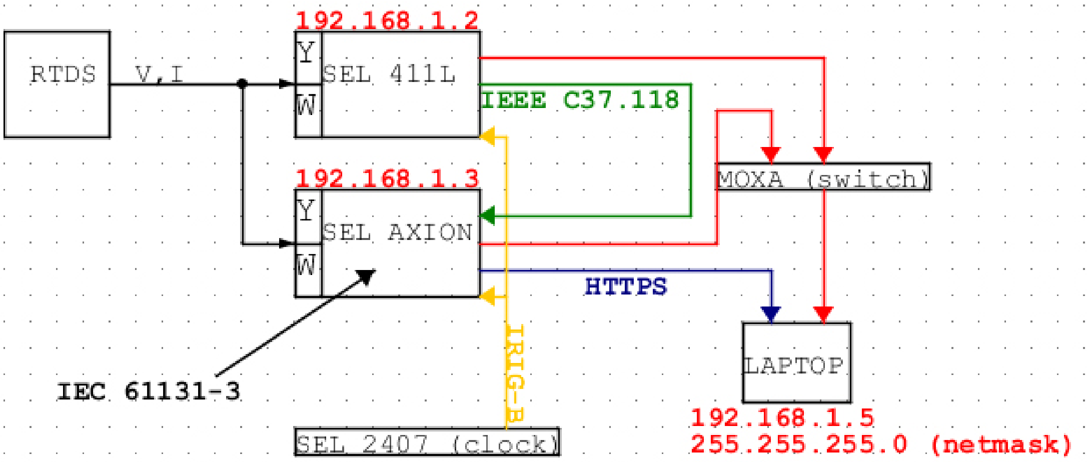

Figure 47 Block scheme of the communication network used during the experiment.

Two different PMU models were chosen for a reason: while the SEL 411L only has basic PMU features (measurement and relaying), the AXION model can also act as a Phasor Data

Collector (PDC) and possesses computational capabilities. After analog input elaboration (sampling and data digitalization), the two machines communicate using the IEEE C37.118 protocol (also called “synchrophasors protocol”, since it is considered the best for phasor data communication as of now). The simpler PMU (SEL 411L) publishes the phasors it created after their elaboration. Then the AXION receives them as well as creating its own ones simultaneously. Further calculations take place in the latter, producing sequence phasor quantities but also running the Validator’s algorithm. The code was in fact implemented in this device through the programming protocol IEC 61131-3, a C-like language, taking the form shown in Appendix A.9.

Since no synchrophasor would have meaning without precise synchronization, a SEL 2407 clock was also installed on the rack with the other devices. Thanks to the IRIG-B protocol, widely used by electric utilities to ensure precise time synchronization of power system devices, both PMUs were able to assure high quality for their outputs. These data, including the network parameters calculated by the AXION, were then made available to the operator via a Human-Machine Interface (HMI). The HMI was both easy to consult and safe thanks to the HTTPS protocol.

As for the transport layer, the communication between devices is enstablished by a dedicated small private network. The IPv4 addresses were assigned as shown in Figure 47.

The complete installation on the rack is shown in Figure 48.

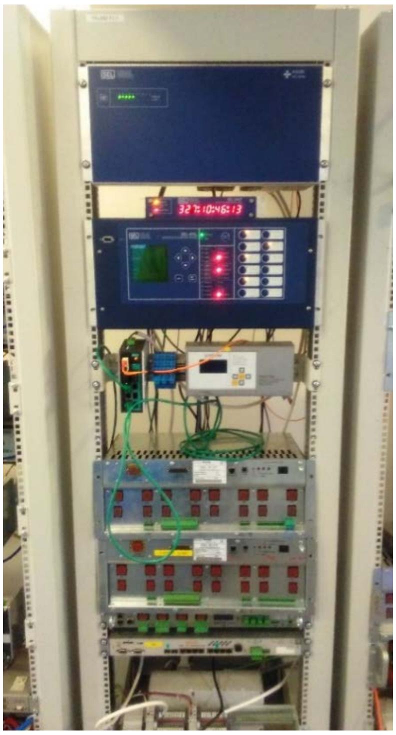

Figure 48 From the top: the AXION PMU model, the SEL 2407 clock, the SEL 411L PMU model.

Due to unforeseen technical issues with the equipment, the experiments could not produce the expected results in due time. However, the work is still in progress and will be subject to further analysis in the near future.

3.5 Clock accuracy requirements for PMUs' distribution applications

Phasor Measurement Units, as shown by this thesis work, have much potential in terms of future applications on the Italian distribution network. The validation – or even from scratch creation – of network parameters' databases is but one of the possible ways their installation could benefit a DSO, as it has been clearly shown in the second chapter of this endeavor. However, from a grid manager point of view, any potential network upgrade must always be evaluated in relationship not only to the technical improvements it could bring, but also to its economic implications. PMUs are, in fact, no cheap devices and because of their intrinsic network-based nature they need to be acquired in vast stocks in order to be employed effectively. The investment could easily become unacceptably high, especially considering the extension of the distribution grid and consequently the number of nodes to be monitored with a PMU.

Since an accurate evaluation of the actual cost/benefit ratio of such an installation would be a matter far too complex and long to be properly analyzed in this paper, a different – and possibly more achievable – alternative is taken in consideration. That is the possibility to upgrade already in place RGDM (*Rilevatore di Guasto Direzionale e Misure*) devices to transform them into proprietary PMUs. Making use of already existing machinery could, in fact, imply a reduction of the initial investment big enough to justify it. Still, in order to get a general idea of the feasibility of such a project, the components needed for the upgrade must be investigated and their costs evaluated. After a consultation meeting with e-distribuzione's experts on the matter, it emerged that there is only one missing component to proceed in that direction: a clock precise enough to guarantee accuracy levels for the phasor measurements high enough to make any of the mentioned applications viable.

The clock accuracy requirements for PMUs' distribution applications not necessarily coincide with the standards used for transmission applications (±500 ns, with a normal distribution), since the angle differences measured in those cases are far greater and suffer less from a lack of synchronization errors. Therefore, a custom study of the matter was needed. It was based on the equation that links time accuracy σ_T (expressed in seconds) and the resulting angle measurement errors σ_A (expressed in degrees or radians). Both of these values are standard deviations, quantities used to describe the degree of dispersion of a set of data values from its expected value.

$$\sigma_A = \frac{\sigma_T}{seconds\ per\ cycle} \cdot degrees\ per\ cycle = \frac{\sigma_T}{0.02} \cdot 360° \qquad \text{Eq. 43}$$

Eq. 43 has a general validity, but here it had to be adapted to the Italian grid characteristics. (50 Hz → 0.02 seconds per cycle) If, for example, σ_T=±10 μs was taken into consideration, then it would imply that the PMU measurements angle accuracy would be equal to σ_A=±0.18°. Is it good enough for distribution applications? If not, what value should be chosen for σ_T in order for it to be considered acceptable? It all depends on the angle differences $\Delta\theta$ between neighboring Secondary Substations: phasor angle accuracy should be at most ±10% of the smallest measurable angle difference.

Experiments conducted with the assistance of the RTDS proved that the smallest angle differences are attested when analyzing voltages. (in the order of the thousandth of degree, while for currents it is always at least some degrees) Therefore, a number of tests were run in order to obtain both said difference (easy to find, since it was obviously measured between the two substations connected by the shorter link) and an average value for the grid used as an example. (the same one examined in the third chapter of this work) The results were the following:

$$\Delta\vartheta_{average} = 0.0313° \rightarrow \sigma_A = \pm 0.1 \cdot \Delta\vartheta_{minimum} = \pm 0.00313° \rightarrow \sigma_T = \pm 173\text{ns} \qquad \text{Eq. 44}$$

$$\Delta\vartheta_{minimum} = 0.0011° \rightarrow \sigma_A = \pm 0.1 \cdot \Delta\vartheta_{average} = \pm 0.00011° \rightarrow \sigma_T = \pm 6.1\text{ns} \qquad \text{Eq. 45}$$

As it can be immediately noticed, the required time accuracy is considerably lower than the standard for transmission lines. This is of course understandable, since longer distances between Substations imply bigger angle differences between the voltage phasors. However, these levels of average time accuracy requirements are nothing that cannot be handled by modern synchronization devices: as for the suggestion of a SEL (*Schweitzer Engineering Laboratories*) technician, a good choice for this kind of upgrade would be the SEL-2401 satellite-synchronized clock. With its ±100 ns time accuracy, intentionally designed to provide timing signals for IEEE C37.118 ("synchrophasors protocol") control applications – such as the ones studied by this paper –, this device is guaranteed to commit errors almost two times lower than the limit calculated through Eq. 44. This is, of course, a very positive result: it means that there is already existing technology that can support the potential RGDM→PMU transition without problematic technical constraints. The same cannot be said, of course, looking at Eq. 45, but here is the kicker: that particular measurement was taken where two Secondary Substations were divided by a very short distance, and connected by a very short link; this situation is extremely rare and unlikely, in this case probably dictated by special needs, thus it cannot be taken as an example of a possible obstacle to the aforementioned transition. In cases like this, in fact, it would be sufficient to just skip one of the Substation (as if it did not exist at all) and base any estimation on the measurements obtained by the next one, which for sure would be far enough to grant an appropriate degree of accuracy.

All of these observations are even more true when the grid is considered unloaded no more and a realistic load scenario is simulated: the differences between the angles widens, and therefore also the tolerated error margins increase accordingly. This further proves the technical feasibility of the RGDM upgrade project, but tells nothing more in terms of financial feasibility.

The economic impact of such an installment, in fact, is very difficult to properly evaluate. However, assuming to be allowed to simplify the matter to a certain degree, a rough estimation can be done. Assuming a cost of 1000 USD for each synchronization device, that is the price of the SEL-2401 unit, and considering all the Secondary Substations spread across the county (around 400000 in total), then the expected CAPEX for the operation would be around 400 million dollars. (more or less 340 million euros) This figure is likely to increase considering all the related operative costs, but it is also presumable it could decrease because of stock discounts or a smaller number of units bought in order to by-pass, as explained before, some Secondary Substations when too close to another one.

In conclusion, whatever the actual amount may be, the GPS clocks' installation has to be valued in relationship to the long time horizon benefits their symbiosis with the RGDMs could produce: if the overall increase in Quality of Service (QoS) is high enough to justify it, then it could prove to be a good investment. (QoS improvements are in fact rewarded with monetary benefits granted to the virtuous DSOs) However, there is another important variable to keep under control: the cost of a μPMU. If this new device, nowadays still under development, in the near future happened to undergo a fast technical and commercial maturation, then it would prove to be a cheaper and more effective alternative to buy and install. It would not be wise, in fact, to disregard the evolution competitive solutions while working on a proprietary one.

CONCLUSION

Phasor Measurement Units technology, thanks to the fast and yet still accelerating growth of telecommunication assets employed in the electrical field, could prove to be a precious asset in a not far future.

The wide range of synchrophasors applications for distribution utilities, both in terms of radical innovation and improvement of already existing control techniques, has an untapped potential that nowadays is yet to be disclosed – or even fully understood. However researches like the one described in this work clearly show that there is much to be learned, and even more to be gained: the creation of the network model Validator, which was the main focus of the thesis, is an example of this. Such an application, as experimented through the use of a complex but powerful MV grid simulator, could in fact grant the DSO the chance not only to update its already existing network parameters' databases, but it could also create new ones from scratches where they are most needed. (e.g. South American networks, after their acquisition, are still in need of an accurate mapping and overall review) This is particularly important while speaking of zero sequence parameters, whose precise estimation has always been a problem for system operators.

The research, however, also offers hints for future development: if the issues with direct sequence parameters' estimation in normal load conditions were to be solved, then their link with load fluctuations could be exploited to develop a real-time high-resolution load profile monitoring system, capable of precisely tracking power flow trends on a small scale. The information produced by such a system could be useful in many different ways: dispatching services planning, more accurate and fast voltage and frequency regulation, strategic network development, etc.

In conclusion, in a world where information is becoming more and more a key-factor for innovation and success, where Smart devices are steadily replacing traditional ones and Big Data production and management is the next big thing, PMUs have the potential to become part of the next generation equipment that will define the shape of the electrical industry's future.

Bibliography

[1] F. Katiraei, M. R. Iravani, P. F. W. P. Lehn, "Micro-grid autonomous operation during and subsequent to islanding process", *IEEE Trans. Power Del.*, vol. 20, no. 1, pp. 248-257, Jan. 2005.

[2] Yingchen Zhang, P. Markham, Tao Xia, Lang Chen, Yanzhu Ye, Zhongyu Wu, Zhiyong Yuan, Lei Wang, J. Bank, J. Burgett, R. W. Conners, Yilu Liu, "Wide-area frequency monitoring network (FNET) architecture and applications", *IEEE Trans. on Smart Grid*, vol. 1, no. 2, pp. 159-167, Sept. 2010.

[3] A. Riepnieks, H. Kirkham, L. Ribickis, "Considerations for phasor measurement unit introduction in distribution systems", *Power and Electrical Engineering of Riga Technical University Conference (RTUCON)*, pp. 1-6, Oct. 2015.

[4] G. Hataway, B. Flerchinger, R. Moxley, "Synchrophasors for Distribution Applications", *Power and Energy Automation Conference*, pp.4-5, Mar. 2013.

[5] R. Moxley, "Synchrophasors in the Real World", *7th Annual Western Power Delivery Automation Conference*, May 2005

[6] E. O. Schweitzer III, D. E. Whithead, "Real-Time Power System Control Using Synchrophasors", *62nd Annual Georgia Tech Protective Relaying Conference*, May 2008

[7] C. Muscas, M. Pau, P.A. Pegoraro, S. Sulis, J. Liu, F. Ponci, A. Monti, "Stima dello stato e della pianificazione ottima di un sistema di misura distribuito robusto per reti elettriche di distribuzione", *XXX Congresso GMEE*, Sep. 2013

[8] "Remedial Action Scheme" Definition Development: Background and Frequently Asked Questions, NERC, June 2014

[9] J. Spears, "Blackout 2003: How Ontario went dark", *The Star*, August 2013

[10] W. O'Brien, E. Udren, K. Garg, D. Haes, B. Sridharan, "Catching Falling Conductors in Midair – Detecting and Tripping Broken Distribution Circuit Conductors at Protection Speeds", *69th Annual Conference for Protective Relay Engineers*, Apr. 2016

[11] A. H. Al-Mohammed, M. A. Abido, "Fault Location Based on Synchronized Measurements: A Comprehensive Survey", *The Scientific World Journal*, vol. 2014, Feb. 2014

[12] Saha M, Izykowski J, Rosolowski E. *Fault Location on Power Network*. New York, NY, USA: Springer; 2010

[13] L. Cibulka, “Synchrophasors: How Are They Making the Electric Grid Smarte”, *The i4Energy Seminar Series*, Feb. 2011

[14] R. Arghandeh, “Towards Micro-synchrophasors (μPMUs) for Distribution Networks”, *IEEE Power Engineering Society Dissertation*, Oct. 2013

APPENDICES

A.1 PI-model distribution line’s sequence parameters calculation

Figure 49 is an alternative representation of the circuit seen in Figure 14. Eq. 17 and Eq. 20 are the starting point of the whole experimental endeavor reported in this thesis, so their validation was of pivotal importance.

The demonstration follows:

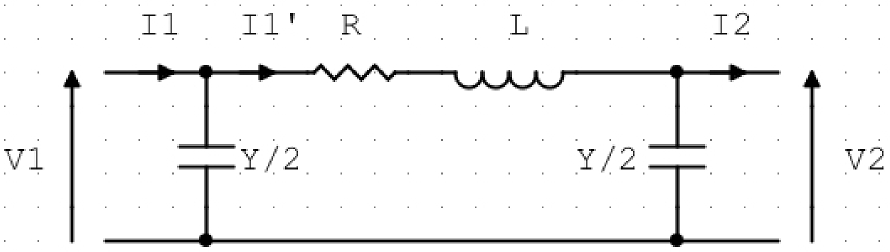

Figure 49 Simplified distribution line model.

Kirchhoff laws are applied to obtain the following equations:

$$\begin{cases} \boldsymbol{V_2} = \boldsymbol{V_1} - \boldsymbol{I_1}'\boldsymbol{Z} \\ \boldsymbol{I_2} = \boldsymbol{I_1} - \boldsymbol{V_1}\frac{\boldsymbol{Y}}{2} - \boldsymbol{V_2}\frac{\boldsymbol{Y}}{2} \end{cases}$$

The first equation is solved for **Z** and the second for **Y**:

$$\begin{cases} \boldsymbol{Z} = \dfrac{\boldsymbol{V_1} - \boldsymbol{V_2}}{\boldsymbol{I_1}'} \\ \boldsymbol{Y} = 2\dfrac{\boldsymbol{I_1} - \boldsymbol{I_2}}{\boldsymbol{V_1} - \boldsymbol{V_2}} \end{cases}$$

The second equation already proves the initial statement, while the first still needs some elaboration. Applying the KCL on the upper left-hand side of the circuit, the expression $\boldsymbol{I_1'} = \boldsymbol{I_1} - \boldsymbol{V_1}\frac{\boldsymbol{Y}}{2}$ can be obtained and used to find **Z**:

$$\boldsymbol{Z} = \frac{\boldsymbol{V_1} - \boldsymbol{V_2}}{\boldsymbol{I_1}'} = \frac{\boldsymbol{V_1} - \boldsymbol{V_2}}{\boldsymbol{I_1} - \boldsymbol{V_1}\dfrac{\boldsymbol{Y}}{2}}$$

Knowing that $\frac{\boldsymbol{Y}}{2} = \frac{\boldsymbol{I_1}-\boldsymbol{I_2}}{\boldsymbol{V_1}-\boldsymbol{V_2}}$ **:**

$$\boldsymbol{Z} = \frac{\boldsymbol{V_1} - \boldsymbol{V_2}}{\boldsymbol{I_1} - \boldsymbol{V_1}\dfrac{\boldsymbol{I_1} - \boldsymbol{I_2}}{\boldsymbol{V_1} - \boldsymbol{V_2}}} = \frac{\boldsymbol{V_1} - \boldsymbol{V_2}}{\dfrac{\boldsymbol{I_1}\boldsymbol{V_1} + \boldsymbol{I_1}\boldsymbol{V_2} - \boldsymbol{I_1}\boldsymbol{V_1} + \boldsymbol{I_2}\boldsymbol{V_1}}{\boldsymbol{V_1} + \boldsymbol{V_2}}} =$$

$$= \frac{(\boldsymbol{V_1} - \boldsymbol{V_2})(\boldsymbol{V_1} + \boldsymbol{V_2})}{\boldsymbol{I_1}\boldsymbol{V_2} + \boldsymbol{I_2}\boldsymbol{V_1}} = \frac{\boldsymbol{V_1^2} - \boldsymbol{V_2^2}}{\boldsymbol{I_1}\boldsymbol{V_2} + \boldsymbol{I_2}\boldsymbol{V_1}}$$

Quod erat demostrandum:

$$\begin{cases} \boldsymbol{Z} = \dfrac{\boldsymbol{V_1^2} - \boldsymbol{V_2^2}}{\boldsymbol{I_1}\boldsymbol{V_2} + \boldsymbol{I_2}\boldsymbol{V_1}} \\ \boldsymbol{Y} = 2\dfrac{\boldsymbol{I_1} - \boldsymbol{I_2}}{\boldsymbol{V_1} - \boldsymbol{V_2}} \end{cases}$$

A.2 Eq.34 and Eq.37 validation test

MATLAB code created to validate Eq. 34 and Eq. 37 by means of comparison of their results with the ones produced by Eq. 17 and Eq. 20:

```
clc
clear all

% Positive sequence parameters computation using Eq.17 and Eq.20
Vd1=11530+5.866i;
Vd2=10250+281.3i;
Id1=106.5-50.76i;
Id2=106.5-50.91i;

Zd=(Vd1^2-Vd2^2)/(Id1*Vd2+Id2*Vd1);
Yd=2*(Id1-Id2)/(Vd1+Vd2);
Rd=real(Zd)
```

```
Xd_L=imag(Zd)
Bd=imag(Yd);
Xd_C=1/Bd

% Zero sequence parameters computation using Eq.17 and Eq.20
Vo1=-163.8+162.8i;
Vo2=-151.1+183.4i;
Io1=0.007981+0.01018i;
Io2=-0.01182-0.01648i;

Zo=(Vo1^2-Vo2^2)/(Io1*Vo2+Io2*Vo1);
Yo=2*(Io1-Io2)/(Vo1+Vo2);
Ro=real(Zo)
Xo_L=imag(Zo)
Bo=imag(Yo);
Xo_C=1/Bo

% Eq.34 and Eq.37 validation test

Vd1r=real(Vd1);
Vd1i=imag(Vd1);
Vd2r=real(Vd2);
Vd2i=imag(Vd2);
Id1r=real(Id1);
Id1i=imag(Id1);
Id2r=real(Id2);
Id2i=imag(Id2);
Vo1r=real(Vo1);
Vo1i=imag(Vo1);
Vo2r=real(Vo2);
Vo2i=imag(Vo2);
Io1r=real(Io1);
Io1i=imag(Io1);
Io2r=real(Io2);
Io2i=imag(Io2);

Rdnew=((Vd1r^2-Vd1i^2-Vd2r^2+Vd2i^2)*(Id1r*Vd2r-Id1i*Vd2i+Id2r*Vd1r-
Id2i*Vd1i)+2*(Vd1r*Vd1i-
Vd2r*Vd2i)*(Id1r*Vd2i+Id1i*Vd2r+Id2r*Vd1i+Id2i*Vd1r))/((Id1r*Vd2r-
Id1i*Vd2i+Id2r*Vd1r-
Id2i*Vd1i)^2+(Id1r*Vd2i+Id1i*Vd2r+Id2r*Vd1i+Id2i*Vd1r)^2)
Xd_Lnew=(2*(Vd1r*Vd1i-Vd2r*Vd2i)*(Id1r*Vd2r-Id1i*Vd2i+Id2r*Vd1r-
Id2i*Vd1i)-(Vd1r^2-Vd1i^2-
Vd2r^2+Vd2i^2)*(Id1r*Vd2i+Id1i*Vd2r+Id2r*Vd1i+Id2i*Vd1r))/((Id1r*Vd2
r-Id1i*Vd2i+Id2r*Vd1r-
Id2i*Vd1i)^2+(Id1r*Vd2i+Id1i*Vd2r+Id2r*Vd1i+Id2i*Vd1r)^2)
Bdnew=2*((Id1i-Id2i)*(Vd1r+Vd2r)-(Id1r-
Id2r)*(Vd1i+Vd2i))/((Vd1r+Vd2r)^2+(Vd1i+Vd2i)^2);
Xd_Cnew=1/Bdnew

Ronew=((Vo1r^2-Vo1i^2-Vo2r^2+Vo2i^2)*(Io1r*Vo2r-Io1i*Vo2i+Io2r*Vo1r-
Io2i*Vo1i)+2*(Vo1r*Vo1i-
Vo2r*Vo2i)*(Io1r*Vo2i+Io1i*Vo2r+Io2r*Vo1i+Io2i*Vo1r))/((Io1r*Vo2r-
Io1i*Vo2i+Io2r*Vo1r-
Io2i*Vo1i)^2+(Io1r*Vo2i+Io1i*Vo2r+Io2r*Vo1i+Io2i*Vo1r)^2)
```

```
Xo_Lnew=(2*(Vo1r*Vo1i-Vo2r*Vo2i)*(Io1r*Vo2r-Io1i*Vo2i+Io2r*Vo1r-
Io2i*Vo1i)-(Vo1r^2-Vo1i^2-
Vo2r^2+Vo2i^2)*(Io1r*Vo2i+Io1i*Vo2r+Io2r*Vo1i+Io2i*Vo1r))/((Io1r*Vo2
r-Io1i*Vo2i+Io2r*Vo1r-
Io2i*Vo1i)^2+(Io1r*Vo2i+Io1i*Vo2r+Io2r*Vo1i+Io2i*Vo1r)^2)
Bonew=2*((Io1i-Io2i)*(Vo1r+Vo2r)-(Io1r-
Io2r)*(Vo1i+Vo2i))/((Vo1r+Vo2r)^2+(Vo1i+Vo2i)^2);
Xo_Cnew=1/Bonew
```

A.3 PMU-based model validator code version 1.0

The following is the code written for the first version of the Validator, the one made to receive synchrophasors directly (as complex numbers):

```
VERSION:
3.001

// Include file below is generated by C-Builder
// and contains the variables declared as -
// PARAMETERS, INPUTS, OUTPUTS . . .
#include "Validator.h"
STATIC:

// ----------------------------------------------
// Variables declared here may be used in both the
// RAM: and CODE: sections below.
// ----------------------------------------------
//    double dt;

double Vd1r;
double Vd1i;
double Vd2r;
double Vd2i;
double Id1r;
double Id1i;
double Id2r;
double Id2i;
double Vo1r;
double Vo1i;
double Vo2r;
double Vo2i;
double Io1r;
double Io1i;
double Io2r;
double Io2i;
double Bd;
double Bo;
double a,b,c,d,e,f,g,h,i,l,m,n;
double sqVd1r;
double sqVd1i;
double sqVd2r;
double sqVd2i;
double sqVo1r;
double sqVo1i;
double sqVo2r;
double sqVo2i;

// - E n d   o f   S T A T I C :   S e c t i o n -

RAM_FUNCTIONS:

// -----------------------------------------------
// This section should contain any 'c' functions
// to be called from the RAM section (either
// RAM_PASS1 or RAM_PASS2). Example:
//
// static double myFunction(double v1, double v2)
// {
//     return(v1*v2);
// }
// -----------------------------------------------

RAM:

// -----------------------------------------------
// Place C code here which computes constants
// required for the CODE: section below.  The C
// code here is executed once, prior to the start
// of the simulation case.
// -----------------------------------------------
//    dt= getTimeStep();

sqVd1r=Vd1r*Vd1r;
sqVd1i=Vd1i*Vd1i;
sqVd2r=Vd2r*Vd2r;
sqVd2i=Vd2i*Vd2i;
a=(Id1r*Vd2r-Id1i*Vd2i+Id2r*Vd1r-Id2i*Vd1i);
b=(Id1r*Vd2i+Id1i*Vd2r+Id2r*Vd1i+Id2i*Vd1r);
c=1/(a*a+b*b);
d=(Vd1r+Vd2r)*(Vd1r+Vd2r);
e=(Vd1i+Vd2i)*(Vd1i+Vd2i);
f=1/(d+e);

sqVo1r=Vo1r*Vo1r;
sqVo1i=Vo1i*Vo1i;
sqVo2r=Vo2r*Vo2r;
sqVo2i=Vo2i*Vo2i;
g=(Io1r*Vo2r-Io1i*Vo2i+Io2r*Vo1r-Io2i*Vo1i);
h=(Io1r*Vo2i+Io1i*Vo2r+Io2r*Vo1i+Io2i*Vo1r);
i=1/(g*g+h*h);
l=(Vo1r+Vo2r)*(Vo1r+Vo2r);
m=(Vo1i+Vo2i)*(Vo1i+Vo2i);
n=1/(l+m);


// ------------- End of RAM: Section -------------

CODE:
```

```
// -----------------------------------------------
// Place C code here which runs on the RTDS. The
// code below is entered once each simulation
// step.
// -----------------------------------------------

Vd1r=Vd1[0];
Vd1i=Vd1[1];
Vd2r=Vd2[0];
Vd2i=Vd2[1];
Id1r=Id1[0];
Id1i=Id1[1];
Id2r=Id2[0];
Id2i=Id2[1];
Vo1r=Vo1[0];
Vo1i=Vo1[1];
Vo2r=Vo2[0];
Vo2i=Vo2[1];
Io1r=Io1[0];
Io1i=Io1[1];
Io2r=Io2[0];
Io2i=Io2[1];

//Code containing squares expressed as "^2"
//Rd=((Vd1r^2-Vd1i^2-Vd2r^2+Vd2i^2)*(Id1r*Vd2r-Id1i*Vd2i+Id2r*Vd1r-
Id2i*Vd1i)+2*(Vd1r*Vd1i-
Vd2r*Vd2i)*(Id1r*Vd2i+Id1i*Vd2r+Id2r*Vd1i+Id2i*Vd1r))/((Id1r*Vd2r-
Id1i*Vd2i+Id2r*Vd1r-
Id2i*Vd1i)^2+(Id1r*Vd2i+Id1i*Vd2r+Id2r*Vd1i+Id2i*Vd1r)^2);
//X_Ld=(2*(Vd1r*Vd1i-Vd2r*Vd2i)*(Id1r*Vd2r-Id1i*Vd2i+Id2r*Vd1r-
Id2i*Vd1i)-(Vd1r^2-Vd1i^2-
Vd2r^2+Vd2i^2)*(Id1r*Vd2i+Id1i*Vd2r+Id2r*Vd1i+Id2i*Vd1r))/((Id1r*Vd2
r-Id1i*Vd2i+Id2r*Vd1r-
Id2i*Vd1i)^2+(Id1r*Vd2i+Id1i*Vd2r+Id2r*Vd1i+Id2i*Vd1r)^2);
//Bd=2*((Id1i-Id2i)*(Vd1r+Vd2r)-(Id1r-
Id2r)*(Vd1i+Vd2i))/((Vd1r+Vd2r)^2+(Vd1i+Vd2i)^2);
//X_Cd=1/Bd;

//Ro=((Vo1r^2-Vo1i^2-Vo2r^2+Vo2i^2)*(Io1r*Vo2r-Io1i*Vo2i+Io2r*Vo1r-
Io2i*Vo1i)+2*(Vo1r*Vo1i-
Vo2r*Vo2i)*(Io1r*Vo2i+Io1i*Vo2r+Io2r*Vo1i+Io2i*Vo1r))/((Io1r*Vo2r-
Io1i*Vo2i+Io2r*Vo1r-
Io2i*Vo1i)^2+(Io1r*Vo2i+Io1i*Vo2r+Io2r*Vo1i+Io2i*Vo1r)^2);
//X_Lo=(2*(Vo1r*Vo1i-Vo2r*Vo2i)*(Io1r*Vo2r-Io1i*Vo2i+Io2r*Vo1r-
Io2i*Vo1i)-(Vo1r^2-Vo1i^2-
Vo2r^2+Vo2i^2)*(Io1r*Vo2i+Io1i*Vo2r+Io2r*Vo1i+Io2i*Vo1r))/((Io1r*Vo2
r-Io1i*Vo2i+Io2r*Vo1r-
Io2i*Vo1i)^2+(Io1r*Vo2i+Io1i*Vo2r+Io2r*Vo1i+Io2i*Vo1r)^2);
//Bo=2*((Io1i-Io2i)*(Vo1r+Vo2r)-(Io1r-
Io2r)*(Vo1i+Vo2i))/((Vo1r+Vo2r)^2+(Vo1i+Vo2i)^2);
//X_Co=1/Bo;

//Code with explicitated squares of two
//Rd=((Vd1r*Vd1r-Vd1i*Vd1i-Vd2r*Vd2r+Vd2i*Vd2i)*(Id1r*Vd2r-
Id1i*Vd2i+Id2r*Vd1r-Id2i*Vd1i)+2*(Vd1r*Vd1i-
Vd2r*Vd2i)*(Id1r*Vd2i+Id1i*Vd2r+Id2r*Vd1i+Id2i*Vd1r))/((Id1r*Vd2r-
Id1i*Vd2i+Id2r*Vd1r-Id2i*Vd1i)*(Id1r*Vd2r-Id1i*Vd2i+Id2r*Vd1r-
Id2i*Vd1i)+(Id1r*Vd2i+Id1i*Vd2r+Id2r*Vd1i+Id2i*Vd1r)*(Id1r*Vd2i+Id1i
*Vd2r+Id2r*Vd1i+Id2i*Vd1r));
//X_Ld=(2*(Vd1r*Vd1i-Vd2r*Vd2i)*(Id1r*Vd2r-Id1i*Vd2i+Id2r*Vd1r-
Id2i*Vd1i)-(Vd1r*Vd1r-Vd1i*Vd1i-
Vd2r*Vd2r+Vd2i*Vd2i)*(Id1r*Vd2i+Id1i*Vd2r+Id2r*Vd1i+Id2i*Vd1r))/((Id
1r*Vd2r-Id1i*Vd2i+Id2r*Vd1r-Id2i*Vd1i)*(Id1r*Vd2r-
Id1i*Vd2i+Id2r*Vd1r-
Id2i*Vd1i)+(Id1r*Vd2i+Id1i*Vd2r+Id2r*Vd1i+Id2i*Vd1r)*(Id1r*Vd2i+Id1i
*Vd2r+Id2r*Vd1i+Id2i*Vd1r));
//Bd=2*((Id1i-Id2i)*(Vd1r+Vd2r)-(Id1r-
Id2r)*(Vd1i+Vd2i))/((Vd1r+Vd2r)*(Vd1r+Vd2r)+(Vd1i+Vd2i)*(Vd1i+Vd2i))
;
//X_Cd=1/Bd;

//Ro=((Vo1r*Vo1r-Vo1i*Vo1i-Vo2r*Vo2r+Vo2i*Vo2i)*(Io1r*Vo2r-
Io1i*Vo2i+Io2r*Vo1r-Io2i*Vo1i)+2*(Vo1r*Vo1i-
Vo2r*Vo2i)*(Io1r*Vo2i+Io1i*Vo2r+Io2r*Vo1i+Io2i*Vo1r))/((Io1r*Vo2r-
Io1i*Vo2i+Io2r*Vo1r-Io2i*Vo1i)*(Io1r*Vo2r-Io1i*Vo2i+Io2r*Vo1r-
Io2i*Vo1i)+(Io1r*Vo2i+Io1i*Vo2r+Io2r*Vo1i+Io2i*Vo1r)*(Io1r*Vo2i+Io1i
*Vo2r+Io2r*Vo1i+Io2i*Vo1r));
//X_Lo=(2*(Vo1r*Vo1i-Vo2r*Vo2i)*(Io1r*Vo2r-Io1i*Vo2i+Io2r*Vo1r-
Io2i*Vo1i)-(Vo1r*Vo1r-Vo1i*Vo1i-
Vo2r*Vo2r+Vo2i*Vo2i)*(Io1r*Vo2i+Io1i*Vo2r+Io2r*Vo1i+Io2i*Vo1r))/((Io
1r*Vo2r-Io1i*Vo2i+Io2r*Vo1r-Io2i*Vo1i)*(Io1r*Vo2r-
Io1i*Vo2i+Io2r*Vo1r-
Io2i*Vo1i)+(Io1r*Vo2i+Io1i*Vo2r+Io2r*Vo1i+Io2i*Vo1r)*(Io1r*Vo2i+Io1i
*Vo2r+Io2r*Vo1i+Io2i*Vo1r));
//Bo=2*((Io1i-Io2i)*(Vo1r+Vo2r)-(Io1r-
Io2r)*(Vo1i+Vo2i))/((Vo1r+Vo2r)*(Vo1r+Vo2r)+(Vo1i+Vo2i)*(Vo1i+Vo2i))
;
//X_Co=1/Bo;

//Optimized code
Rd=((sqVd1r-sqVd1i-sqVd2r+sqVd2i)*(Id1r*Vd2r-Id1i*Vd2i+Id2r*Vd1r-
Id2i*Vd1i)+2*(Vd1r*Vd1i-
Vd2r*Vd2i)*(Id1r*Vd2i+Id1i*Vd2r+Id2r*Vd1i+Id2i*Vd1r))*c;
X_Ld=(2*(Vd1r*Vd1i-Vd2r*Vd2i)*(Id1r*Vd2r-Id1i*Vd2i+Id2r*Vd1r-
Id2i*Vd1i)-(sqVd1r-sqVd1i-
sqVd2r+sqVd2i)*(Id1r*Vd2i+Id1i*Vd2r+Id2r*Vd1i+Id2i*Vd1r))*c;
Bd=2*((Id1i-Id2i)*(Vd1r+Vd2r)-(Id1r-Id2r)*(Vd1i+Vd2i))*f;
X_Cd=1/Bd;

Ro=((sqVo1r-sqVo1i-sqVo2r+sqVo2i)*(Io1r*Vo2r-Io1i*Vo2i+Io2r*Vo1r-
Io2i*Vo1i)+2*(Vo1r*Vo1i-
Vo2r*Vo2i)*(Io1r*Vo2i+Io1i*Vo2r+Io2r*Vo1i+Io2i*Vo1r))*i;
X_Ld=(2*(Vo1r*Vo1i-Vo2r*Vo2i)*(Io1r*Vo2r-Io1i*Vo2i+Io2r*Vo1r-
Io2i*Vo1i)-(sqVo1r-sqVo1i-
sqVo2r+sqVo2i)*(Io1r*Vo2i+Io1i*Vo2r+Io2r*Vo1i+Io2i*Vo1r))*i;
Bd=2*((Io1i-Io2i)*(Vo1r+Vo2r)-(Io1r-Io2r)*(Vo1i+Vo2i))*n;
X_Co=1/Bo;

// ------------ End of CODE: Section -------------
```

The code mentions, at the beginning, the inclusion of a “Validator.h” file. It is simply the automatic initialization of input and output parameters, so it is not worth reporting here.

A.4 Symmetrical components and Fortescue matrix

Symmetrical components’ transformation (also known as “sequence transformation”) is an effective technique used to study three-phase sinusoidal systems. It exploits the three-phase symmetry of variables and parameters to simplify the relationships among them. It is applied in the phasor domain (complex constants that share a bijective correspondence with sinusoidal iso-frequential waveforms) to triad of variable, like voltages, currents, fluxes, etc.

Symmetrical components’ transformation is applied using the following matrix, filled with constant complex coefficients:

$$\boldsymbol{T} = \frac{1}{3}\begin{bmatrix} 1 & \boldsymbol{\alpha} & \boldsymbol{\alpha^2} \\ 1 & \boldsymbol{\alpha^2} & \boldsymbol{\alpha} \\ 1 & 1 & 1 \end{bmatrix} \qquad \text{with} \quad \begin{cases} \boldsymbol{\alpha} = e^{j\frac{2}{3}\pi} = -\frac{1}{2} + j\frac{\sqrt{3}}{2} \\ \boldsymbol{\alpha^2} = e^{-j\frac{2}{3}\pi} = -\frac{1}{2} - j\frac{\sqrt{3}}{2} \end{cases}$$

The complex constant $\boldsymbol{\alpha}$ is a unit vector that, when multiplied to another vector, makes it rotate by 120° counterclockwise. (positive direction) The complex constant $\boldsymbol{\alpha^2}$ makes it rotate by -120° counterclockwise. (negative direction) It is useful to know that $\boldsymbol{\alpha^3} = \boldsymbol{1}$ and $1 + \boldsymbol{\alpha} + \boldsymbol{\alpha^2} = \boldsymbol{0}$.

When applied, for example, to the three phase voltages $\mathbf{V_a}$, $\mathbf{V_b}$, $\mathbf{V_c}$, the transformation produces the direct (positive) sequence phasor $\mathbf{V_d}$, the inverse (negative) sequence phasor $\mathbf{V_i}$ and the omopolar (zero) sequence phasor $\mathbf{V_o}$.

$$\begin{bmatrix} \mathbf{Vd} \\ \mathbf{Vi} \\ \mathbf{Vo} \end{bmatrix} = \boldsymbol{T} \begin{bmatrix} \mathbf{Va} \\ \mathbf{Vb} \\ \mathbf{Vc} \end{bmatrix} = \frac{1}{3}\begin{bmatrix} 1 & \boldsymbol{\alpha} & \boldsymbol{\alpha^2} \\ 1 & \boldsymbol{\alpha^2} & \boldsymbol{\alpha} \\ 1 & 1 & 1 \end{bmatrix} \begin{bmatrix} \mathbf{Va} \\ \mathbf{Vb} \\ \mathbf{Vc} \end{bmatrix}$$

The inverse transformation is obtained as:

$$\begin{bmatrix} \mathbf{Va} \\ \mathbf{Vb} \\ \mathbf{Vc} \end{bmatrix} = \boldsymbol{T}^{-1} \begin{bmatrix} \mathbf{Vd} \\ \mathbf{Vi} \\ \mathbf{Vo} \end{bmatrix} = \frac{1}{3}\begin{bmatrix} 1 & 1 & 1 \\ \boldsymbol{\alpha^2} & \boldsymbol{\alpha} & 1 \\ \boldsymbol{\alpha} & \boldsymbol{\alpha^2} & 1 \end{bmatrix} \begin{bmatrix} \mathbf{Va} \\ \mathbf{Vb} \\ \mathbf{Vc} \end{bmatrix}$$

A.5 PMU-based model validator code version 2.0

The following is the code written for the final version of the Validator, the one made to receive synchrophasors indirectly (as a combination of separate magnitude and phase):

```
VERSION:
```

```
3.001

// Include file below is generated by C-Builder
// and contains the variables declared as -
// PARAMETERS, INPUTS, OUTPUTS . . .
#include "Validator.h"
STATIC:

// -----------------------------------------------
// Variables declared here may be used in both the
// RAM: and CODE: sections below.
// -----------------------------------------------
//    double dt;

double Vd1r;
double Vd1i;
double Vd2r;
double Vd2i;
double Vo1r;
double Vo1i;
double Vo2r;
double Vo2i;
double Id1r;
double Id1i;
double Id2r;
double Id2i;
double Io1r;
double Io1i;
double Io2r;
double Io2i;
double Bd;
double Bo;
double a,b,c,d,e,f,g,h,i,l,m,n;
double sqVd1r;
double sqVd1i;
double sqVd2r;
double sqVd2i;
double sqVo1r;
double sqVo1i;
double sqVo2r;
double sqVo2i;

// -End of STATIC: Section-

RAM_FUNCTIONS:

// -----------------------------------------------
// This section should contain any 'c' functions
// to be called from the RAM section (either
// RAM_PASS1 or RAM_PASS2). Example:
//
// static double myFunction(double v1, double v2)
// {
//     return(v1*v2);
// }
// -----------------------------------------------
```

```
RAM:

// ----------------------------------------------
// Place C code here which computes constants
// required for the CODE: section below.  The C
// code here is executed once, prior to the start
// of the simulation case.
// ----------------------------------------------
//    dt= getTimeStep();

//Variables’ initialization:

Vd1r=0;
Vd1i=0;
Vd2r=0;
Vd2i=0;
Vo1r=0;
Vo1i=0;
Vo2r=0;
Vo2i=0;
Id1r=0;
Id1i=0;
Id2r=0;
Id2i=0;
Io1r=0;
Io1i=0;
Io2r=0;
Io2i=0;
Bd=0;
Bo=0;
a=0;
b=0;
c=0;
d=0;
e=0;
f=0;
g=0;
h=0;
i=0;
l=0;
m=0;
n=0;
sqVd1r=0;
sqVd1i=0;
sqVd2r=0;
sqVd2i=0;
sqVo1r=0;
sqVo1i=0;
sqVo2r=0;
sqVo2i=0;


// ------------- End of RAM: Section -------------

CODE:
```

```
// ---------------------------------------------------
// Place C code here which runs on the RTDS. The
// code below is entered once each simulation
// step.
// ---------------------------------------------------



//Optimized code:



Vd1r=Vd1*cos(tetaVd1-tetaRIF);
Vd1i=Vd1*sin(tetaVd1-tetaRIF);
Vd2r=Vd2*cos(tetaVd2-tetaRIF);
Vd2i=Vd2*sin(tetaVd2-tetaRIF);
Vo1r=Vo1*cos(tetaVo1-tetaRIF);
Vo1i=Vo1*sin(tetaVo1-tetaRIF);
Vo2r=Vo2*cos(tetaVo2-tetaRIF);
Vo2i=Vo2*sin(tetaVo2-tetaRIF);
Id1r=Id1*cos(tetaId1-tetaRIF);
Id1i=Id1*sin(tetaId1-tetaRIF);
Id2r=-Id2*cos(tetaId2-tetaRIF);
Id2i=-Id2*sin(tetaId2-tetaRIF);
Io1r=Io1*cos(tetaIo1-tetaRIF);
Io1i=Io1*sin(tetaIo1-tetaRIF);
Io2r=-Io2*cos(tetaIo2-tetaRIF);
Io2i=-Io2*sin(tetaIo2-tetaRIF);

sqVd1r=Vd1r*Vd1r;
sqVd1i=Vd1i*Vd1i;
sqVd2r=Vd2r*Vd2r;
sqVd2i=Vd2i*Vd2i;
a=(Id1r*Vd2r-Id1i*Vd2i+Id2r*Vd1r-Id2i*Vd1i);
b=(Id1r*Vd2i+Id1i*Vd2r+Id2r*Vd1i+Id2i*Vd1r);
if (a*a+b*b==0)
{
c=1e20;
}
else
{
c=1/(a*a+b*b);

}

d=(Vd1r+Vd2r)*(Vd1r+Vd2r);
e=(Vd1i+Vd2i)*(Vd1i+Vd2i);
if (d+e==0)
{
f=1e20;
}
else
{
f=1/(d+e);
}



sqVo1r=Vo1r*Vo1r;
sqVo1i=Vo1i*Vo1i;
sqVo2r=Vo2r*Vo2r;
sqVo2i=Vo2i*Vo2i;
g=(Io1r*Vo2r-Io1i*Vo2i+Io2r*Vo1r-Io2i*Vo1i);
h=(Io1r*Vo2i+Io1i*Vo2r+Io2r*Vo1i+Io2i*Vo1r);
if (g*g+h*h==0)
{
i=1e20;
}
else
{
i=1/(g*g+h*h);

}


l=(Vo1r+Vo2r)*(Vo1r+Vo2r);
m=(Vo1i+Vo2i)*(Vo1i+Vo2i);
if (l+m==0)
{
n=1e20;
}
else
{
n=1/(l+m);

}


Rd=((sqVd1r-sqVd1i-sqVd2r+sqVd2i)*(Id1r*Vd2r-Id1i*Vd2i+Id2r*Vd1r-
Id2i*Vd1i)+2*(Vd1r*Vd1i-
Vd2r*Vd2i)*(Id1r*Vd2i+Id1i*Vd2r+Id2r*Vd1i+Id2i*Vd1r))*c;
X_Ld=(2*(Vd1r*Vd1i-Vd2r*Vd2i)*(Id1r*Vd2r-Id1i*Vd2i+Id2r*Vd1r-
Id2i*Vd1i)-(sqVd1r-sqVd1i-
sqVd2r+sqVd2i)*(Id1r*Vd2i+Id1i*Vd2r+Id2r*Vd1i+Id2i*Vd1r))*c;
Bd=2*((Id1i-Id2i)*(Vd1r+Vd2r)-(Id1r-Id2r)*(Vd1i+Vd2i))*f;
if (Bd==0)
{
X_Cd=1e20;
}
else
{
X_Cd=1/Bd;

}

Ro=((sqVo1r-sqVo1i-sqVo2r+sqVo2i)*(Io1r*Vo2r-Io1i*Vo2i+Io2r*Vo1r-
Io2i*Vo1i)+2*(Vo1r*Vo1i-
Vo2r*Vo2i)*(Io1r*Vo2i+Io1i*Vo2r+Io2r*Vo1i+Io2i*Vo1r))*i;
```

```
X_Lo=(2*(Vo1r*Vo1i-Vo2r*Vo2i)*(Io1r*Vo2r-Io1i*Vo2i+Io2r*Vo1r-
Io2i*Vo1i)-(sqVo1r-sqVo1i-
sqVo2r+sqVo2i)*(Io1r*Vo2i+Io1i*Vo2r+Io2r*Vo1i+Io2i*Vo1r))*i;
Bo=2*((Io1i-Io2i)*(Vo1r+Vo2r)-(Io1r-Io2r)*(Vo1i+Vo2i))*n;
if (Bo==0)
{
X_Co=1e20;
}
else
{
X_Co=1/Bo;

}



// ------------ End of CODE: Section -------------
```

A.6 Single pi-model equivalence to a cascade of pi-models: equations and MATLAB algorithm

In order to obtain a single pi-model that results to be equivalent to a cascade of many different ones, it is needed to make use of transmission matrices. A transmission matrix is a 2x2 matrix able to relate output and input variables of any given two-port network, as it is shown below:

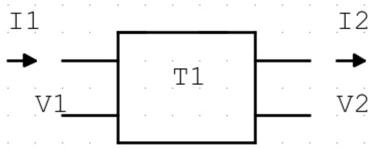

$$\begin{bmatrix} \boldsymbol{V_1} \\ \boldsymbol{I_1} \end{bmatrix} = \begin{bmatrix} \boldsymbol{A} & \boldsymbol{C} \\ \boldsymbol{B} & \boldsymbol{D} \end{bmatrix} \begin{bmatrix} \boldsymbol{V_2} \\ \boldsymbol{I_2} \end{bmatrix} = \boldsymbol{T_1} \begin{bmatrix} \boldsymbol{V_2} \\ \boldsymbol{I_2} \end{bmatrix}$$

The four elements that compose the matrix are:

- $\boldsymbol{A} = \left.\frac{\boldsymbol{V_1}}{\boldsymbol{V_2}}\right|_{\boldsymbol{I_2=0}}$ is adimensional, being the ratio between two voltages;
- $\boldsymbol{B} = \left.\frac{\boldsymbol{V_1}}{\boldsymbol{I_2}}\right|_{\boldsymbol{V_2=0}}$ is an impedance, being the ratio between a voltage and a current;
- $\boldsymbol{C} = \left.\frac{\boldsymbol{I_1}}{\boldsymbol{V_2}}\right|_{\boldsymbol{I_2=0}}$ is an admittance, being the ratio between a current and a voltage;
- $\boldsymbol{D} = \left.\frac{\boldsymbol{I_1}}{\boldsymbol{I_2}}\right|_{\boldsymbol{V_2=0}}$ is an admittance, being the ratio between two currents.

In this case, the two-port network is a pi-model. The cascade of two pi-models can then be represented as either one of the following:

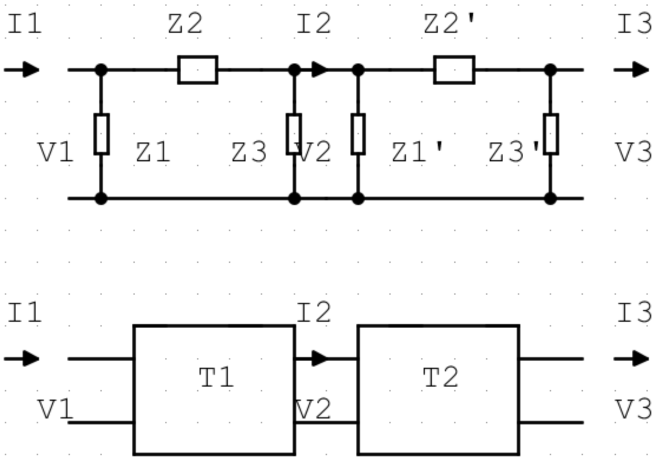

The transmission matrix parameters for a pi-model (e.g. the first one) are computed as follows:

$$V_2 = I_1' Z_3 = Z_3 \left(I_1 - \frac{V_1}{Z_1} \right) =$$

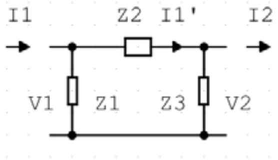

$$A = \left. \frac{V_1}{V_2} \right|_{I_2=0}$$

$$= Z_3 \left(\frac{V_1}{\frac{Z_1(Z_2+Z_3)}{Z_1+Z_2+Z_3}} - \frac{V_1}{Z_1} \right) =$$

$$= Z_3 V_1 \left(\frac{Z_1+Z_2+Z_3}{Z_1(Z_2+Z_3)} - \frac{1}{Z_1} \right) =$$

$$= V_1 \frac{Z_3}{Z_1} \left(\frac{Z_1+Z_2+Z_3-Z_2-Z_3}{Z_2+Z_3} \right) =$$

$$= V_1 \frac{Z_3}{Z_1} \left(\frac{Z_1}{Z_2+Z_3} \right) = V_1 \frac{Z_3}{Z_2+Z_3}$$

$$A = \left. \frac{V_1}{V_2} \right|_{I_2=0} = \frac{Z_2+Z_3}{Z_3}$$

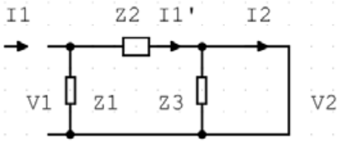

$$B = \left. \frac{V_1}{I_2} \right|_{V_2=0}$$

$$I_2 = I_1 \frac{Z_1}{Z_1+Z_2} = \frac{V_1}{\frac{Z_1 Z_2}{Z_1+Z_2}} \frac{Z_1}{Z_1+Z_2} = \frac{V_1}{Z_2}$$

$$B = \left. \frac{V_1}{I_2} \right|_{V_2=0} = Z_2$$

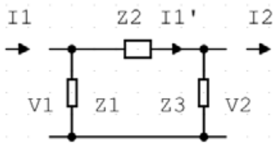

$$C = \left.\frac{I_1}{V_2}\right|_{I_2=0}$$

$$V_2 = I_1' Z_3 = I_1 \frac{Z_1}{Z_1 + Z_2 + Z_3} Z_3$$

$$C = \left.\frac{I_1}{V_2}\right|_{I_2=0} = \frac{Z_1 + Z_2 + Z_3}{Z_1 Z_3}$$

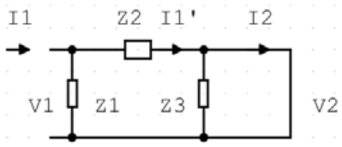

$$D = \left.\frac{I_1}{I_2}\right|_{V_2=0}$$

$$I_2 = I_1 \frac{Z_1}{Z_1 + Z_2}$$

$$D = \left.\frac{I_1}{I_2}\right|_{V_2=0} = \frac{Z_1 + Z_2}{Z_1}$$

As already mentioned, in order to produce an equivalent for the cascade, all the transmission matrices should be multiplied in the correct order. This can be done thanks to the fact that the output variables of the first two-port network, in a cascade, are at the same time the input variables of the second one; and this is true for the output of the second and the input of the third, for the output of the third and the input of the fourth, etc.

Thanks to this property, the equivalent transmission matrix **T** for *n* cascading elements can be obtained as:

$$\boldsymbol{T} = \boldsymbol{T_1} \cdot \boldsymbol{T_2} \cdot \ldots \cdot \boldsymbol{T_n}$$

Only one step is left: obtaining an equivalent p-model from this matrix. It is an easy task, considering that it suffices to take the equations obtained above for **A, B, C** and **D** and solve them for **Z1, Z2** and **Z3** instead, which can be done by mere substitution:

$$\begin{cases} Z_1 = \dfrac{B}{D-1} \\ Z_2 = B \\ Z_3 = \dfrac{B}{A-1} \end{cases}$$

The following code is the MATLAB algorithm that implements this whole procedure, in particular, for the line “Feeder 3” mentioned in the sub-chapter 3.3.1:

```
clc
clear all

%Line parameters for each of the 8 pi-models
Rd1=0.45854;
```

```
X_Ld1=0.20498;
X_Cd1=0.0064093e+006;
X_Cd1t=2*X_Cd1;
Zsd1=Rd1+X_Ld1*1i;
Ztd1=X_Cd1t*1i;
Ro1=2.0679;
X_Lo1=1.5525;
X_Co1=0.0064093e+006;
X_Co1t=2*X_Co1;
Zso1=Ro1+X_Lo1*1i;
Zto1=X_Co1t*1i;

Rd2=0.1248;
X_Ld2=0.04992;
X_Cd2=0.028144e+006;
X_Cd2t=2*X_Cd2;
Zsd2=Rd2+X_Ld2*1i;
Ztd2=X_Cd2t*1i;
Ro2=0.468;
X_Lo2=0.39;
X_Co2=0.028144e+006;
X_Co2t=2*X_Co2;
Zso2=Ro2+X_Lo2*1i;
Zto2=X_Co2t*1i;

Rd3=0.0928;
X_Ld3=0.03712;
X_Cd3=0.037849e+006;
X_Cd3t=2*X_Cd3;
Zsd3=Rd3+X_Ld3*1i;
Ztd3=X_Cd3t*1i;
Ro3=0.348;
X_Lo3=0.29;
X_Co3=0.037849e+006;
X_Co3t=2*X_Co3;
Zso3=Ro3+X_Lo3*1i;
Zto3=X_Co3t*1i;

Rd4=0.15104;
X_Ld4=0.060416;
X_Cd4=0.023255e+006;
X_Cd4t=2*X_Cd4;
Zsd4=Rd4+X_Ld4*1i;
Ztd4=X_Cd4t*1i;
Ro4=0.5664;
X_Lo4=0.472;
X_Co4=0.023255e+006;
X_Co4t=2*X_Co4;
Zso4=Ro4+X_Lo4*1i;
Zto4=X_Co4t*1i;

Rd5=0.13588;
X_Ld5=0.054897;
X_Cd5=0.025392e+006;
X_Cd5t=2*X_Cd5;
Zsd5=Rd5+X_Ld5*1i;
```

```
Ztd5=X_Cd5t*1i;
Ro5=0.51689;
X_Lo5=0.42821;
X_Co5=0.025392e+006;
X_Co5t=2*X_Co5;
Zso5=Ro5+X_Lo5*1i;
Zto5=X_Co5t*1i;

Rd6=0.2768;
X_Ld6=0.11072;
X_Cd6=0.012689e+006;
X_Cd6t=2*X_Cd6;
Zsd6=Rd6+X_Ld6*1i;
Ztd6=X_Cd6t*1i;
Ro6=1.038;
X_Lo6=0.865;
X_Co6=0.012689e+006;
X_Co6t=2*X_Co6;
Zso6=Ro6+X_Lo6*1i;
Zto6=X_Co6t*1i;

Rd7=0.024;
X_Ld7=0.0096;
X_Cd7=0.14635e+006;
X_Cd7t=2*X_Cd7;
Zsd7=Rd7+X_Ld7*1i;
Ztd7=X_Cd7t*1i;
Ro7=0.09;
X_Lo7=0.075;
X_Co7=0.14635e+006;
X_Co7t=2*X_Co7;
Zso7=Ro7+X_Lo7*1i;
Zto7=X_Co7t*1i;

Rd8=0.14592;
X_Ld8=0.058368;
X_Cd8=0.024071e+006;
X_Cd8t=2*X_Cd8;
Zsd8=Rd8+X_Ld8*1i;
Ztd8=X_Cd8t*1i;
Ro8=0.5472;
X_Lo8=0.456;
X_Co8=0.024071e+006;
X_Co8t=2*X_Co8;
Zso8=Ro8+X_Lo8*1i;
Zto8=X_Co8t*1i;

%Transmision matrix computation for the positive sequence

A1d=(Zsd1+Ztd1)/Ztd1;
B1d=Zsd1;
C1d=(2*Ztd1+Zsd1)/Ztd1^2;
D1d=A1d;

T1d= [A1d B1d; C1d D1d];
```

```
A2d=(Zsd2+Ztd2)/Ztd2;
B2d=Zsd2;
C2d=(2*Ztd2+Zsd2)/Ztd2^2;
D2d=A2d;

T2d= [A2d B2d; C2d D2d];

A3d=(Zsd3+Ztd3)/Ztd3;
B3d=Zsd3;
C3d=(2*Ztd3+Zsd3)/Ztd3^2;
D3d=A3d;

T3d= [A3d B3d; C3d D3d];

A4d=(Zsd4+Ztd4)/Ztd4;
B4d=Zsd4;
C4d=(2*Ztd4+Zsd4)/Ztd4^2;
D4d=A4d;

T4d= [A4d B4d; C4d D4d];

A5d=(Zsd5+Ztd5)/Ztd5;
B5d=Zsd5;
C5d=(2*Ztd5+Zsd5)/Ztd5^2;
D5d=A5d;

T5d= [A5d B5d; C5d D5d];

A6d=(Zsd6+Ztd6)/Ztd6;
B6d=Zsd6;
C6d=(2*Ztd6+Zsd6)/Ztd6^2;
D6d=A6d;

T6d= [A6d B6d; C6d D6d];

A7d=(Zsd7+Ztd7)/Ztd7;
B7d=Zsd7;
C7d=(2*Ztd7+Zsd7)/Ztd7^2;
D7d=A7d;

T7d= [A7d B7d; C7d D7d];

A8d=(Zsd8+Ztd8)/Ztd8;
B8d=Zsd8;
C8d=(2*Ztd8+Zsd8)/Ztd8^2;
D8d=A8d;

T8d= [A8d B8d; C8d D8d];

%Transmision matrix computation for the zero sequence

A1o=(Zso1+Zto1)/Zto1;
B1o=Zso1;
C1o=(2*Zto1+Zso1)/Zto1^2;
D1o=A1o;
```

```
T1o= [A1o B1o; C1o D1o];

A2o=(Zso2+Zto2)/Zto2;
B2o=Zso2;
C2o=(2*Zto2+Zso2)/Zto2^2;
D2o=A2o;

T2o= [A2o B2o; C2o D2o];

A3o=(Zso3+Zto3)/Zto3;
B3o=Zso3;
C3o=(2*Zto3+Zso3)/Zto3^2;
D3o=A3o;

T3o= [A3o B3o; C3o D3o];

A4o=(Zso4+Zto4)/Zto4;
B4o=Zso4;
C4o=(2*Zto4+Zso4)/Zto4^2;
D4o=A4o;

T4o= [A4o B4o; C4o D4o];

A5o=(Zso5+Zto5)/Zto5;
B5o=Zso5;
C5o=(2*Zto5+Zso5)/Zto5^2;
D5o=A5o;

T5o= [A5o B5o; C5o D5o];

A6o=(Zso6+Zto6)/Zto6;
B6o=Zso6;
C6o=(2*Zto6+Zso6)/Zto6^2;
D6o=A6o;

T6o= [A6o B6o; C6o D6o];

A7o=(Zso7+Zto7)/Zto7;
B7o=Zso7;
C7o=(2*Zto7+Zso7)/Zto7^2;
D7o=A7o;

T7o= [A7o B7o; C7o D7o];

A8o=(Zso8+Zto8)/Zto8;
B8o=Zso8;
C8o=(2*Zto8+Zso8)/Zto8^2;
D8o=A8o;

T8o= [A8o B8o; C8o D8o];

%Equivalent transmission matrix computation for both positive and
zero sequence

Tdeq=T1d*T2d*T3d*T4d*T5d*T6d*T7d*T8d;
```

```
Adeq=Tdeq(1,1);
Bdeq=Tdeq(1,2);
Cdeq=Tdeq(2,1);
Ddeq=Tdeq(2,2);


Toeq=T1o*T2o*T3o*T4o*T5o*T6o*T7o*T8o;

Aoeq=Toeq(1,1);
Boeq=Toeq(1,2);
Coeq=Toeq(2,1);
Doeq=Toeq(2,2);

%Equivalent p-model computation for both positive and zero sequence

Ztdeq_sx=Bdeq/(Ddeq-1);
Zsdeq=Bdeq;
Ztdeq_dx=Bdeq*Ddeq/(Bdeq*Cdeq-Ddeq+1);
Ztdeq=Ztdeq_sx*Ztdeq_dx/(Ztdeq_dx+Ztdeq_sx);
Rdeq=real(Zsdeq)
X_Ldeq=imag(Zsdeq)
X_Cdeq=imag(Ztdeq)

Ztoeq_sx=Boeq/(Doeq-1);
Zsoeq=Boeq;
Ztoeq_ox=Boeq*Doeq/(Boeq*Coeq-Doeq+1);
Ztoeq=Ztoeq_sx*Ztoeq_ox/(Ztoeq_ox+Ztoeq_sx);
Roeq=real(Zsoeq)
X_Loeq=imag(Zsoeq)
X_Coeq=imag(Ztoeq)
```

A.7 Branching line section circuital equivalent and MATLAB model

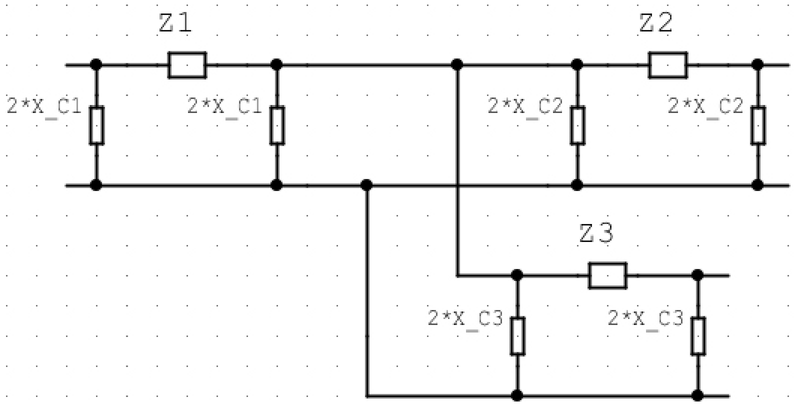

Figure 50 Circuital representation of a branching section of a feeder.

In order to include in the MATLAB model already developed in Appendix A.6 the branching section shown in the equivalent of Figure 50, some circuital elaborations were in order. The following equivalent is elaborated under the assumptions of no loads connected to any of the ports and for any of the three sequences, just to keep the process as general as possible.

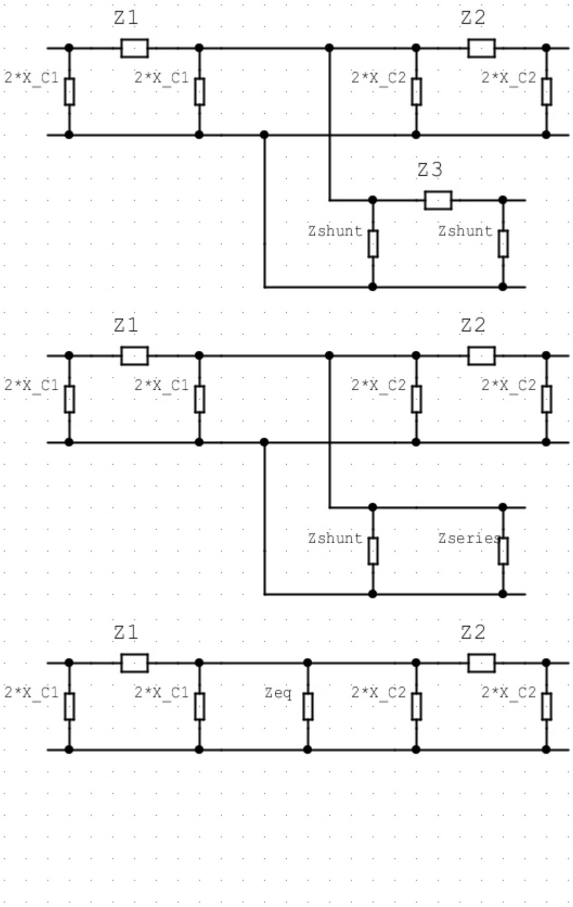

$$\boldsymbol{Z_{shunt}} = jX_{C3}$$

$$\boldsymbol{Z_{series}} = \boldsymbol{Z_3} + \boldsymbol{Z_{shunt}}$$

$$\boldsymbol{Z_{eq}} = \frac{\boldsymbol{Z_{series}}\boldsymbol{Z_{shunt}}}{\boldsymbol{Z_{series}}\boldsymbol{Z_{shunt}}}$$

Once $\mathbf{Z_{eq}}$ is computed, the element can be implemented in the two-ports cascade by simply calculating its transformation matrix and including it in the ordered multiplication already shown in Appendix A.6. It’s transformation matrix can be easily found as show below:

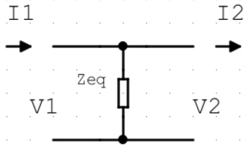

$$\boldsymbol{A} = \left.\frac{\boldsymbol{V_1}}{\boldsymbol{V_2}}\right|_{\boldsymbol{I_2=0}}$$

$$\boldsymbol{V_2} = \boldsymbol{V_1}$$

$$\boldsymbol{A} = \left.\frac{\boldsymbol{V_1}}{\boldsymbol{V_2}}\right|_{\boldsymbol{I_2=0}} = 1$$

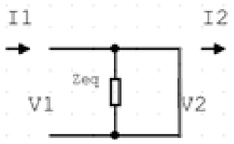

$$B = \left.\frac{V_1}{I_2}\right|_{V_2=0}$$

$$I_2 = \frac{V_1}{0} = \infty$$

$$B = \left.\frac{V_1}{I_2}\right|_{V_2=0} = 0$$

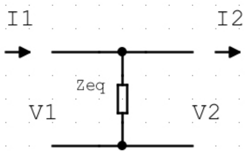

$$C = \left.\frac{I_1}{V_2}\right|_{I_2=0}$$

$$V_2 = V_1 = I_1 Z_{eq}$$

$$C = \left.\frac{I_1}{V_2}\right|_{I_2=0} = \frac{1}{Z_{eq}}$$

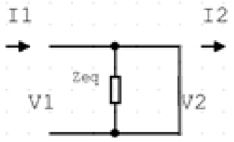

$$D = \left.\frac{I_1}{I_2}\right|_{V_2=0}$$

$$I_2 = I_1$$

$$D = \left.\frac{I_1}{I_2}\right|_{V_2=0} = 1$$

The following is the MATLAB code that implements what has been analytically elaborated up until now:

```
clc
clear all

%Known sequence line parameters for the three pi models under
analysis

Rd1=0.46552;
X_Ld1=0.20842;
X_Cd1=0.0063063e+006;
X_Cd1t=2*X_Cd1;
Zsd1=Rd1+X_Ld1*1i;
Ztd1=X_Cd1t*1i;
Ro1=2.1557;
X_Lo1=1.5895;
X_Co1=0.0064311e+006;
X_Co1t=2*X_Co1;
Zso1=Ro1+X_Lo1*1i;
Zto1=X_Co1t*1i;

Rd2=0.18751;
X_Ld2=0.077496;
X_Cd2=0.019773e+006;
X_Cd2t=2*X_Cd2;
Zsd2=Rd2+X_Ld2*1i;
Ztd2=X_Cd2t*1i;
Ro2=0.70128;
```

```
X_Lo2=0.58152;
X_Co2=0.019773e+006;
X_Co2t=2*X_Co2;
Zso2=Ro2+X_Lo2*1i;
Zto2=X_Co2t*1i;

Rd3=0.065305;
X_Ld3=0.02695;
X_Cd3=5.0525e+006;
X_Cd3t=2*X_Cd3;
Zsd3=Rd3+X_Ld3*1i;
Ztd3=X_Cd3t*1i;
Ro3=0.075665;
X_Lo3=0.11361;
X_Co3=11.3682e+006;
X_Co3t=2*X_Co3;
Zso3=Ro3+X_Lo3*1i;
Zto3=X_Co3t*1i;

%Zeq computation for both positive and zero sequence

Zseried=Ztd3+Zsd3;
Zeqd=(Ztd3*Zseried)/(Ztd3+Zseried);

Zserieo=Zto3+Zso3;
Zeqo=(Zto3*Zserieo)/(Zto3+Zserieo);

%Pi model transformation for Zeq (positive and zero sequence)

Rdline=0;
X_Ldline=0;
X_Cdline=imag(Zeqd);
X_Cdlinet=2*X_Cdline;
Zsdline=Rdline+X_Ldline*1i;
Ztdline=X_Cdlinet*1i;

Roline=0;
X_Loline=0;
X_Coline=imag(Zeqo);
X_Colinet=2*X_Coline;
Zsoline=Roline+X_Loline*1i;
Ztoline=X_Colinet*1i;

%Transmission matrices computation for direct sequence

A1d=(Zsd1+Ztd1)/Ztd1;
B1d=Zsd1;
C1d=(2*Ztd1+Zsd1)/Ztd1^2;
D1d=A1d;

T1d= [A1d B1d; C1d D1d];

A2d=(Zsd2+Ztd2)/Ztd2;
B2d=Zsd2;
C2d=(2*Ztd2+Zsd2)/Ztd2^2;
D2d=A2d;
```

```
T2d= [A2d B2d; C2d D2d];

Alined=(Zsdline+Ztdline)/Ztdline;
Blined=Zsdline;
Clined=(2*Ztdline+Zsdline)/Ztdline^2;
Dlined=Alined;

Tlined= [Alined Blined; Clined Dlined];

%Transmission matrices computation for homopolar sequence

A1o=(Zso1+Zto1)/Zto1;
B1o=Zso1;
C1o=(2*Zto1+Zso1)/Zto1^2;
D1o=A1o;

T1o= [A1o B1o; C1o D1o];

A2o=(Zso2+Zto2)/Zto2;
B2o=Zso2;
C2o=(2*Zto2+Zso2)/Zto2^2;
D2o=A2o;

T2o= [A2o B2o; C2o D2o];

Alineo=(Zsoline+Ztoline)/Ztoline;
Blineo=Zsoline;
Clineo=(2*Ztoline+Zsoline)/Ztoline^2;
Dlineo=Alineo;

Tlineo= [Alineo Blineo; Clineo Dlineo];

%Equivalent matrix computation for both positive and zero sequence

Tdeq=T1d*Tlined*T2d;

Adeq=Tdeq(1,1);
Bdeq=Tdeq(1,2);
Cdeq=Tdeq(2,1);
Ddeq=Tdeq(2,2);


Toeq=T1o*Tlineo*T2o;

Aoeq=Toeq(1,1);
Boeq=Toeq(1,2);
Coeq=Toeq(2,1);
Doeq=Toeq(2,2);

%Pi equivalent model derivation for both positive and zero sequence

Ztdeq_sx=Bdeq/(Ddeq-1);
Zsdeq=Bdeq;
Ztdeq_dx=Bdeq*Ddeq/(Bdeq*Cdeq-Ddeq+1);
Ztdeq=Ztdeq_sx*Ztdeq_dx/(Ztdeq_dx+Ztdeq_sx);
```

```
Rdeq=real(Zsdeq)
X_Ldeq=imag(Zsdeq)
X_Cdeq=imag(Ztdeq)

Ztoeq_sx=Boeq/(Doeq-1);
Zsoeq=Boeq;
Ztoeq_dx=Boeq*Doeq/(Boeq*Coeq-Doeq+1);
Ztoeq=Ztoeq_sx*Ztoeq_dx/(Ztoeq_dx+Ztoeq_sx);
Roeq=real(Zsoeq)
X_Loeq=imag(Zsoeq)
X_Coeq=imag(Ztoeq)
```

A.8 Parallel three-phase delta load circuital sequence equivalent

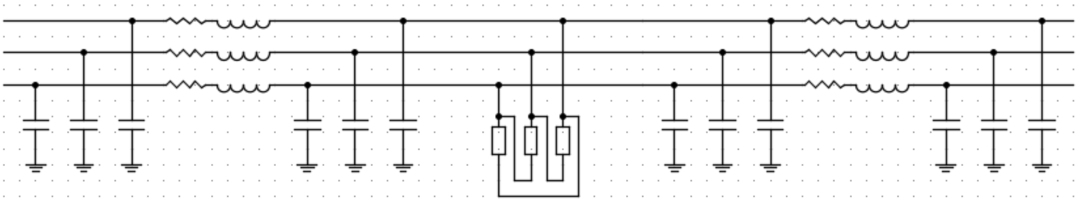

Figure 51 Delta-connection of a load onto a three-phase distribution line section.

Figure 51 shows a three-phase equivalent representation of the “line section – load – line section” system seen before in Figure 45. In order to analyze more easily this kind of situation, symmetrical components are often resorted to: from a three-phase circuit, through the application of specific equations, three single-phase equivalent circuits can be obtained and studied with reduced computational burdens. Applying these transformations, however, is not as straightforward as it could appear: each circuital component, due to its peculiar connection pattern and nature, is related to its symmetrical equivalent in a unique way.

A delta-connection load, as in this example, must be examined accurately in order to obtain from it a proper equivalent. First things first, its connection’s schematics are handled in order to have a clearer overview of applied voltages and flowing currents:

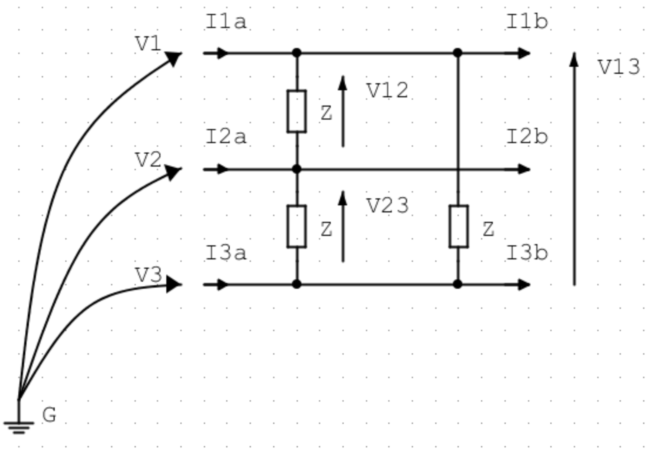

Figure 52 Delta-connected three-phase load.

The circuit of Figure 52 reveals the hypothesis upon which the following elaboration is based: the three-phased load is of unknown nature but perfectly balanced. The logic behind the considerations below could still be applicable to an unbalanced load, but calculations would prove to be more difficult. Using Kirchhoff's Current Law for each phase the following is obtained:

$$\begin{cases} \boldsymbol{I_{1a}} = \boldsymbol{I_{1b}} + \boldsymbol{V_{12}}\dfrac{1}{\boldsymbol{Z}} + \boldsymbol{V_{13}}\dfrac{1}{\boldsymbol{Z}} = \boldsymbol{I_{1b}} + 2\dfrac{\boldsymbol{V_1}}{\boldsymbol{Z}} - \dfrac{\boldsymbol{V_2}}{\boldsymbol{Z}} - \dfrac{\boldsymbol{V_3}}{\boldsymbol{Z}} \\ \boldsymbol{I_{2a}} = \boldsymbol{I_{2b}} + \boldsymbol{V_{21}}\dfrac{1}{\boldsymbol{Z}} + \boldsymbol{V_{23}}\dfrac{1}{\boldsymbol{Z}} = \boldsymbol{I_{1b}} - \dfrac{\boldsymbol{V_1}}{\boldsymbol{Z}} + 2\dfrac{\boldsymbol{V_2}}{\boldsymbol{Z}} - \dfrac{\boldsymbol{V_3}}{\boldsymbol{Z}} \\ \boldsymbol{I_{3a}} = \boldsymbol{I_{3b}} + \boldsymbol{V_{31}}\dfrac{1}{\boldsymbol{Z}} + \boldsymbol{V_{32}}\dfrac{1}{\boldsymbol{Z}} = \boldsymbol{I_{1b}} - \dfrac{\boldsymbol{V_1}}{\boldsymbol{Z}} - \dfrac{\boldsymbol{V_2}}{\boldsymbol{Z}} + 2\dfrac{\boldsymbol{V_3}}{\boldsymbol{Z}} \end{cases}$$

This equation set can be written in matrix form as:

$$\begin{bmatrix} \boldsymbol{I_{1a}} \\ \boldsymbol{I_{2a}} \\ \boldsymbol{I_{3a}} \end{bmatrix} = \begin{bmatrix} \boldsymbol{I_{1b}} \\ \boldsymbol{I_{2b}} \\ \boldsymbol{I_{3b}} \end{bmatrix} + \begin{bmatrix} \dfrac{2}{\boldsymbol{Z}} & -\dfrac{1}{\boldsymbol{Z}} & -\dfrac{1}{\boldsymbol{Z}} \\ -\dfrac{1}{\boldsymbol{Z}} & \dfrac{2}{\boldsymbol{Z}} & -\dfrac{1}{\boldsymbol{Z}} \\ -\dfrac{1}{\boldsymbol{Z}} & -\dfrac{1}{\boldsymbol{Z}} & \dfrac{2}{\boldsymbol{Z}} \end{bmatrix} \begin{bmatrix} \boldsymbol{V_1} \\ \boldsymbol{V_2} \\ \boldsymbol{V_3} \end{bmatrix}$$

How does the admittance matrix obtain translate in terms of symmetrical components? The answer is the following:

$$\begin{bmatrix} \boldsymbol{I_{1a}} \\ \boldsymbol{I_{2a}} \\ \boldsymbol{I_{3a}} \end{bmatrix} = \begin{bmatrix} \boldsymbol{I_{1b}} \\ \boldsymbol{I_{2b}} \\ \boldsymbol{I_{3b}} \end{bmatrix} + \begin{bmatrix} \frac{2}{\boldsymbol{Z}} & -\frac{1}{\boldsymbol{Z}} & -\frac{1}{\boldsymbol{Z}} \\ -\frac{1}{\boldsymbol{Z}} & \frac{2}{\boldsymbol{Z}} & -\frac{1}{\boldsymbol{Z}} \\ -\frac{1}{\boldsymbol{Z}} & -\frac{1}{\boldsymbol{Z}} & \frac{2}{\boldsymbol{Z}} \end{bmatrix} \begin{bmatrix} \boldsymbol{V_1} \\ \boldsymbol{V_2} \\ \boldsymbol{V_3} \end{bmatrix}$$

$$\downarrow$$

$$[\boldsymbol{T}]^{-1} \begin{bmatrix} \boldsymbol{I_{da}} \\ \boldsymbol{I_{ia}} \\ \boldsymbol{I_{oa}} \end{bmatrix} = [\boldsymbol{T}]^{-1} \begin{bmatrix} \boldsymbol{I_{db}} \\ \boldsymbol{I_{ib}} \\ \boldsymbol{I_{ob}} \end{bmatrix} + \begin{bmatrix} \frac{2}{\boldsymbol{Z}} & -\frac{1}{\boldsymbol{Z}} & -\frac{1}{\boldsymbol{Z}} \\ -\frac{1}{\boldsymbol{Z}} & \frac{2}{\boldsymbol{Z}} & -\frac{1}{\boldsymbol{Z}} \\ -\frac{1}{\boldsymbol{Z}} & -\frac{1}{\boldsymbol{Z}} & \frac{2}{\boldsymbol{Z}} \end{bmatrix} [\boldsymbol{T}]^{-1} \begin{bmatrix} \boldsymbol{V_d} \\ \boldsymbol{V_i} \\ \boldsymbol{V_o} \end{bmatrix}$$

where $[\boldsymbol{T}]$ is the Fortescue matrix already discussed in Appendix A.4. If both sides of the equation are then multiplied on the left by $[\boldsymbol{T}]$, then the result is:

$$\begin{bmatrix} \boldsymbol{I_{da}} \\ \boldsymbol{I_{ia}} \\ \boldsymbol{I_{oa}} \end{bmatrix} = \begin{bmatrix} \boldsymbol{I_{db}} \\ \boldsymbol{I_{ib}} \\ \boldsymbol{I_{ob}} \end{bmatrix} + [\boldsymbol{T}] \begin{bmatrix} \frac{2}{\boldsymbol{Z}} & -\frac{1}{\boldsymbol{Z}} & -\frac{1}{\boldsymbol{Z}} \\ -\frac{1}{\boldsymbol{Z}} & \frac{2}{\boldsymbol{Z}} & -\frac{1}{\boldsymbol{Z}} \\ -\frac{1}{\boldsymbol{Z}} & -\frac{1}{\boldsymbol{Z}} & \frac{2}{\boldsymbol{Z}} \end{bmatrix} [\boldsymbol{T}]^{-1} \begin{bmatrix} \boldsymbol{V_d} \\ \boldsymbol{V_i} \\ \boldsymbol{V_o} \end{bmatrix}$$

In case of a balanced load (and only in that particular case), the resulting sequence admittance matrix is diagonal and has a null homopolar parameter. (that will translate to an infinite zero sequence impedance, as it was predictable since a delta-connected load lack any kind of link to the ground)

The last obtained equation then is used to build the symmetrical component's equivalent circuits as follows:

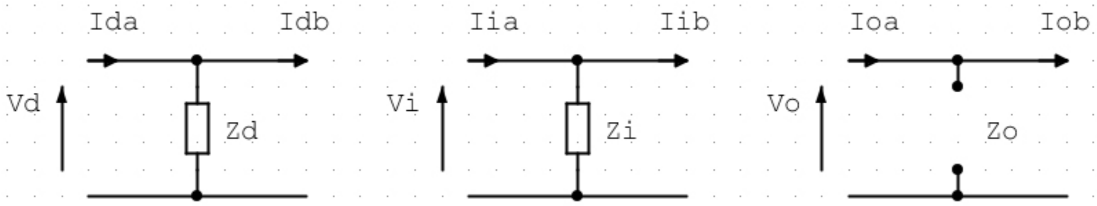

Figure 53 Delta-connected three-phase load sequence equivalent circuits.

A.9 IEEE C37.118 Validator’s algorithm

The code, originally written on RSCAD in C, has been translated into the IEEE C37.118 synchrophasor-specific language in order to be run on the AXION SEL device working as a PDC.

The algorithm is the following:

```
PROGRAM Validator’s Algorithm

VAR

 Vd1r            : REAL;

 Vd1i            : REAL;

 Vd2r            : REAL;

 Vd2i            : REAL;

 Vo1r            : REAL;

 Vo1i            : REAL;

 Vo2r            : REAL;

 Vo2i            : REAL;

 Id1r            : REAL;

 Id1i            : REAL;

 Id2r            : REAL;

 Id2i            : REAL;

 Io1r            : REAL;

 Io1i            : REAL;

 Io2r            : REAL;

 Io2i            : REAL;

 Bd              : REAL;

 Bo              : REAL;

 a,b,c,d,e,f,g,h,i,l,m,n : REAL;

 sqVd1r          : REAL;

 sqVd1i          : REAL;
```

```
sqVd2r          : REAL;
sqVd2i          : REAL;
sqVo1r          : REAL;
sqVo1i          : REAL;
sqVo2r          : REAL;
sqVo2i          : REAL;
xcd             : REAL;
Rd              : REAL;
X_Ld            : REAL;
Ro              : REAL;
X_Lo            : REAL;
X_Co            : REAL;


IA_R, IA_I  : REAL;
IB_R, IB_I  : REAL;
IC_R, IC_I  : REAL;
I0_R, I0_I  : REAL;



VA_R, VA_I  : REAL;
VB_R, VB_I  : REAL;
VC_R, VC_I  : REAL;
V0_R, V0_I  : REAL;


I0_MAG, I0_ANG : REAL;
END_VAR
```

```
// AXION PMU VOLTAGES

Vd1r     := SEL_CTPT_1_ECAT.V1_PM.instCVal.mag * COS
(SEL_CTPT_1_ECAT.V1_PM.instCVal.ang/180*3.14);

Vd1i     := SEL_CTPT_1_ECAT.V1_PM.instCVal.mag * SIN
(SEL_CTPT_1_ECAT.V1_PM.instCVal.ang/180*3.14);

Vo1r     := SEL_CTPT_1_ECAT.V0_PM.instCVal.mag * COS
(SEL_CTPT_1_ECAT.V0_PM.instCVal.ang/180*3.14);

Vo1i     := SEL_CTPT_1_ECAT.V0_PM.instCVal.mag * SIN
(SEL_CTPT_1_ECAT.V0_PM.instCVal.ang/180*3.14);


Vd2r     := SEL_CTPT_2_ECAT.V1_PM.instCVal.mag *COS
(SEL_CTPT_2_ECAT.V1_PM.instCVal.ang/180*3.14);

Vd2i     := SEL_CTPT_2_ECAT.V1_PM.instCVal.mag * SIN
(SEL_CTPT_2_ECAT.V1_PM.instCVal.ang/180*3.14);

Vo2r     := SEL_CTPT_2_ECAT.V0_PM.instCVal.mag * COS
(SEL_CTPT_2_ECAT.V0_PM.instCVal.ang/180*3.14);

Vo2i     := SEL_CTPT_2_ECAT.V0_PM.instCVal.mag * SIN
(SEL_CTPT_2_ECAT.V0_PM.instCVal.ang/180*3.14);


// AXION PMU CURRENTS

Id1r     :=SEL_CTPT_1_ECAT.I1_PM.instCVal.mag * COS
(SEL_CTPT_1_ECAT.I1_PM.instCVal.ang/180*3.14);

Id1i     :=SEL_CTPT_1_ECAT.I1_PM.instCVal.mag * SIN
(SEL_CTPT_1_ECAT.I1_PM.instCVal.ang/180*3.14);

Io1r     :=SEL_CTPT_1_ECAT.I0_PM.instCVal.mag * COS
(SEL_CTPT_1_ECAT.I0_PM.instCVal.ang/180*3.14);

Io1i     :=SEL_CTPT_1_ECAT.I0_PM.instCVal.mag * SIN
(SEL_CTPT_1_ECAT.I0_PM.instCVal.ang/180*3.14);


Id2r     :=SEL_CTPT_2_ECAT.I1_PM.instCVal.mag * COS
(SEL_CTPT_2_ECAT.I1_PM.instCVal.ang/180*3.14);

Id2i     :=SEL_CTPT_2_ECAT.I1_PM.instCVal.mag * SIN
(SEL_CTPT_2_ECAT.I1_PM.instCVal.ang/180*3.14);
```

```
Io2r      :=SEL_CTPT_2_ECAT.I0_PM.instCVal.mag * COS
(SEL_CTPT_2_ECAT.I0_PM.instCVal.ang/180*3.14);

Io2i      :=SEL_CTPT_2_ECAT.I0_PM.instCVal.mag * SIN
(SEL_CTPT_2_ECAT.I0_PM.instCVal.ang/180*3.14);


Bd        :=0;

Bo        :=0;

a         :=0;

b         :=0;

c         :=0;

d         :=0;

e         :=0;

f         :=0;

g         :=0;

h         :=0;

i         :=0;

l         :=0;

m         :=0;

n         :=0;

sqVd1r :=0;

sqVd1i  :=0;

sqVd2r :=0;

sqVd2i  :=0;

sqVo1r :=0;

sqVo1i  :=0;

sqVo2r :=0;

sqVo2i  :=0;
```

```
sqVd1r :=Vd1r*Vd1r;

sqVd1i  :=Vd1i*Vd1i;

sqVd2r :=Vd2r*Vd2r;

sqVd2i  :=Vd2i*Vd2i;

a           :=(Id1r*Vd2r-Id1i*Vd2i+Id2r*Vd1r-Id2i*Vd1i);

b           :=(Id1r*Vd2i+Id1i*Vd2r+Id2r*Vd1i+Id2i*Vd1r);

            IF ((a*a+b*b)=0) THEN

                        c :=1E20;

            ELSE

                        c:=1/(a*a+b*b);

            END_IF



d :=(Vd1r+Vd2r) * (Vd1r+Vd2r);

e := (Vd1i+Vd2i) * (Vd1i+Vd2i);

IF ((d+e)=0) THEN

            f:=1E20;

ELSE

            f:=1/(d+e);

END_IF




sqVo1r:=Vo1r*Vo1r;

sqVo1i:=Vo1i*Vo1i;

sqVo2r:=Vo2r*Vo2r;

sqVo2i:=Vo2i*Vo2i;

g:= (Io1r*Vo2r-Io1i*Vo2i+Io2r*Vo1r-Io2i*Vo1i);

h:= (Io1r*Vo2i+Io1i*Vo2r+Io2r*Vo1i+Io2i*Vo1r);
```

```
IF ((g*g+h*h)=0) THEN

        i:=1E20;

ELSE

        i:=1/(g*g+h*h);

END_IF



l:= (Vo1r+Vo2r) * (Vo1r+Vo2r);

m:= (Vo1i+Vo2i) * (Vo1i+Vo2i);


IF ((l+m)=0) THEN

        n:=1E20;

ELSE

        n:=1/(l+m);

END_IF



Rd := ((sqVd1r-sqVd1i-sqVd2r+sqVd2i) * (Id1r*Vd2r-Id1i*Vd2i+Id2r*Vd1r-
Id2i*Vd1i)+2*(Vd1r*Vd1i-Vd2r*Vd2i) * (Id1r*Vd2i+Id1i*Vd2r+Id2r*Vd1i+Id2i*Vd1r))*c;

X_Ld:= (2*(Vd1r*Vd1i-Vd2r*Vd2i) * (Id1r*Vd2r-Id1i*Vd2i+Id2r*Vd1r-Id2i*Vd1i)-(sqVd1r-
sqVd1i-sqVd2r+sqVd2i) * (Id1r*Vd2i+Id1i*Vd2r+Id2r*Vd1i+Id2i*Vd1r))*c;

Bd:=2*((Id1i-Id2i) * (Vd1r+Vd2r)-(Id1r-Id2r) * (Vd1i+Vd2i))*f;


IF (Bd=0) THEN

        xcd := 1E20;

ELSE

        xcd := 1/Bd;

END_IF
```

```
Ro:= ((sqVo1r-sqVo1i-sqVo2r+sqVo2i) * (Io1r*Vo2r-Io1i*Vo2i+Io2r*Vo1r-
Io2i*Vo1i)+2*(Vo1r*Vo1i-Vo2r*Vo2i) * (Io1r*Vo2i+Io1i*Vo2r+Io2r*Vo1i+Io2i*Vo1r))*i;

X_Lo:= (2*(Vo1r*Vo1i-Vo2r*Vo2i) * (Io1r*Vo2r-Io1i*Vo2i+Io2r*Vo1r-Io2i*Vo1i)-(sqVo1r-
sqVo1i-sqVo2r+sqVo2i) * (Io1r*Vo2i+Io1i*Vo2r+Io2r*Vo1i+Io2i*Vo1r))*i;

Bo:=2*((Io1i-Io2i) * (Vo1r+Vo2r)-(Io1r-Io2r) * (Vo1i+Vo2i))*n;


IF (Bo=0) THEN

        X_Co:=1E20;

ELSE

        X_Co:=1/Bo;

END_IF
```